RESEARCH ON THE DYNAMIC INTERNAL SHEAR BEHAVIOR OF A NEEDLE-PUNCHED GEOSYNTHETIC CLAY LINER

A Thesis

Presented in Partial Fulfillment of the Requirements for

the Degree Master of Science in the

Graduate School of The Ohio State University

By

Christopher John Nye, B.S.

* * * * *

The Ohio State University

2006

Masters Examination Committee:

Dr. Patrick J. Fox, Adviser

Dr. William E. Wolfe

Dr. Tien H. Wu

Approved by:

Adviser
Civil Engineering Graduate Program

ABSTRACT

A large direct shear machine for static and dynamic shear strength testing of geosynthetic clay liners (GCLs) and GCL interfaces is described. The basic design concept for the device is to shear a GCL specimen between a bidirectional pullout plate and a stationary reaction plate, each covered with an aggressive gripping surface. The maximum normal stress is 2000 kPa, the maximum shear stress is 750 kPa, and the shearing system is capable of imposing general stress-controlled or displacement-controlled dynamic loading to a test specimen. The maximum displacement rate for burst loading (i.e., single thrust) at zero force is 1 m/s. Four main components of the machine are described: (1) the shearing system, (2) the normal stress and vertical displacement measurement system, (3) the specimen hydration system, and (4) the process control and data acquisition system.

Monotonic and cyclic shear tests were performed to investigate the effects of displacement rate, displacement amplitude, number of cycles, excitation frequency, and motion waveform on the dynamic internal shear behavior of a hydrated woven/nonwoven needle-punched GCL with no thermal bonding. Monotonic tests indicate that peak shear strength first increased and then decreased with increasing displacement rate. Cyclic shear tests indicate that dynamic response was primarily controlled by displacement amplitude. Number of cycles (≥ 10), excitation frequency, and waveform had little effect

on cyclic shear behavior or post-cyclic static shear strengths. Shear stress-displacement diagrams displayed hysteresis similar to those for natural soils with some differences observed due to the presence of GCL reinforcement. Secant shear stiffness displayed strong reduction with increasing displacement amplitude and degradation with continued cycling. Values of damping ratio were significantly higher than those typically measured for natural clays at lower shear strain levels. Finally, cyclic tests with increasing displacement amplitude yielded progressively lower post-cyclic static peak strengths due to greater levels of reinforcement damage. Post-cyclic static residual strengths were unaffected by prior cyclic loading.

Dedicated to my parents for getting me here

ACKNOWLEDGMENTS

The completion of this thesis would not have been possible without the help of many people. First, I would like to thank my adviser, Dr. Patrick Fox, for his continued support during my Master's program. His tireless efforts and collaboration made the process efficient and expedient. I would also like to acknowledge Drs. William Wolfe and Tien Wu for serving on my graduate committee. Their comments on this thesis are greatly appreciated, as is their willingness to share their knowledge in the classroom. The work of Todd Morrison must also not be overlooked, since his efforts brought about the successful operation of the dynamic direct shear machine. David Varathungarajan's assistance with the experimental work presented herein is also greatly appreciated. Finally, I would like to thank my wife, Elizabeth, for her constant love and encouragement, which has helped me more than she will ever know.

Financial support for this work was provided by a grant from CETCO of Arlington Heights, Illinois, and a University Fellowship from The Ohio State University.

VITA

May 1, 1982	Born – Toledo, Ohio
2005	B.S. Civil Engineering, The Ohio State University, Columbus, Ohio
2005 – 2006	University Fellow, The Ohio State University, Columbus, Ohio

PUBLICATIONS

Research Publications

1. Fox, P. J., Morrison, T. C., Nye, C. J., Hunter, J. G., and Olsta, J. T. (2005). "Current Research on Dynamic Shear Behavior of Needle-Punched Geosynthetic Clay Liners," *Proceedings, Geosynthetics '05,* North American Geosynthetics Society, Las Vegas (CD-Rom).

2. Fox, P. J., Nye, C. J., Morrison, T. C., Hunter, J. G. and Olsta, J. T. (2006) "Large Dynamic Direct Shear Machine for Geosynthetic Clay Liners," *Geotechnical Testing Journal*, Vol. 29, No. 5, in press.

3. Nye, C.J. and Fox, P.F. (2006). "Dynamic Shear Behavior of a Needle-Punched Geosynthetic Clay Liner," *Journal of Geotechnical and Geoenvironmental Engineering*, in review.

FIELDS OF STUDY

Major Field: Civil Engineering

Specialization: Geotechnical Engineering

TABLE OF CONTENTS

LIST OF TABLES

LIST OF FIGURES

CHAPTER 1

INTRODUCTION

Since the inception of the Resource Conservation and Recovery Act, modern solid waste landfills in the United States are required to incorporate a liner system that will encapsulate waste materials and prevent migration of leachate and gases into the surrounding ecosystem. Over the past thirty years, designers have increasingly used specialized geosynthetics to comprise the multiple layers of these liner systems. A typical cross section of a liner prior to the widespread availability of geosynthetics is shown in Figure 1.1a, and a contemporary liner cross section is depicted in Figure 1.1b. Note that the sand filter layer has been replaced by thin geotextiles, geonets and geocomposite drains. Similarly, the hydraulic barriers constructed with compacted clay in the past are being replaced by geomembranes (GMs) and geosynthetic clay liners (GCLs).

With the increasing use of geosynthetics in landfill liner systems, interface shear strength behavior of these materials is very important for stability analysis. This is especially true since landfills are typically constructed with sloping sides in order to maximize internal volume. These side slopes introduce several modes of stability failure, two of which are illustrated in Figure 1.2. The rotational failure surface shown in Figure

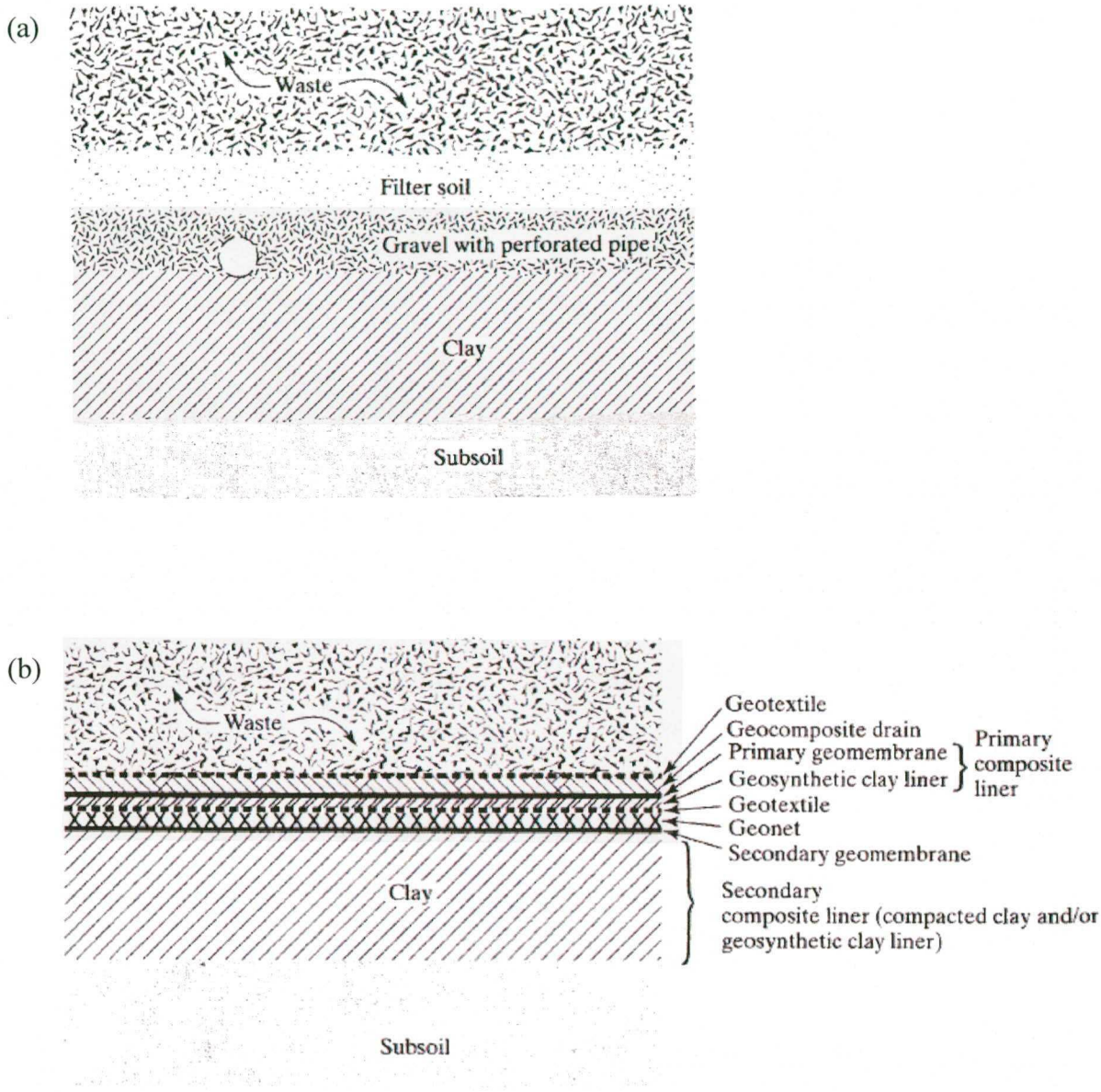

Figure 1.1: Typical landfill liner cross-section (a) prior to use of geosynthetics and (b) after widespread availability of geosynthetics (Koerner 2005).

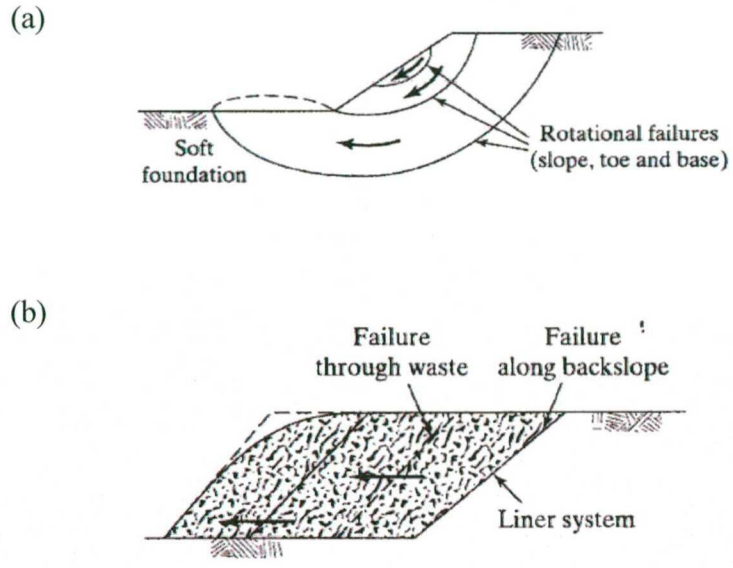

Figure 1.2: Modes of stability failure typical for landfills: (a) rotational and (b) translational (Qian et al. 2002).

1.2a will be controlled by the shear properties of the solid waste since the majority of the failure surface passes through the waste. This type of failure can be classified as a slope, toe or base failure depending on the depth of the slip surface and location at which the slip surface daylights. The translational failure surface depicted in Figure 1.2b will be controlled by the internal or interface shear strength of the various geosynthetic and natural material layers within the liner system.

The interface shear behavior of geosynthetics has been shown to be frictional in nature and the failure envelope for these materials is often nonlinear over a wide range of normal stress (Gilbert et al. 1996 Chiu and Fox 2004). However across a narrow normal stress range, a simplified linear envelope is often employed. This linear relationship, known as the Mohr-Coulomb failure criterion, is characterized by two parameters,

friction angle, ϕ, and cohesion intercept, c. Accurate determination of these parameters is vital to high quality, economical engineering design practices. At present, a vast literature is available on the static interface shear behavior of many geosynthetics used in landfill liners, including geomembranes, geotextiles, geogrids, and GCLs. This data is useful for design under static conditions, where gravity comprises the dominant driving force in stability calculations. However for dynamic loading conditions, such as the lateral displacements that occur during an earthquake, the literature is much less complete for behavior of these interfaces. In the case of geosynthetic clay liners, the available data is very limited and there is a significant need for such information (Fox and Stark 2004).

Geosynthetic clay liners are hydraulic barriers comprised of a thin layer of bentonite clay supported by one or more layers of geosynthetic material. GCLs can be subdivided into unreinforced and reinforced products. Unreinforced GCLs have no geosynthetic reinforcing that spans the bentonite layer and therefore the shear behavior is controlled by the bentonite clay. An example of this type of GCL is the Claymax 200R product manufactured by CETCO (Arlington Heights, IL, USA). This product contains bentonite adhesively bonded to an upper and a lower woven geotextile. Unreinforced GCLs can also be geomembrane supported, such as Gundseal, manufactured by Gundle/SLT Environmental, Inc. (Houston, TX, USA). In this case, the bentonite is adhered to one side of either a smooth or textured geomembrane. Reinforced GCLs use needle-punched or stitched geosynthetic reinforcement to transfer shear forces across the weak bentonite layer. Needle-punching draws fibers from the nonwoven geotextile and locks them into the other geotextile (either woven or nonwoven) in such a way that a random web of reinforcement is created. An example of this type of product is Bentomat

ST, manufactured by CETCO (Arlington Heights, IL, USA). In the stitch-bonding process, lines of stitching run in the machine direction and fasten the upper and lower geotextiles together allowing shear forces to be transmitted across the bentonite layer. NaBento manufactured by HUESKER Synthetic GmbH (Gescher, Germany) is an example of this type of product. A schematic diagram of each GCL type is provided in Figure 1.3.

Since compacted clay liners (CCLs) have been used extensively in the past, it is prudent to compare the relative quality of GCLs as a replacement material. Koerner (2005) and Qian et al. (2002) provide a complete discussion, with some of the advantages of GCLs being:

- a consistent and uniform low hydraulic conductivity (10^{-8} to 10^{-10} cm/s),
- the typical thickness is 0.6 – 2.0% of that for CCLs, resulting in additional landfill space for waste,
- the construction process is rapid and simple, with decreased environmental impact,
- less susceptibility to desiccation, freeze/thaw and shrink/swell damage,
- and on-site clay materials are not required for construction.

On the other hand, there are some advantages to CCLs as compared to GCLs:

- high number of experienced CCL contractors due to the large history of use,
- increased puncture resistance due to its larger thickness,
- increased capacity for leachate absorption,
- on-site materials may be used, which decreases the cost of removal.

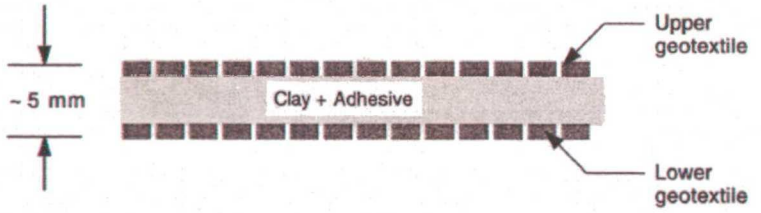

(a) Unreinforced GCL with adhesive-bound clay between upper and lower geotextiles,

(b) Unreinforced GCL with adhesive-bound clay to a geomembrane,

(c) Reinforced GCL with needle-punched clay through upper and lower geotextiles,

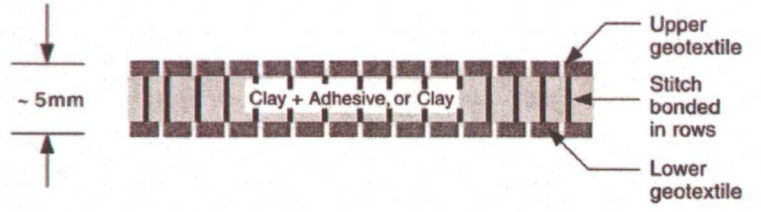

(d) Reinforced GCL with stitch-bonded clay through upper and lower geotextiles.

Figure 1.3: Illustration of GCL product types (Koerner 2005).

Quality control measures during construction are equally important for both CCLs and GCLs. With proper design, either can produce an adequate liner material, but GCLs have become increasingly popular over the last 15 years due to their many advantages.

The shear behavior of unreinforced GCLs is equal to that of the bentonite clay, which has one of the lowest friction angles of any naturally occurring material when hydrated, with typical values of 3-5° (Mesri and Olson 1970). Due to this low shear strength, these products are limited to applications on very shallow slopes (Stark et al. 1998), which means they are not well suited for use in landfill liners. One exception is the encapsulated GCL consisting of GM/bentonite/GM in which the bentonite essentially remains dry throughout the design life of the facility. For hydrated conditions, it is therefore most common to specify needle-punched or stitch-bonded GCLs, in conjunction with other geosynthetics, to comprise the liner system. If the weakest shear plane within the liner involves a reinforced GCL, there are two mechanisms of failure that may occur. At low normal stress, an interface shear failure is more likely where the plane of sliding is located at the interface of the GCL and an adjacent geosynthetic or natural material. At high normal stress, the shear resistance along the interface is typically sufficient such that the reinforcement is ruptured and sliding occurs within the GCL, termed an internal failure. Studies have shown that such displacement occurs at the interface of the bentonite and one of the supporting geotextiles, not within the bentonite layer (Fox et al. 1998, Zornberg et al. 2005).

Significant research has been performed on the internal shear behavior of geosynthetic clay liners, which is typically accomplished using a direct shear device. Figure 1.4 illustrates the general stress-strain behavior for the monotonic internal shear of

a reinforced GCL. The resistance to shearing increases rapidly at the onset of displacement until reaching a peak stress, typically at a displacement less than 50 mm (Fox and Stark 2004). In general, needle-punched products exhibit higher peak strengths than stitch-bonded, and both are higher than unreinforced GCLs (Fox et al. 1998, Zornberg et al. 2005). A post-peak strength reduction effect is present as additional displacement occurs, the reinforcement is ruptured, and clay particles are reoriented along the failure surface. At large displacement, a steady-state or residual condition is achieved. Since the reinforcement no longer contributes to the shearing resistance, the residual condition is equivalent to the behavior of the bentonite. The peak and residual shear stress values increase as normal stress increases, but the peak stress is influenced to a much higher extent. Once stress-strain plots are obtained for several normal stresses, a failure envelope can be constructed utilizing the Mohr-Coulomb failure parameters, ϕ and c.

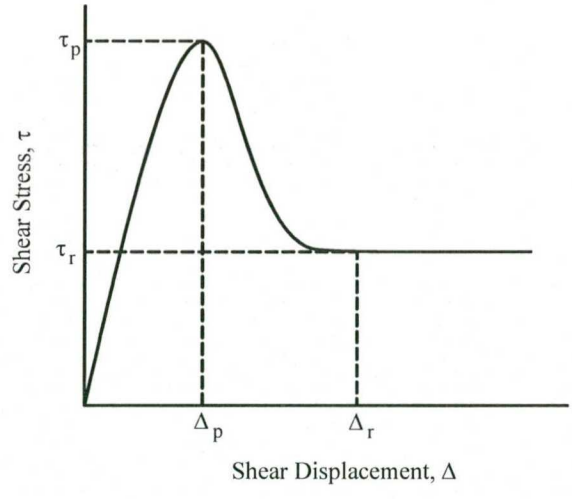

Figure 1.4: Typical GCL shear stress-shear displacement curve (Fox and Stark 2004).

During an earthquake, dynamic movement is experienced at ground level that does not mimic the static testing conditions described above; therefore it is necessary to perform testing that will simulate such a loading condition in order to determine the material response. However, relatively little data is available on the dynamic shear behavior of geosynthetic liner systems. For example, Lai et al. (1998), Lo Grasso et al. (2002) and Kim et al. (2005) have presented the only information concerning the effect of dynamic loading on GCLs. Both of these studies were conducted on small specimens at low normal stress and frequency. A complete discussion of these works is provided in Chapter 2.

A large direct shear machine has been developed at Ohio State University to obtain quality data on the dynamic shear behavior of geosynthetic clay liners and GCL liner systems (Fox et al. 2006). This machine incorporates many of the improved design features discussed by Fox et al. (1997), such as large specimen size, large displacement capability, large range of displacement rate, an improved specimen gripping system, negligible machine friction, and continuous measurement of specimen volume change. The main feature of this new machine is the capability to apply dynamic displacement-controlled and stress-controlled loading to the specimen. It also has the ability to test at a maximum normal stress of 2000 kPa, which simulates landfills approaching 150 m in height. The objective of this research is to investigate the internal shear behavior of a needle-punched geosynthetic clay liner at a single normal stress. Monotonic shear tests were conducted for displacement rates of 0.1 to 30,000 mm/min. Cyclic load tests were then performed to investigate the effect of displacement amplitude, number of cycles, input frequency, and loading waveform. From this data, the general shear behavior of a

needle-punched GCL is discussed, and the analysis produced curves for shear stiffness reduction and damping ratio, which are the first of their kind for any GCL product.

This thesis is divided into five chapters. Chapter 2 presents a literature review on the methods used to test the shear response of geosynthetics, the static shear behavior of GCLs, and the dynamic behavior of clays, geosynthetics and GCLs. A description of the machine and its capabilities is provided in Chapter 3. Chapter 4 presents testing procedures used in this study, all testing results and a discussion of the data significance. Finally, Chapter 5 provides conclusions and recommendations for future work.

CHAPTER 2

BACKGROUND AND PREVIOUS RESEARCH

2.1 Introduction

The assessment of geosynthetic and geosynthetic interface shear behavior under dynamic loading is important for the design of liner systems in seismically active regions. Significant research has been performed on the shear characteristics of these materials when subjected to both static and dynamic loading. This chapter provides 1) a review of the testing devices commonly used for laboratory shear testing of geosynthetics and some of the advantages and disadvantages of each method, 2) a discussion of the static shear behavior of geosynthetic clay liners (GCLs) along with factors that influence the response, 3) a review of the dynamic shear behavior of geosynthetics, including GCLs, and 4) a brief discussion of the dynamic shear behavior of clays.

2.2 Testing Devices

The laboratory measurement of geosynthetic shear strength is difficult due to the variability of the material, possible anisotropy, material extensibility, influence of normal stress, presence of machine friction and many other factors. Several testing devices have been developed to measure the internal and interface shear strength of geosynthetics

under both static and dynamic loading conditions. Some of the more common devices are discussed in this section along with important advantages and disadvantages of each.

2.2.1 Tilt Table

The tilt table apparatus provides a simple method for measuring shear behavior of geosynthetics, and is more commonly used in Europe than the United States. Ling et al. (2002), Narejo (2003) and Lalarakotoson et al. (1999) provide examples of this type of test procedure, an illustration of which is shown in Figure 2.1. The concept of this device is that one geosynthetic is attached to a rigid, tilting plate with a second geosynthetic or natural material placed on top. Dead load is added and the table is gradually tilted, typically at a constant angular rate, until slippage along the interface is observed. Lalarakotoson et al. utilized instrumentation to record relative displacement along the interface, while other researchers visually observed such movement. The angle of inclination that causes slip displacement is measured and standard equilibrium equations are implemented to determine the frictional resistance of the interface. Briancon et al. (2002) used force transducers to aid in this calculation and also enabled their apparatus to test submerged interfaces.

An inclined plane or tilt table has the advantage that large specimens (often up to a meter or more) can be tested, shearing occurs in a single direction which directly simulates field conditions, and shearing is generally uniform across the interface which minimizes progressive failure effects. However, this testing device is severely limited in that it tests under low normal stresses since dead weights are utilized, shearing is force controlled (i.e., gravity) so stress-controlled tests are unfeasible, and no information on

post-peak response is typically obtained since data collection ceases with initial displacements.

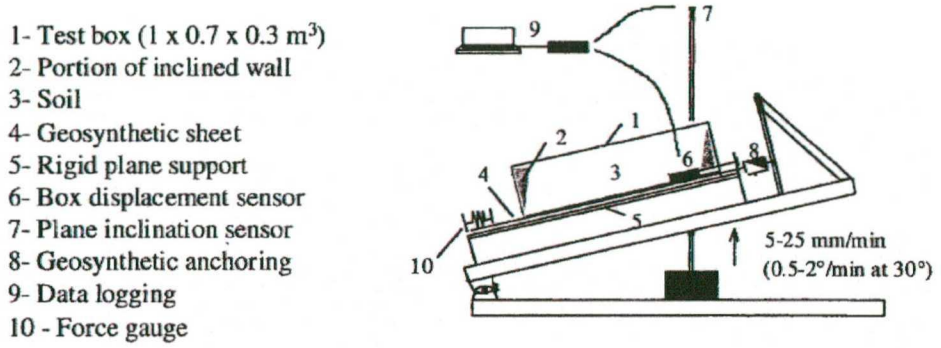

Figure 2.1: Illustration of a typical tilt table device (Lalarakotoson et al. 1999).

2.2.2 Direct Shear

The primary method of measuring internal and interface shear strength of GCLs has been using direct shear devices. Figure 2.2 shows a schematic of a simple direct shear machine. In this configuration, the geosynthetic specimen is placed in a shear box that permits translation of either the upper or lower container with respect to the other. Normal stress is applied using various methods, including dead weight (Martin et al. 1984), air pressure (Triplett and Fox 2001) or pneumatic devices (Gilbert et al. 1995), and shear resistance is typically measured using proving rings (Martin et al. 1984) or load cells (Triplett and Fox 2001). This testing method has been standardized for both geosynthetics (ASTM D 5321) and GCLs (ASTM D 6243). These standards require a minimum specimen size of 300 x 300 mm in order to lessen the impact of edge effects, that the device be capable of applying a constant rate of horizontal displacement (strain controlled) or horizontal stress (stress controlled), and that precise normal stress be

maintained during testing. In the case of GCLs, the specimen must have access to water to allow for proper hydration.

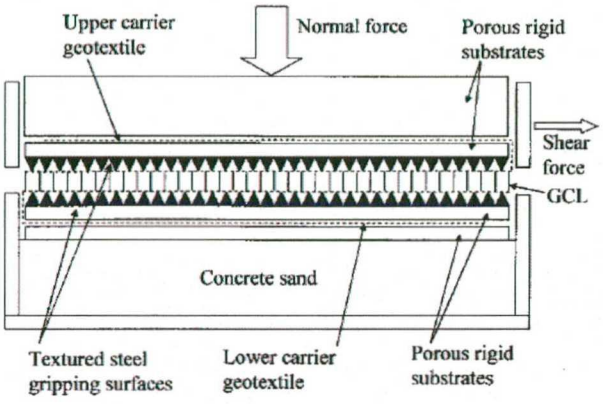

Figure 2.2: Illustration of a typical direct shear device (Zornberg et al. 2005).

The advantages of using a direct shear device are similar to those of the tilt table. Shearing occurs in one direction, which closely imitates field behavior, specimens can be relatively large depending on the machine capabilities, and shearing is relatively uniform over the surface. The primary disadvantage of the standard direct shear method is that maximum displacement of most devices which use 300 x 300 mm test samples are insufficient to measure residual conditions of most GCL and geosynthetic interfaces (Gilbert et al. 1996; Fox and Stark 2004). This problem can be avoided by using a shearing block that moves across a longer stationary half, which allows the shearing area to remain constant during the test, however this raises some concern since previously unconsolidated and unsheared material moves into the failure surface. Another disadvantage of the direct shear device is that a specimen gripping surface is required to

transmit shear forces to the geosynthetics. Fox et al. (1997) showed that the quality of the test data is highly dependent on the effectiveness of the gripping system for the internal shear of a needle-punched GCL. In some cases, end clamping is employed to ensure that failure will occur at the desired geosynthetic interface, however this can distress the geosynthetics and produce an uneven shear distribution across the failure plane, termed progressive failure. While such distress may be present in field conditions, it creates uncertainty in accurately determining material response.

2.2.3 Torsional Ring Shear

The primary advantage of the torsional ring shear device, shown in Figure 2.3, is that continuous unlimited shear displacements are capable, which allow for measurement of true residual strengths (Stark and Eid 1996; Eid and Stark 1997; Hillman and Stark 2001). This may require more than a meter of displacement in some cases (Stark and Poeppel 1994). The torsional ring shear device utilizes circular specimens set against one another with a stationary shaft passing through the center. Normal stress is applied and the specimens are rotated about the shaft while measurements of applied torque and cumulative displacement are recorded. Since the specimens are circular, the shearing surface is constant during testing which eliminates area correction factors from analysis calculations. However, because shearing occurs on an annular surface, the displacement rate and hence cumulative displacement is not equal across the specimen. In other words, at any given angular displacement, the material at the outer diameter has moved farther than the material at the inner diameter. This results in an uneven stress distribution

across the interface and progressive failure effects must be considered, which may be significant if the geosynthetic exhibits significant anisotropy (Gilbert et al. 1995).

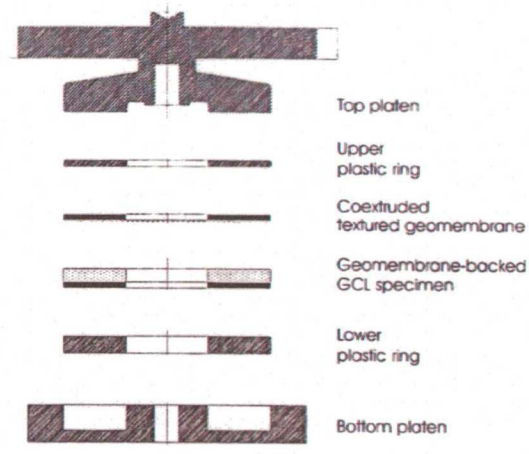

Figure 2.3: Schematic of a typical torsional ring shear device (Eid and Stark 1997).

2.2.4 Shake Table

Measurement of dynamic interface shear behavior of geosynthetics is not possible with the testing devices discussed above because dynamic (either cyclic or seismic) loading cannot be produced. An exception to this is the direct shear device provided that the loading mechanism is capable of applying bi-directional displacements. Regardless, the predominant device used by researchers to investigate the dynamic shear behavior of geosynthetics has been the shake table. Illustrated in Figure 2.4, this device consists of a table upon which one geosynthetic is attached. Typically, an actuator is fastened to the table which permits cyclic loading (Yegian and Lahlaf 1992; Kim et al. 2005) and sometimes application of an earthquake time-history (Yegian and Kadakal 1998; Yegian

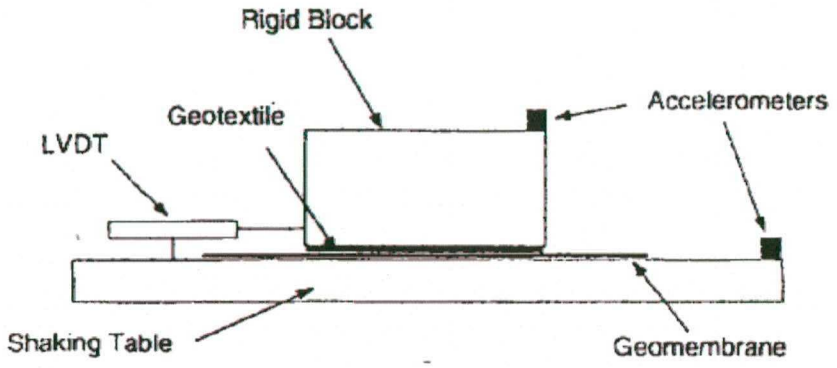

Figure 2.4: Schematic of a typical shake table device (Yegian et al. 1998).

et al. 1995). A separate block with a second geosynthetic attached to it is smaller than and rests on top of the table. This block can be in either a fixed or free configuration. In the fixed block method, the block is rigidly fixed to prevent movement when excitations are applied to the underlying table and load cells are used to measure the shear forces transmitted across the interface. Yegian and Kadakal (1998) and Kim et al. (2005) both used this type of setup. The second configuration is the free block, where the upper block is not rigidly fixed but simply rests on the shaking table. Displacement transducers and accelerometers are utilized to measure relative displacement between the upper and lower geotextiles. This setup was used by De and Zimmie (1998) and Yegian and Harb (1995), among others.

Shake tables are useful for measurement of dynamic interface shear behavior since large specimens can be tested, however some limitations exist. This apparatus is limited to low normal stress since dead weight is typically used. While this accurately models a cover system where low overburden is expected, proper application of stresses expected on a bottom liner system are unattainable. Another limitation of the shake table

is that unconsolidated and unsheared material becomes part of the failure plane as relative displacement occurs between the table and the block, which introduces uncertainty into the measurements. Also, while the fixed block method allows for measurement of post-peak response, the free block method implicitly assumes a rigid-plastic material response and therefore only provides peak shear behavior. Regardless of these limitations, the use of shake tables has greatly contributed to the current knowledge of the dynamic interface shear behavior of geosynthetics.

2.2.5 Geotechnical Centrifuge

Due to the normal stress limitation encountered with shake tables, researchers have resorted to geotechnical centrifuges to accurately model the stresses expected for a bottom liner system. A centrifuge subjects the model test specimens to centripetal accelerations that are greater than gravity (Viswanadham and Jessberger 2005). Since the mass of the material remains constant while the acceleration increases, the applied force increases proportionally. Researchers place shaking tables inside the centrifuge and conduct dynamic loading tests while subjecting them to this increased normal stress. The most important consideration for a geotechnical centrifuge is that all model dimensions and test parameters must be scaled properly according to prototype conditions (De and Zimmie 1998; Viswanadham and Jessberger 2005). Although a detailed discussion of scaling laws are beyond the scope of this report, the importance of this topic is noted. Centrifuges have enabled dynamic geosynthetic behavior to be observed at normal stress levels greater than those used with shake tables.

2.3 Static Shear Characteristics of Geosynthetic Clay Liners

Geosynthetic clay liners are hydraulic barriers consisting of a thin layer of bentonite clay supported between one or more layers of geosynthetic material. GCLs can be divided into reinforced and unreinforced products, as discussed in Chapter 1. Since the shear behavior of an unreinforced GCL is controlled by the shear characteristics of the bentonite clay, which is one of the weakest natural materials (Mesri and Olson 1970), manufactures began incorporating geosynthetic reinforcement to increase the internal shear strength. Currently, reinforced GCLs are available as needle-punched or stitch-bonded products, where the reinforcing fibers pass through the clay layer to transmit shear force between the geotextiles. The needle-punching process pulls fibers from the nonwoven geotextile through the bentonite layer and locks them into the other (woven or nonwoven) geotextile creating a random web of reinforcing. The stitch-bonding process creates lines of stitching parallel to the machine direction and fastens the upper and lower geotextiles together. The reinforcement has a profound effect on the shear characteristics of the GCL, as discussed below. Also discussed are considerations for laboratory measurement of shear strength.

2.3.1 Internal Shear Behavior

Fox et al. (1998) performed static internal shear tests on three geosynthetic clay liners: a geomembrane-supported unreinforced GCL (GCL-1), a stitch-bonded GCL (GCL-2) and a needle-punched GCL (GCL-3). All specimens were hydrated prior to testing and sheared on a large direct shear machine. The stress-displacement curves for these three products are shown in Figure 2.5. The behavior is characterized by a sharp

increase in shear stress at small displacement until a peak shear resistance is achieved. The shear resistance then decreases markedly with further displacement until a residual value is obtained. The unreinforced GCL exhibits the weakest peak strength while the needle-punched GCL exhibits the largest. The displacement required to achieve peak strength is smallest for GCL-1 (1.4 mm) and larger for GCL-2 (39.7 mm) and GCL-3 (22.9 mm). The initial response (< 1 mm) of all three products was identical, as shown in the detail portion in Figure 2.5. Interestingly, all three specimens have similar residual strengths, which indicates that the reinforcement does not contribute to large-displacement behavior. Chiu and Fox (2004) and Zornberg et al. (2005) also observed this phenomenon.

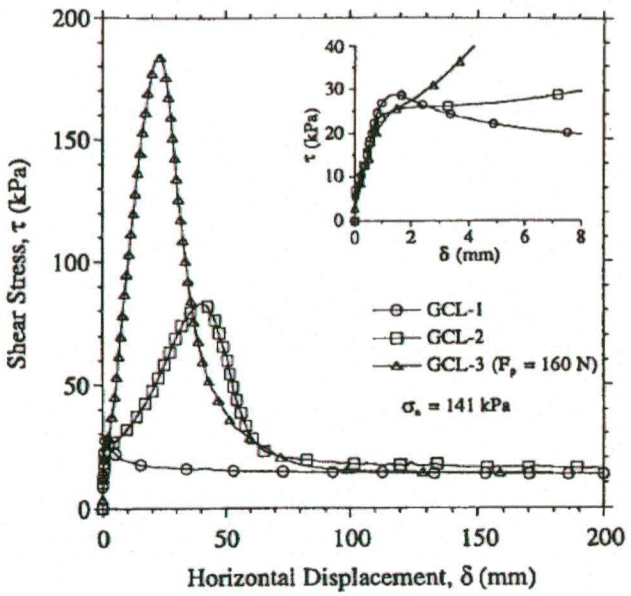

Figure 2.5: Stress-displacement curves for an unreinforced (GCL-1), a stitch-bonded (GCL-2), and a needle-punched (GCL-3) geosynthetic clay liner (Fox et al. 1998).

Figure 2.6 shows the peak and residual failure envelopes for the internal shear of these three GCLs. Both linear and nonlinear envelopes are included and Table 2.1 lists the linear Mohr-Coulomb failure parameters; the nonlinear failure parameters are provided in Fox et al. (1998). The 4.4° residual friction angle for the GCLs is in good agreement with the 4.0° value obtained from ring shear tests on sodium montmorillonite (Müller-Vonmoos and Løken 1989). Note that increasing normal stress results in increased peak and residual strengths, which illustrates the frictional nature of the response. In addition, the importance of the reinforcement can be assessed by considering the y-intercept of each failure envelope. This value is very low for the unreinforced product, which is in fact a cohesive characteristic of the bentonite, and is higher for the reinforced GCLs, which reflects the effect of the reinforcement (Qian et al. 2002). The peel strength, F_p, of a needle-punched GCL is the force required to separate the geotextiles (ASTM D 6496), thus it provides a measure of the inherent strength of the reinforcement. Figure 2.6 indicates that the peel strength also has an effect on the response of the needle-punched GCL, where a higher F_p results in higher peak shear resistance. Eid et al. (1999) also noted that increased peak strength resulted with increasing peel strength after comparing test results from torsional ring shear tests to other literature values. However, Zornberg et al. (2005) compiled a large database of commercially-performed internal shear tests and concluded that peel strength had no significant effect on measured peak shear resistance. Final water content data of the hydrated bentonite is also provided in Figure 2.6, which shows that the post-shearing water content decreases nonlinearly with increasing normal stress. The effect of water content on shearing behavior is discussed later in this section.

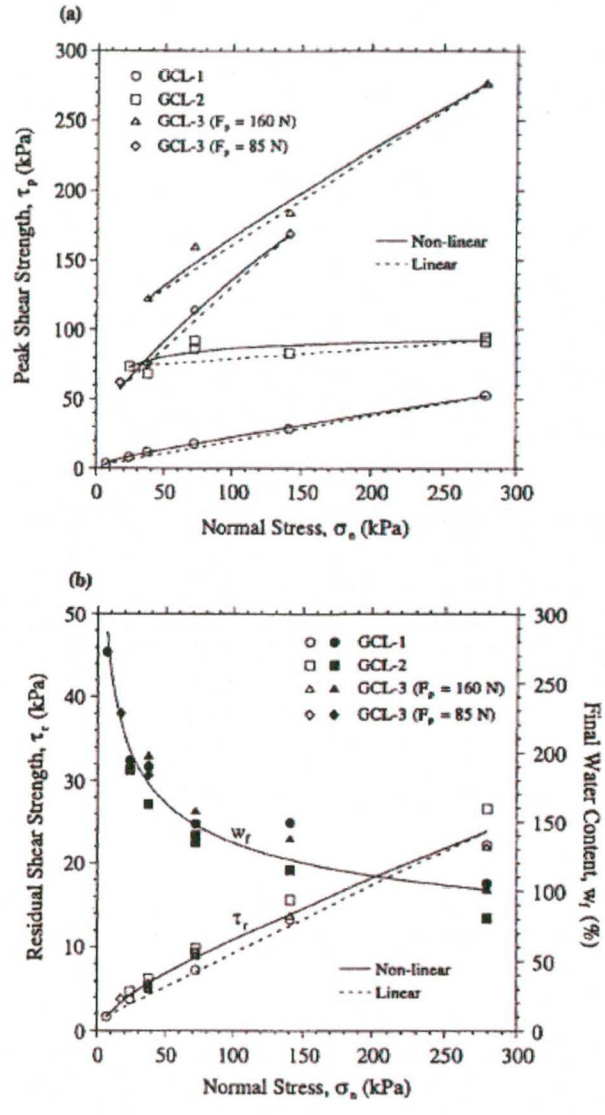

Figure 2.6: Failure envelopes for (a) peak and (b) residual strength of an unreinforced (GCL-1), a stitch-bonded (GCL-2), and a needle-punched (GCL-3) geosynthetic clay liner (Fox et al. 1998).

GCL type	Normal stress range (kPa)	Mohr-Coulomb strength parameters	
		c (kPa)	ϕ (°)
Unreinforced	7 - 279	2.4	10.2
Stitch-bonded	24 - 279	71.6	4.3
Needle-punched (F_p = 160 N)	38 - 279	98.2	32.6
Needle-punched (F_p = 85 N)	17 - 141	42.3	41.9

Table 2.1: Peak shear strength parameters for three GCL products (Fox et al. 1998).

2.3.2 Interface Shear Behavior

The primary interface of interest for geosynthetic clay liners is the GM/GCL interface. This interface is commonly encountered due to the composite liner concept that utilizes two hydraulic barriers to dramatically reduce flow through the system (Koerner 2005). Eid and Stark (1997) performed interface torsional ring shear tests on a geomembrane-supported unreinforced GCL with 1) a smooth geomembrane (GMS) and 2) a textured geomembrane (GMX). These tests were conducted under dry and hydrated conditions, where the dry condition refers to the as-received GCL water content (10-15%), at a displacement rate of 0.015 mm/min. Figure 2.7 shows normalized stress-displacement curves for the dry condition under two different normal stresses. This curve is similar in shape to that for internal shear of GCLs in that a peak resistance is reached and then a post-peak reduction occurs, ultimately leading to a residual condition. At higher normal stresses, failure occurred within the adhesive and resulting slip displacements took place at the smooth, supporting geomembrane/bentonite interface

rather than at the unreinforced GCL/GMX interface. Figure 2.8 shows peak and residual failure envelopes for the unreinforced GCL/GMS and unreinforced GCL/GMX interfaces. Note that in both cases beyond a limiting normal stress, failure of the adhesive occurred which resulted in a decreased residual interface friction angle. Table 2.2 lists shear strength values for these tests, along with interfaces tested by other researchers. Interface shear strength parameters are characterized by peak and large displacement adhesion intercepts (a_p, a_{ld}) and interface friction angles (Δ_p, Δ_{ld}).

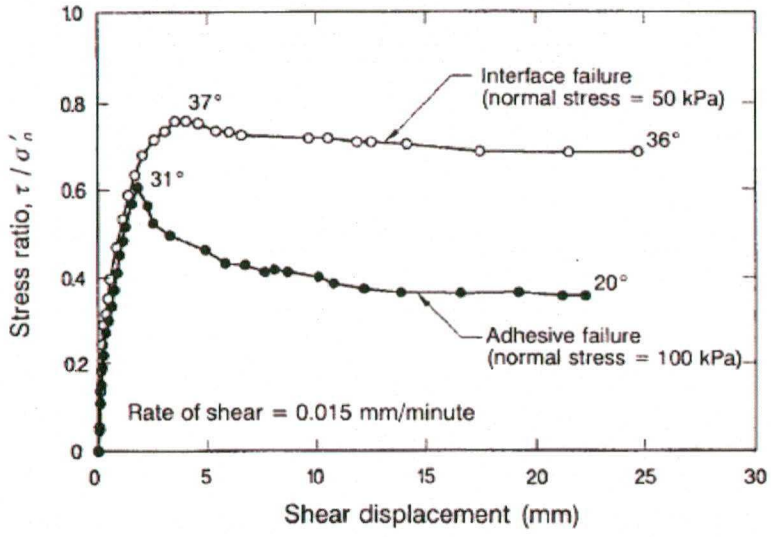

Figure 2.7: Stress-displacement curves for a dry smooth geomembrane-supported GCL/textured geomembrane interface (Eid and Stark 1997).

(a)

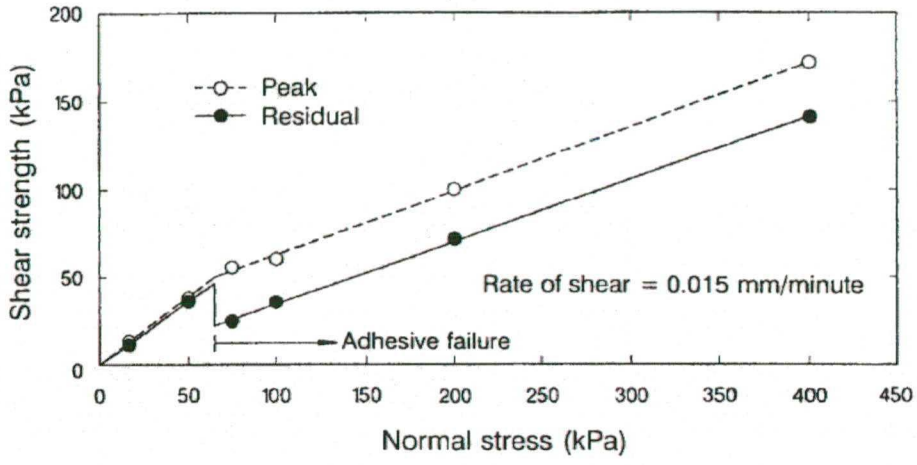

(b)

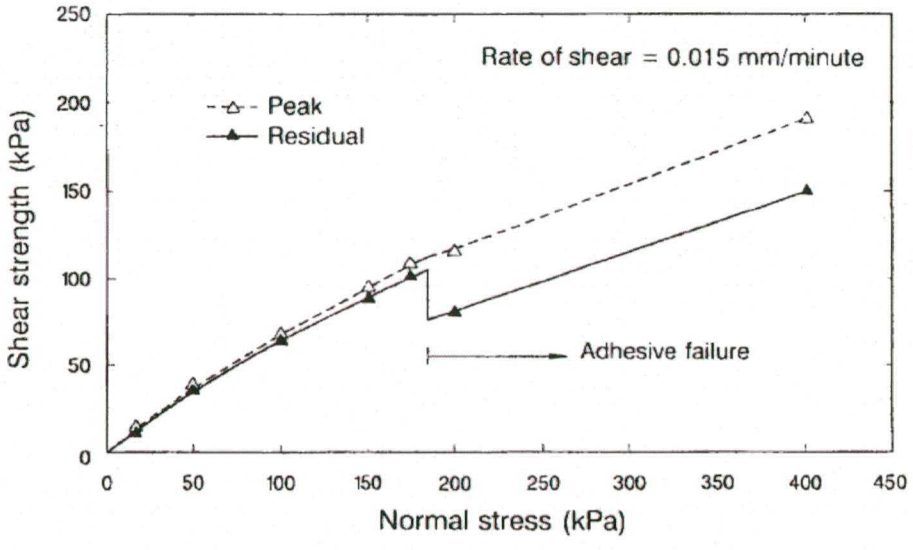

Figure 2.8: Peak and residual failure envelopes from interface shear tests between (a) dry smooth geomembrane-supported GCL and (b) dry textured geomembrane-supported GCL with a textured geomembrane (Eid and Stark 1997).

Reference	GCL	Interface Geosynthetic	GCL Hydration	Displacement Rate	Maximum Displacement (mm)	Peak Strength			Large Displacement Strength		
						Normal Stress (kPa)	a_p (kPa)	Δ_p (°)	Normal Stress (kPa)	a_{ld} (kPa)	Δ_{ld} (°)
Gilbert et al. (1996)	NP (woven)	GMS	hydrated	0.5 mm/min	43	3.45 - 69.0	0	8.4	3.45 - 69.0	0	8.1
	NP (nonwoven)	drainage geocomposite	hydrated	0.5 mm/min	43	3.45 - 69.0	0.4	23	3.45 - 69.0	0	22
Eid and Stark (1997)	Unreinforced, GM-supported	GMS	dry	0.015 mm/min	70	0 - 70	0	37	0 - 70	0	36
						70 - 400	0	31	70 - 400	0	20
	Unreinforced, GM-supported	GMX	dry	0.015 mm/min	70	0 - 180	0	39	0 - 180	0	30
						180 - 400	0	24	180 - 400	0	22
	Unreinforced, GM-supported	GMX	hydrated	0.015 mm/min	30	0 - 400	0	19	0 - 400	0	10
Triplett and Fox (2001)	NP (woven)	GMS	hydrated	0.1 mm/min	203	6.9 - 486	0.3	9.8	6.9 - 127	0.3	8.1
									127 - 486	3.0	6.9
	NP (woven)	GMX (LM)	hydrated	0.1 mm/min	203	6.9 - 124	2.2	21.6	6.9 - 134	1.0	12.7
						124 - 486	22.0	13.3	134 - 486	15.7	6.6
	NP (woven)	GMX (CX)	hydrated	0.1 mm/min	203	6.9 - 279	0	23.7	6.9 - 71.9	0	15.0
									71.9 - 279	4.9	11.3
	NP (nonwoven)	GMS	hydrated	0.1 mm/min	203	6.9 - 486	0.4	9.9	6.9 - 127	0.6	9.2
									127 - 486	5.8	6.9
	NP (nonwoven)	GMX (LM)	hydrated	0.1 mm/min	203	6.9 - 279	7.4	31.7	6.9 - 69.6	2.3	18.5
									69.6 - 279	11.8	11.2
	NP (nonwoven)	GMX (CX)	hydrated	0.1 mm/min	203	6.9 - 279	7.2	28.3	6.9 - 135	3.4	14.4
									135 - 279	16.0	9.3

Table 2.2: Summary of shear strength parameters for static shear of GCL interfaces.

Extensive interface shear testing has also been conducted using reinforced GCLs, however the discussion herein will concentrate on needle-punched products. Triplett and Fox (2001) conducted large-scale (406 x 1067 mm) direct shear tests on smooth and textured geomembrane interfaces with a woven/nonwoven NP GCL at a shearing rate of 0.1 mm/min. The testing program investigated laminated (LM) versus coextruded (CX) geomembranes and woven (W) versus nonwoven (NW) geotextile interfaces. The stress-displacement curves for the six interfaces, Figure 2.9, show again peak strengths at small shear displacements and pronounced post-peak strength reduction. The peak strength for the GCL/GMS interface is considerably less than that for the GCL/GMX interface and is not significantly influenced by the geotextile type (woven versus nonwoven). In addition, displacement required to achieve both peak and residual strengths is also considerably less for the smooth geomembrane interface. The laminated geomembrane exhibits stronger peak strength than the coextruded geomembrane, and both textured products display greater peak strength when sheared against the nonwoven geotextile. The maximum displacement of the Triplett and Fox testing device (203 mm) was not sufficient to induce residual shear behavior at all normal stresses for the textured geomembrane interfaces, therefore these are termed large displacement strengths. The effect of the geotextile type for the textured geomembrane interfaces was less pronounced for large displacement behavior than for peak behavior.

Figure 2.10 shows peak and large displacement shear strength envelopes for the six interfaces (Table 2.2 provides strength parameters for these interfaces) and also includes the internal GCL shear strength envelopes from Fox et al. (1998) for comparison. The same GCL product was used by both studies, however the peel strength

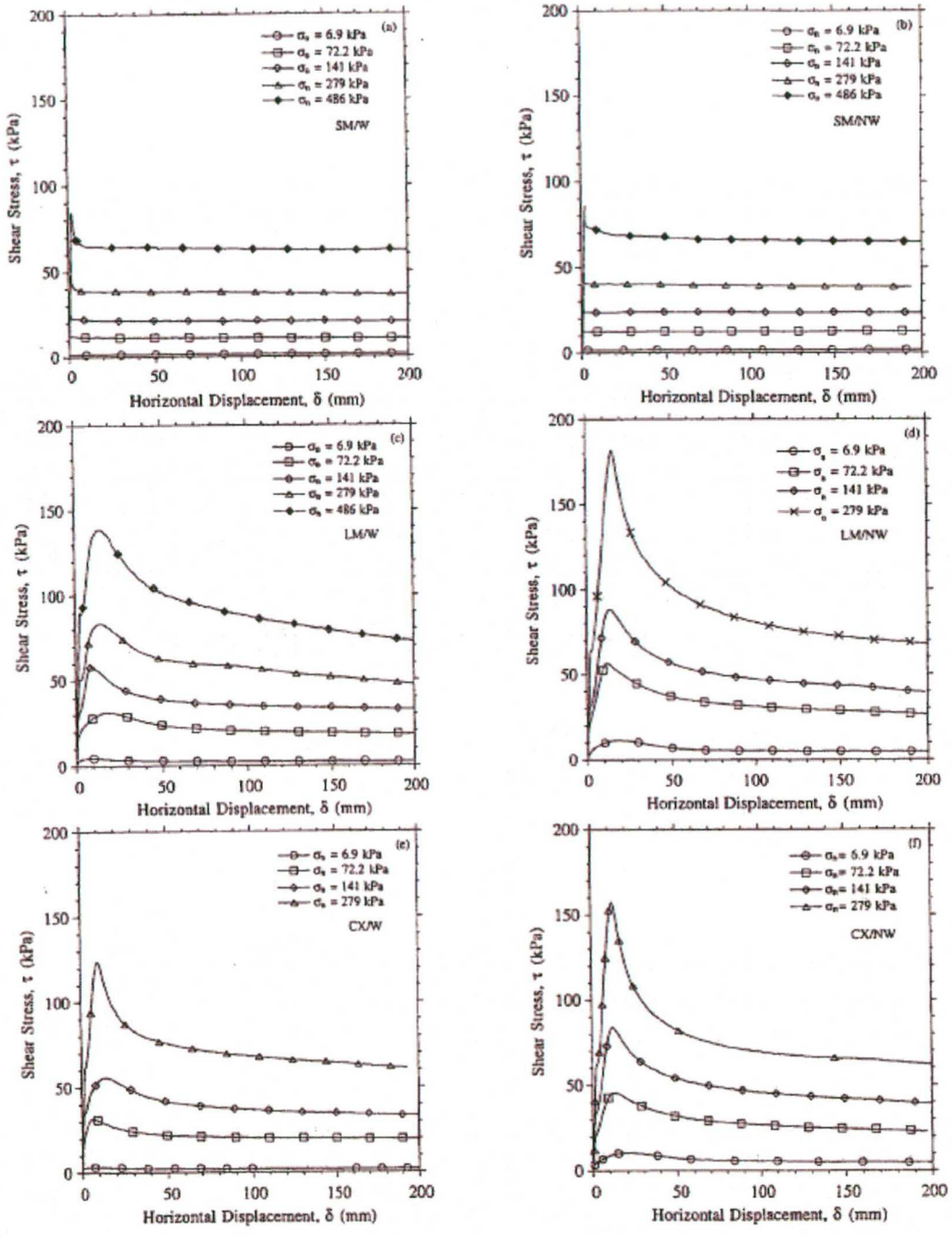

Figure 2.9: Stress-displacement curves for interface shear of a NP GCL with both a textured and smooth geomembrane (Triplett and Fox 2001).

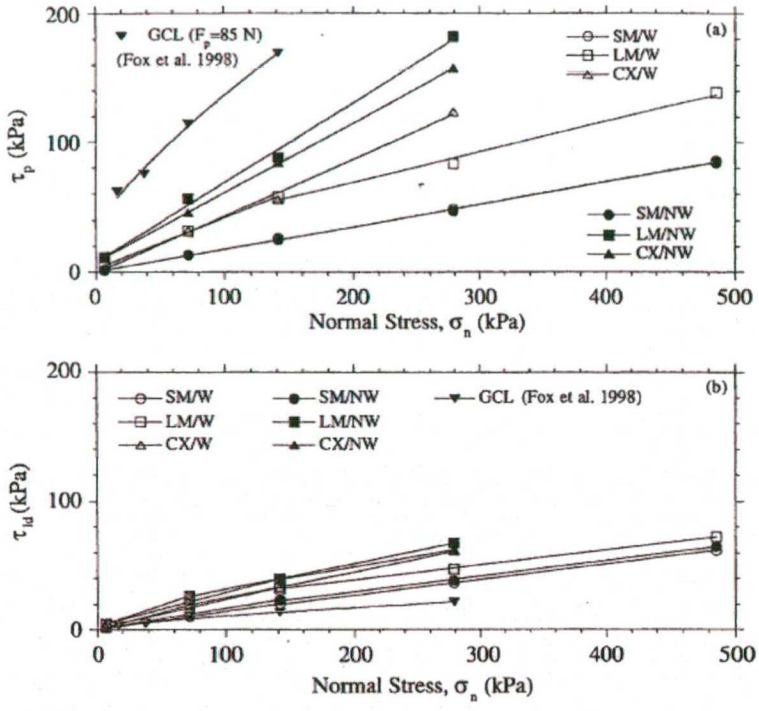

Figure 2.10: Failure envelopes for (a) peak and (b) large displacement shear strengths of a NP GCL against a smooth and a textured geomembrane (Triplett and Fox 2001).

for the Fox et al. study (85 N) was less than that for Triplett and Fox (94 N). Peel strength has been shown to be an indicator of peak shear strength, with higher peel strength resulting in higher peak strength, but to have no effect on residual strength (Fox et al. 1998; Eid et al. 1999). Thus, the peak internal failure envelope for the Triplett and Fox study is expected to be greater than that shown in Figure 2.10a and the residual internal shear strength envelope equal to that shown in Figure 2.10b. Therefore, for the normal stress range investigated, the interface large displacement shear strength of all GCL/GM interfaces studied was greater than the residual internal GCL shear strength, and the peak interface shear strength was less than the peak internal GCL strength.

It is important to note that Gilbert et al. (1996) observed that the failure mechanism in direct shear tests of a needle-punched GCL/laminated GMX interface was a function of normal stress. For normal stresses up to 13.8 kPa, failure occurred at the interface between the GCL (woven geotextile) and the GMX. For normal stresses of 27.6 and 69.0 kPa, internal failure of the GCL was observed, and at the highest normal stress tested (345 kPa) the failure mechanism was a combination of internal and interface failure. Triplett and Fox (2001), however observed failure at the GCL/GMX interface under all normal stresses (6.9 – 486 kPa). There may be several factors that contributed to this difference in observed failure mechanism. An increased GCL peel strength could cause the failure surface to remain at the GCL/GMX interface, however peel strength was not reported for the Gilbert et al. study so a comparison cannot be made.

2.3.3 Laboratory Measurement of GCL Shear Strength

The American Society for Testing and Materials has standardized the procedure for determining the internal and interface shear resistance of geosynthetic clay liners using a direct shear device (ASTM D 6243). Currently, the standard recommends that square or rectangular specimens are used and requires that the minimum dimension be greater than 300 mm, fifteen times d_{35} of the coarser soil used in the test, or five times the maximum opening size in the geosynthetic. The shearing surfaces should be covered with a gripping system that is capable of inducing uniform specimen failure and must also permit flow of water into and out of the test specimen. End clamping is also permitted so long as it does not interfere with the measured shear strength. Conditioning of the test specimens must be specified by the user, including test configuration,

hydration procedure, testing normal stress, soil compaction criteria (if applicable), and shearing method (i.e., stress- or displacement-controlled). For displacement-controlled testing, the shearing rate to provide drained conditions can be estimated using

$$R = \frac{d_p}{50 t_{50} \eta} \tag{2-1}$$

where R is the maximum displacement rate; d_p is the estimated horizontal displacement at peak shear stress; t_{50} is the time required for the specimen to reach 50% consolidation assuming double-drained conditions under the current normal stress; and $\eta = 1$ for internal shear of a GCL with drainage at both boundaries, 4 for interface shear between a GCL and an impermeable material, and 0.002 for interface shear between a GCL and a pervious material. If pore pressures are not expected to develop on the failure surface during a GCL interface test, then ASTM D 6243 allows for a maximum displacement rate of 1 mm/min. Following completion of the test, the specimen should be inspected for failure location, failure mechanism and any distress to the geosynthetic caused by the gripping/clamping system.

The specimen size for testing GCLs and their interfaces is typically larger than for shear tests on natural soils. Fox and Stark (2004) note that this is necessary because:

- greater shear displacements are often required to achieve peak and residual strength conditions,
- textured elements of many geosynthetics (e.g., geonet, textured geomembrane) are larger than for most soils, and
- the spacing of some types of GCL reinforcement (e.g., stitch-bonding) may be as large as 100 mm.

The ASTM D 6243 dimension requirements indicate that smaller specimens are also more influenced by edge effects and do not account for large-scale variations in material behavior. The disadvantage of having a large specimen size is that the testing equipment becomes bulky and expensive, tests are more difficult to perform, and the maximum attainable normal stress is often limited (Fox and Stark 2004). For these reasons, some researchers recommend that tests be performed on small specimens in order to complement large-scale shear tests (Stark and Eid 1996; Gilbert et al. 1997).

The specimen gripping/clamping system is vital to the success and accuracy of the direct shear device since it transfers all applied shear forces to the geosynthetic specimens. Typical gripping surfaces used in many GCL shear devices are composed of wood, plastic or metal plates, sandpaper, or coarse soil (Fox and Stark 2004). ASTM D 6243 discourages the use of adhesive to fasten the GCL to a substrate since it may influence the strength behavior. However, typical gripping surfaces are not sufficient to induce failure for strong interfaces, therefore it is common for production laboratories to utilize end clamping (Figure 2.11) to avoid unsuccessful shear tests. These clamps usually consist of a bolted bar or mechanical compression that fix the geosynthetics to one or both ends of the shearing blocks. Fox et al. (1997) provided an excellent study on the gripping system's effect on GCL internal shear strength. Three different static shear tests were performed on a needle-punched GCL with different gripping surfaces, and the resulting stress-displacement curves are shown in Figure 2.12. For the lowermost curve, the GCL was clamped and a medium coarse sandpaper was used as the gripping surface. The failure surface for this configuration was at the GCL/sandpaper interface and significant stretching of the geotextile at the clamp was observed. A second test was

Figure 2.11: Direct shear configurations illustrating end-clamping for (a) GCL internal and (b) GM/GCL interface shear tests (Fox and Stark 2004).

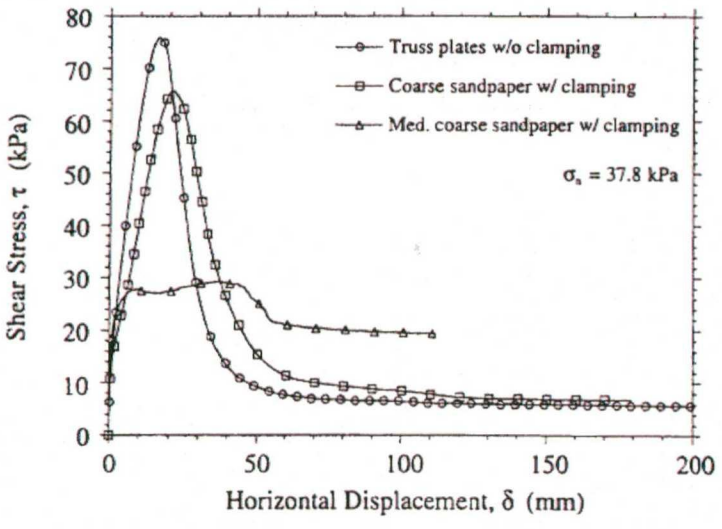

Figure 2.12: Stress-displacement curves for internal shear of a needle-punched GCL using three gripping systems (Fox et al. 1997).

performed using the same clamping procedure, however a coarse sandpaper was used for the gripping surface. For this case, the post-test inspection revealed that some slipping occurred at the GCL/sandpaper interface, however internal failure of the GCL did occur. The final test was performed with no end clamping and a modified steel truss plate used in wood construction for the gripping surface. The truss plate consisted of metal teeth (density of 0.93 teeth/cm^2) machined at an angle such that they had a triangular profile and a maximum height of 2 mm. This configuration yielded internal failure of the GCL with no interface slippage and, compared to the other two gripping systems, produced the largest peak shear strength and slightly lower residual shear strength. There is currently no standard on gripping surfaces, however it is evident that ASTM is moving toward a system that does not require end clamping, such as that described by Fox et al. (1997).

The normal stress under which a shear test is conducted for a GCL internal or interface test is left to the user's discretion. As shear behavior is very much dependant on applied normal stress, especially since failure envelopes are often nonlinear (Gilbert et al. 1996; Fox et al. 1998; Chiu and Fox 2004), it is important to select an appropriate range for the field conditions being investigated. It is typical for the failure envelopes to be simplified using a linear envelope, consisting of a cohesion intercept and a friction angle, however these parameters may not be valid for normal stresses outside of the range under which the shear tests were conducted. GCLs used for bottom liner systems are subjected to normal stress that is initially low and increases over time. Therefore tests should be conducted over a wide stress range. However, GCLs used for cover liner systems are subjected to low normal stresses throughout the design life and therefore a more narrow normal stress range would be appropriate. ASTM D 6243 requires a minimum of three

shear tests be performed at different normal stresses to define a failure envelope, however more tests should be conducted if the normal stress range is large or initial data points exhibit considerable scatter (Fox and Stark 2004).

The designer who is having a GCL internal or interface strength test performed must also stipulate hydration procedures for the test. Specifically, "conditions must be defined during soaking/hydration for the type of fluid, duration of soaking, criteria to define completion of consolidation during soaking, normal stress to be applied during soaking, and whether the GCL is to be hydrated by itself or with other interface components assembled" (ASTM D 6243). Full hydration is always expected in the field unless the GCL is encapsulated between two geomembranes (Gilbert et al. 1997). Therefore, shear tests should be conducted under hydrated conditions when hydration in the field is anticipated. This is an important aspect of the test to define because studies have shown that GCL shear strength is highly dependent on the hydration conditions (Stark and Eid 1996; Eid and Stark 1997; Zornberg et al. 2005). Figure 2.13 shows stress-displacement curves for ring shear tests performed on an unreinforced GCL/textured geomembrane interface at 17 kPa normal stress and displacement rate of 0.5 mm/min. The weakest specimen was fully hydrated, a process that required ten days to complete, and the strongest specimen was exposed to water for only two minutes prior to shearing. Data from Koerner et al. (1996) for the same interface is also provided, where direct shear tests were performed at 17.2 kPa normal stress and displacement rate of 1.0 mm/min. This plot clearly shows that dry bentonite exhibits much stronger peak and residual strength values than a hydrated specimen. Similar observations were made by Zornberg et al. (2005) for internal shear of an unreinforced GCL.

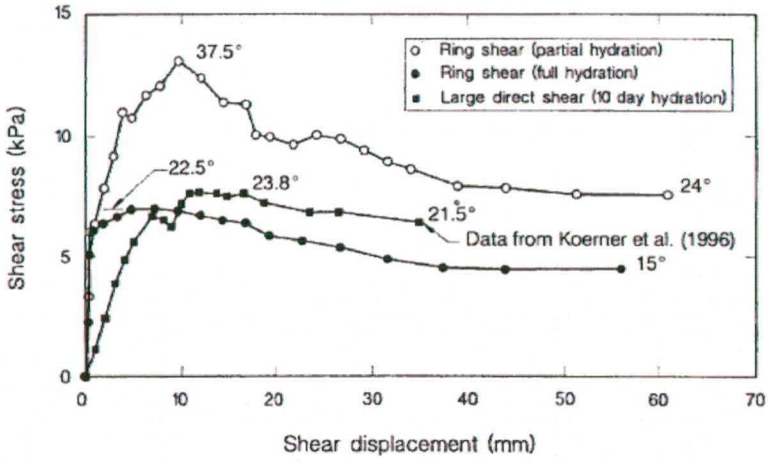

Figure 2.13: Ring shear and direct shear results of a GCL/geomembrane interface showing effect of GCL hydration (Stark and Eid 1996).

The hydrating liquid must also be specified for the test, and tap water is typically used due to its availability and convenience, however a site-specific liquid may also be utilized. In addition, the normal stress during hydration must be defined, as this too can have an influence on measured shear strength. Eid and Stark (1997) performed an interesting study on encapsulated, GMX-supported GCL specimens in which two different hydration procedures were followed. The first set of tests (Figure 2.14a) was performed with the hydration and shearing normal stresses being equal. For the second set of tests (Figure 2.14b), the specimens were hydrated under 17 kPa and then consolidated to the shearing normal stress. Note that hydrating under a lower normal stress resulted in lower shear and residual strength values. This is attributed to additional

(a)

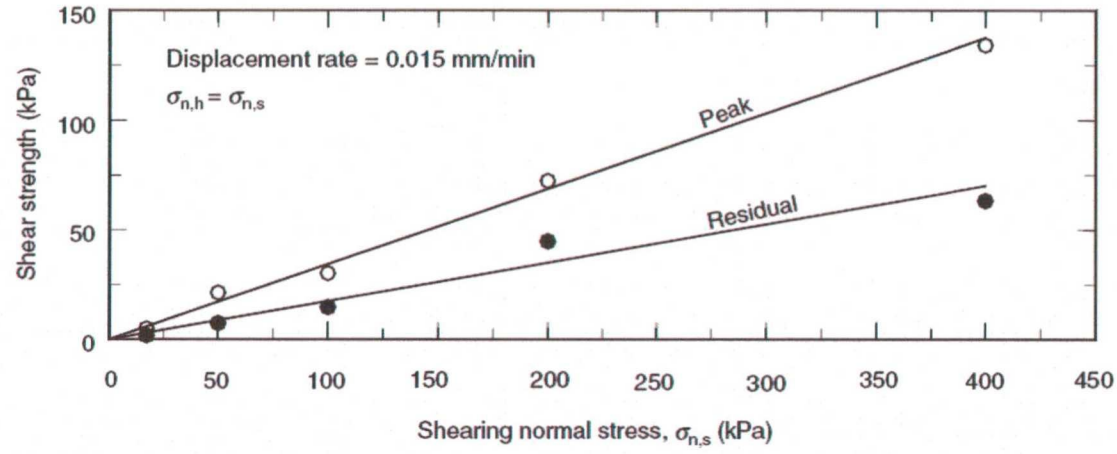

(b)

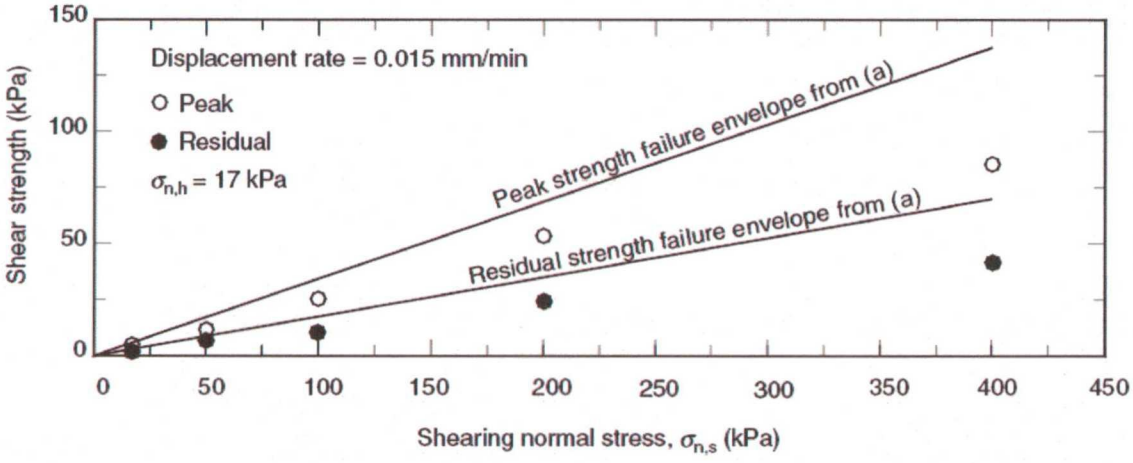

Figure 2.14: Peak and residual strengths for a textured geomembrane/geomembrane-encapsulated GCL (a) hydrated at the shearing normal stress and (b) hydrated at 17 kPa normal stress and then consolidated to the shearing normal stress (Eid and Stark 1997).

water that is adsorbed into the bentonite double layers when hydrated at the lower normal stress. Not all of this water is expelled during consolidation therefore higher water content and, consequently, lower shear strength results (Fox and Stark 2004). Hydration/consolidation procedures may also have an effect on shear strengths of reinforced GCLs. Tensioning of the reinforcing occurs during hydration which will likely reduce the fiber tensile strength and the hydrated bentonite may lubricate the reinforcing strands, which could facilitate fiber pull-out from the geotextiles (Stark and Eid 1996).

The final aspect of the hydration/consolidation procedure that must be addressed is the manner in which hydration is accomplished. It is common for hydration to occur within the shearing device under the desired normal stress until volume change ceases. However, this procedure may require hydration periods up to three weeks (Gilbert et al. 1997; Stark and Eid 1996). An alternative, two-stage accelerated hydration method was described by Fox et al. (1998) to address the significant time required to achieve full hydration. According to this method, the GCL is initially hydrated outside of the shearing device for two days under low normal stress (1 kPa) with just enough water to reach the expected final hydration water content (estimated from previous tests). The GCL is then placed in the testing device and provided free access to water for two additional days under the desired hydration normal stress. Most GCLs attained equilibrium in less than 24 hours using this method (Fox et al. 1998; Triplett and Fox 2001, Fox et al. 2006).

Another parameter that has a significant effect on GCL shear strength is the shearing displacement rate. Since the testing rate will control the time required to

perform a test, it has a significant impact on the cost associated with testing. Hydrated GCLs would be expected to be rate-dependent because shear-induced excess pore pressures would develop in the bentonite, however dry GCLs would not be expected to exhibit this behavior. Indeed, Eid and Stark (1997) showed that the peak and residual shear strength of dry encapsulated GCLs are essentially constant at displacement rates below 1 mm/min (Figure 2.15). Hydrated specimens, however, show significant rate dependency. Figure 2.16 shows peak and residual shear strength values for large direct shear tests performed by Berard (1997) and Fox et al. (1998) on two different needle-punched GCL products. It can be seen that the peak internal shear strength increases with increasing displacement rate between 0.01 and 10 mm/min, and this trend is more prominent for higher normal stresses. The residual shear strength, however, appears independent of displacement rate for this range. Stark and Eid (1996) performed an investigation into the mechanism of rate dependency on GCL internal shear strength. Ring shear tests were performed on a needle-punched GCL with thermal locking at a normal stress of 17 kPa and displacement rates up to 36.5 mm/min. The tests were performed in two configurations; for the first series of tests the bentonite was removed from the specimens by gently tapping the geotextiles until all the clay was removed, and the second series was performed with the clay not removed and the specimens fully hydrated under the shearing normal stress. Figure 2.17 shows results of these shear tests as a function of displacement rate. It can be seen that the unfilled specimen peak shear strength increased with increasing displacement rate. This increase is attributed to tearing of the geosynthetic reinforcing strands at higher shear rates, as opposed to the gradual pull-out of fibers from the woven geotextile. Interestingly, the bentonite-filled

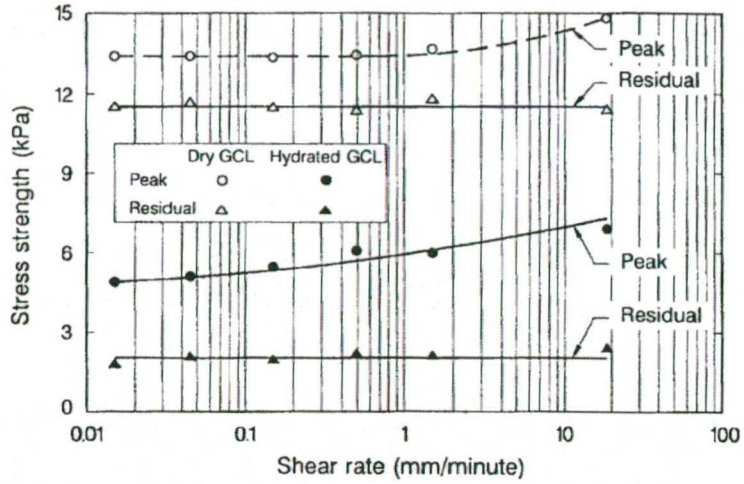

Figure 2.15: Effect of shear displacement rate on the interface strength of dry and hydrated smooth geomembrane-supported GCL/textured geomembrane specimens at a normal stress of 17 kPa (Eid and Stark 1997).

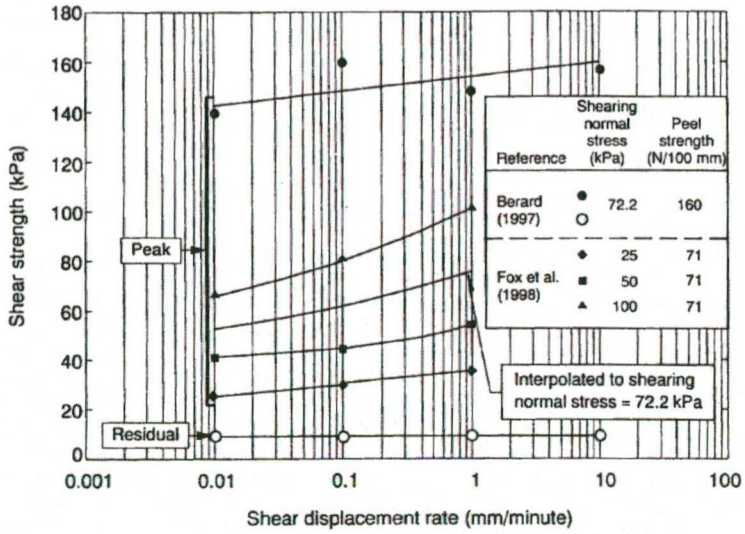

Figure 2.16: Summary of displacement rate effects on needle-punched GCL internal shear strength (Eid et al. 1999).

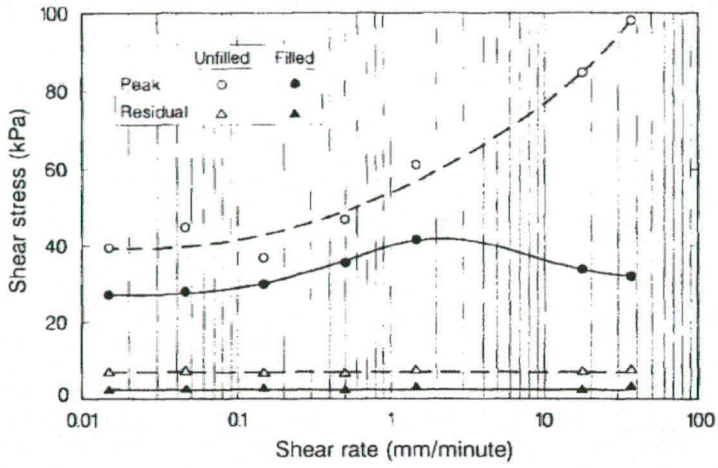

Figure 2.17: Measured effect of displacement rate on needle-punched GCL internal shear strength (Stark and Eid 1996).

GCLs are slightly weaker, which is attributed to 1) the reinforcing fibers being tensioned during hydration, 2) bentonite extrusion lubricating the fibers and facilitating pull-out, 3) contact between the geotextiles in the unfilled specimens increasing the measured strength, and 4) creation of positive excess pore pressures in the bentonite-filled GCLs (Stark and Eid 1996). However, comparison of the two GCL strengths suggests that shear-induce pore pressures do not significantly affect the internal shear strength until a displacement rate of 1.5 mm/min is exceeded. In addition, no significant change is noticed below a shear rate of 0.04 mm/min. The data in Figure 2.17 also indicates that the residual shear strength of this GCL is independent of displacement rate.

Eid et al. (1999) extended this study by performing internal ring shear tests on a needle-punched GCL at high normal stresses (100 – 400 kPa) with displacement rates up to 36.5 mm/min. All of the specimens were hydrated under 17 kPa normal stress and then consolidated to the shearing normal stress. Figure 2.18 shows peak and residual

shear strengths for the GCL specimens as a function of shear displacement rate. At lower normal stresses (17 and 100 kPa), the peak strength increased due to rapid tearing or pull-out of the reinforcement (Stark and Eid 1996), however the presumed development of positive excess pore pressures overtook this effect and resulted in decreased strength at higher displacement rates. The effect of presumed shear-induced pore pressures is more pronounced for the 100 kPa test, which is likely due to increasing pore pressures with increasing normal stress. For higher normal stress tests (200 and 400 kPa), the apex in peak strength is not present, but rather remains relatively constant up to a displacement rate of 10 mm/min. This observation is attributed to a larger undrained frictional resistance mobilized within the bentonite at lower water contents. Therefore, the strength increase from rapid tearing of the reinforcement was nearly equally countered by the decrease in strength due to positive excess pore pressures, thus constant shear strength was observed (Eid et al. 1999). Figure 2.18 also includes residual shear strength, which agrees with Stark and Eid (1996) and Eid and Stark (1997) that residual internal shear strength is essentially independent of displacement rate.

Triplett and Fox (2001) reported displacement rate tests on interfaces between the woven geotextile (W) of a needle-punched GCL and a smooth geomembrane (SM), a laminated textured geomembrane (LM), and a coextruded textured geomembrane (CX). Figure 2.19 shows the peak and large displacement strength results of this study, however no consistent trend for this data could be established.

(a)

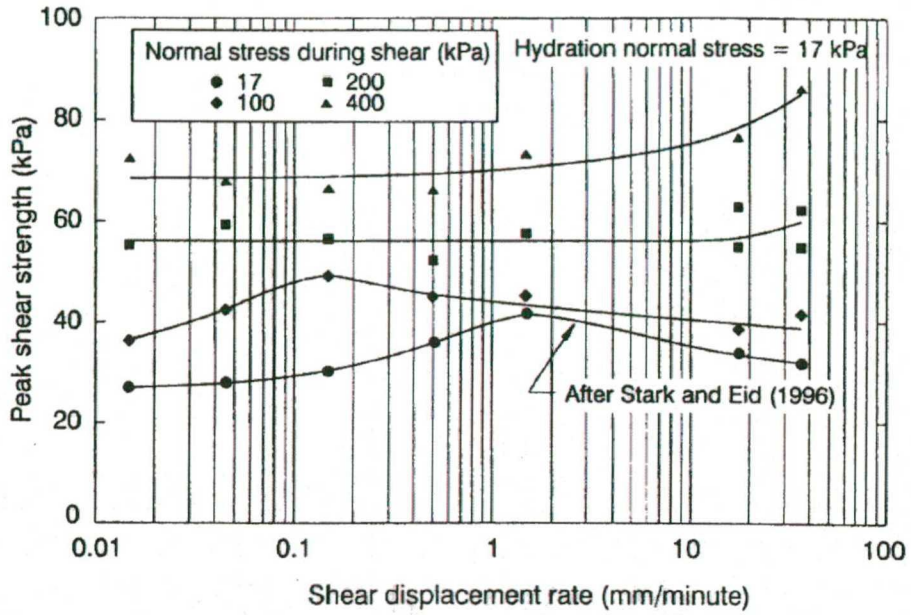

(b)

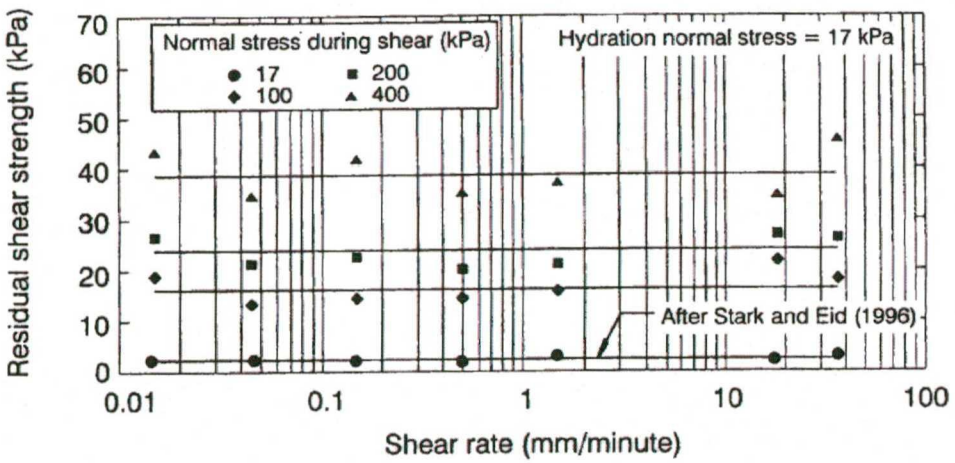

Figure 2.18: Displacement rate effect on (a) peak and (b) residual internal shear strength of a needle-punched GCL (Eid et al. 1999).

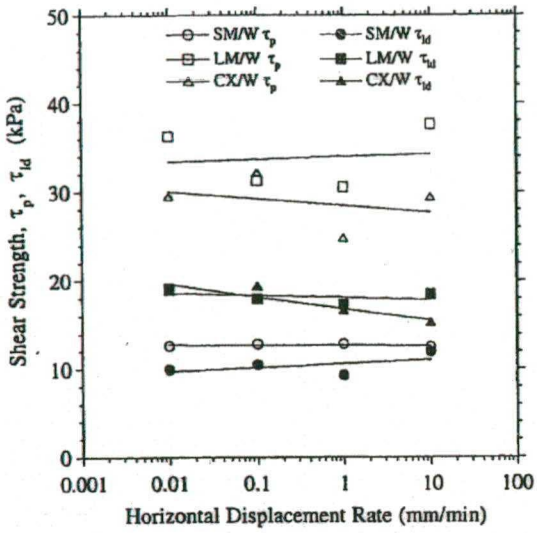

Figure 2.19: Displacement rate study performed on needle-punched GCL/geomembrane interfaces (Triplett and Fox 2001).

2.4 Dynamic Shear Characteristics of Geosynthetic Interfaces

Dynamic or cyclic loading is applied to soil in various ways, including earthquakes, wind, waves, traffic, or machinery. However, geosynthetics used in hydraulic barrier applications typically only experience dynamic loading during a seismic event. Anderson (1995) described post-seismic investigations performed at sixteen landfill sites in California, USA over the course of eight years. This includes investigations following the Northridge Earthquake of 1994. He reported that no catastrophic slope or foundation failures occurred, however varying degrees of damage were observed, typically affecting the cover and environmental control systems. Damage involving the liner systems was limited to tears in the geosynthetics and cracks in the soil. Only visual inspections were conducted at these sites so any damage or distress to portions of the liner covered by waste and/or soil was not observed. Augello et al. (1995)

presented seven case histories of landfill performance during the Northridge Earthquake, three of which were geosynthetic-lined. Again, the only observed damage at these sites included tears in the geosynthetic liners and cracks in the soil. Back-analyses were performed to determine the dynamic shear strengths of liner interfaces. This analysis indicated that the calculated shear strengths were generally consistent with values commonly used in practice.

The shear strength values typically used in practice are determined through research investigations of the dynamic interface shear properties of geosynthetics. These studies are often conducted using cyclic direct shear or shake table devices. In some instances, geotechnical centrifuges have been utilized to increase the normal stress capabilities of the shake tables. The following discussion presents studies performed on geosynthetic interfaces that are typical in landfill liner systems.

2.4.1 Geotextile / Geomembrane Interface

The interface between a geotextile and a geomembrane is likely the most common interface found in landfill liners. Geomembranes are desirable due to their low hydraulic conductivity and geotextiles have a range of uses, from supporting bentonite in a GCL to providing a drainage, separation, or protection layer. Yegian and Lahlaf (1992) provided an excellent study on the dynamic interface shear characteristics between a nonwoven geotextile and a smooth geomembrane. First, they performed static tests to provide a comparison with subsequent dynamic tests. Under monotonic loading with a constant displacement rate of approximately 1.27 mm/min, the typical stress-displacement curve resembled a rigid-plastic system, with a high initial modulus until a peak shear resistance

was reached and then constant stress with additional displacement. The main difference was that following peak stress, a slight reduction in resistance was observed as further displacement occurred until a residual condition was achieved. The residual friction angle was approximately 1° less than the peak friction angle. To determine the dynamic shear behavior, shake table tests were then performed on this interface. The researchers determined that there exists a limiting acceleration that is transmitted between the geosynthetics, beyond which relative displacement occurs. Assuming a Mohr-Coulomb failure criterion, the shear strength can be written as

$$F = W \tan \phi_d \tag{2-2}$$

where W is the applied normal force and ϕ_d is the interface dynamic friction angle. This limiting force can be expressed as a limiting acceleration, a_b, given by

$$F = \frac{W}{g} a_b \tag{2-3}$$

where g is Earth's gravitational acceleration. Rearranging these equations gives

$$\phi_d = \tan^{-1}\left(\frac{a_b}{g}\right) \tag{2-4}$$

Figure 2.20 shows a typical peak block acceleration versus table acceleration for a shake table test on the nonwoven geotextile/smooth geomembrane interface. The dashed line indicates zero relative movement between the geosynthetics and that all acceleration (and therefore, force) is transmitted across the interface. This occurs up to a limiting block acceleration of 0.20g, corresponding to a dynamic friction angle of 11.3° from Equation 2-4. Immediately after sliding initiates, the block acceleration becomes slightly less than the peak strength, which is attributed to the residual shear strength of the interface

(Yegian and Lahlaf 1992). Shake table tests were also conducted to investigate the interface response to changes in normal stress and loading frequency, and the effect of dry versus submerged conditions. It was concluded that neither normal stress nor frequency had an effect on shear behavior and that the submerged condition provided slightly lower shear strength as compared to the dry condition. In general, the dynamic shear resistance was found to be similar to that under static loading, with typical increased shear strength of approximately 1°. The measured peak and residual friction angles for both the static and dynamic conditions are provided in Table 2.3.

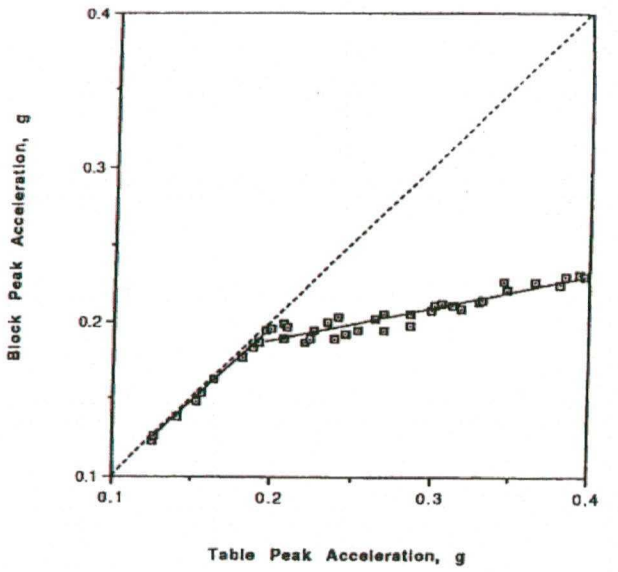

Figure 2.20: Shake table results for dry geomembrane-geotextile interface with a normal stress of 8.5 kPa and a frequency of 2 Hz (Yegian and Lahlaf 1992).

Interface Condition	Static Loading		Dynamic Loading	
	Peak friction angle	Residual friction angle	Peak friction angle	Residual friction angle
Nonwoven geotextile/Smooth geomembrane (dry)	10.7°	10.0°	11.3°	10.7-13.5°
Nonwoven geotextile/Smooth geomembrane (submerged)	9.6°	8.5°	10.7°	9.6-13.0°

Table 2.3: Geotextile/geomembrane interface friction angles (Yegian and Lahlaf 1992).

Other studies have performed friction tests on a geotextile/geomembrane interface and have likewise concluded that a limiting shear resistance exists, beyond which relative displacements occur (Yegian et al. 1995; De and Zimmie 1998; Yegian and Kadakal 1998). In addition, each of these studies concluded that frequency had no significant influence on the dynamic shear behavior, and Yegian et al. and De and Zimmie concluded that normal stress also had no influence on the shear response. Tests performed using a cyclic direct shear device showed reduction in shear resistance with increasing number of cycles, which was attributed to polishing of the geomembrane surface (De and Zimmie 1998; Kim et al. 2005). A decrease of 2° in peak friction angle due to this phenomenon was reported by De and Zimmie for a test duration of 50 cycles. Some studies also observed a stick-slip behavior along the geosynthetics, which momentarily increased the shear resistance of the interface (Yegian et al. 1995; Yegian and Kadakal 1998; Yegian et al. 1998). Figure 2.21 shows the block acceleration-relative displacement relationships for a nonwoven geotextile/smooth geomembrane interface. Note that the peak block acceleration can be used to determine the interface shear force using Equation 2-4. Yegian et al. (1998) analyzed this hysteretic curve by assuming the

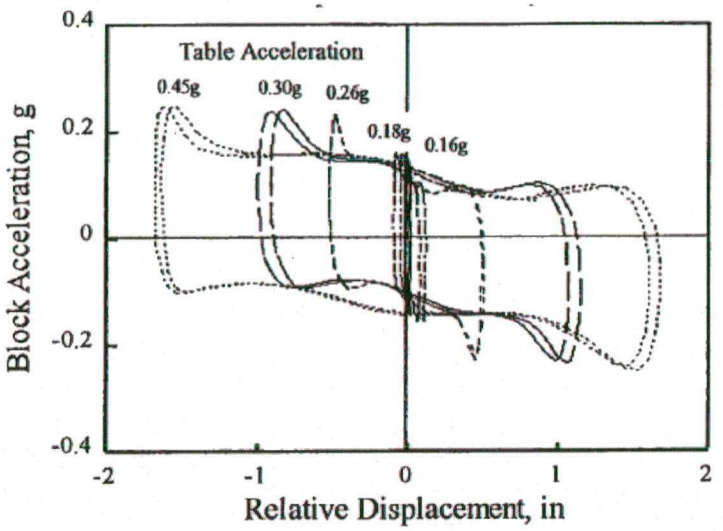

Figure 2.21: Block acceleration-relative displacement curves for shake table tests of geotextile/geomembrane interface at various table accelerations (Yegian et al. 1998).

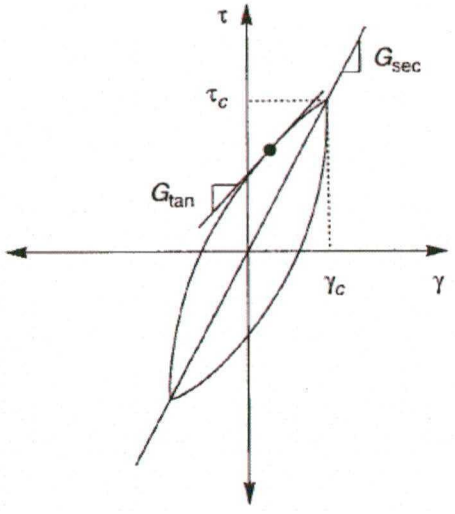

Figure 2.22: Secant and tangent shear modulus for hysteretic curve typical of cyclic loading on natural soil (Kramer 1996).

behavior to be linear elastic, with an equivalent shear stiffness that is dependent on slip amplitude. This method has been used extensively for dynamic characterization of natural materials that display hysteretic behavior (e.g., Mitchell 1993; Kramer 1996). In this method, the equivalent shear modulus is defined as the line joining the two peaks of the force-slip hysteresis loop, thus from Figure 2.22,

$$G_{\text{sec}} = \frac{\tau_c}{\gamma_c} \tag{2-5}$$

where τ_c and γ_c are the shear stress and strain amplitudes, respectively. The damping ratio, ξ, provides a measure of the breadth of the hysteresis loop (Kramer 1996) and is given by

$$\xi = \frac{W_D}{4\pi W_S} = \frac{1}{2\pi} \frac{A}{G_{\text{sec}} \gamma_c^2} \tag{2-6}$$

where W_D is the dissipated energy, W_S is the maximum strain energy, and A_{loop} is the area of the hysteresis loop. In the case of interface shear, displacement amplitude is used rather than strain for these calculations (Yegian et al. 1998). The reduction in shear modulus with increasing displacement (or strain) can be expressed through either the backbone curve or the modulus reduction curve, shown in Figure 2.23. The backbone curve is "the locus of points corresponding to the tips of hysteresis loops of various cyclic strain amplitudes" (Kramer 1996). Its slope at the origin represents the largest shear modulus value, G_{max}. The modulus reduction curve illustrates the decrease in secant shear modulus with increasing displacement amplitude, and is often normalized by dividing by G_{max}. These two curves provide the same information and one can be determined from the other (Kramer 1996). Figure 2.24 shows a plot of equivalent

stiffness as a function of displacement amplitude for the geotextile/geomembrane interface tested by Yegian et al. (1998). The stiffness K has the same conceptual meaning as the secant shear modulus but is more applicable to geosynthetic interfaces. Here it has been normalized by dividing by the applied normal stress and decreases nonlinearly with increasing amplitude. It was also determined that the damping ratio for this interface was not dependent on level of slip or frequency of excitation, but maintained a constant value of 0.43 (Yegian et al. 1998).

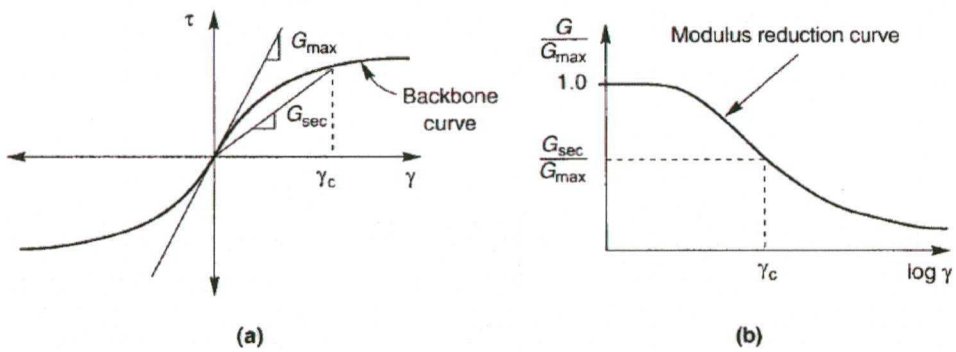

Figure 2.23: Cyclic shear analysis of natural soil using (a) backbone curve and (b) modulus reduction curve (Kramer 1996).

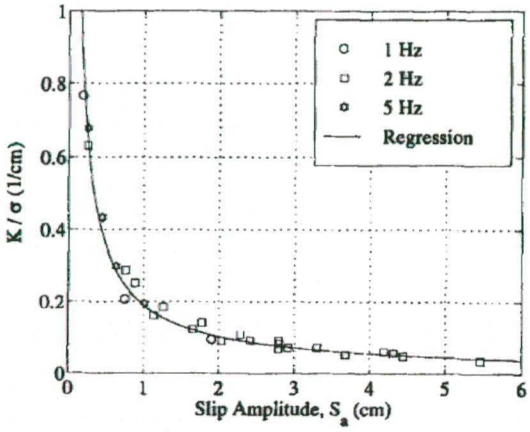

Figure 2.24: Equivalent stiffness reduction with displacement amplitude for a geotextile/geomembrane interface (Yegian et al. 1998).

2.4.2 Geonet / Geomembrane Interface

Geonets are used primarily for water drainage in geoenvironmental applications (Koerner 2005), such as a landfill liner system, thus the dynamic interface shear characteristics are of interest. De and Zimmie (1998) performed cyclic direct shear and shake table tests using a geotechnical centrifuge on a geonet/smooth geomembrane interface. The geonet shear behavior was found to be dependent on its orientation relative to the direction of shear, thus three different orientations were tested: transverse, longitudinal and aligned, as shown in Figure 2.25. The results of cyclic direct shear tests on the transverse geonet direction are provided in Figure 2.26. At all normal stress levels, the peak friction angle for the first cycle was approximately 11°. Then the friction angle value increased rapidly over the next five to ten cycles, beyond which the rate of increase slowed. This rate of increase is related to the normal stress, where the test with the lowest normal stress (20.7 kPa) exhibited the most rapid increase and the test with the

highest normal stress (41.4 kPa) showed the slowest increase. The friction angle after 50 cycles of loading ranged from 14 to 18°, for the highest and lowest normal stresses, respectively. The basic trend for these curves was observed to be the same for the longitudinal and aligned geonet orientations, however the aligned orientation did not show a significant dependence on normal stress. Peak friction values for these tests are provided in Table 2.4.

Shake table tests were also performed on the transverse and longitudinal orientations, as well as shake table tests using a geotechnical centrifuge, for a normal stress range of 2.1 to 84 kPa. The peak dynamic friction angle values for these tests are included in Table 2.4. In general, neither interface showed any dependence on the frequency of excitation, the transverse orientation exhibited the same dependence on normal stress as the cyclic direct shear tests, and the longitudinal orientation tests showed no dependence on normal stress (De and Zimmie 1998).

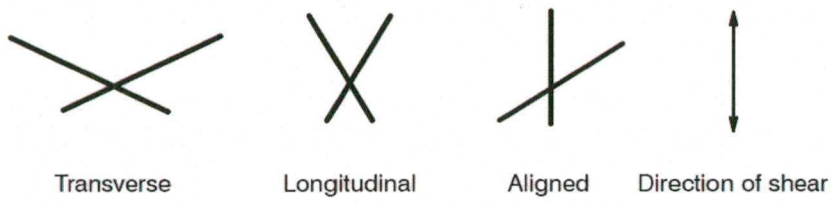

Figure 2.25: Orientation of geonet mesh (De and Zimmie 1998).

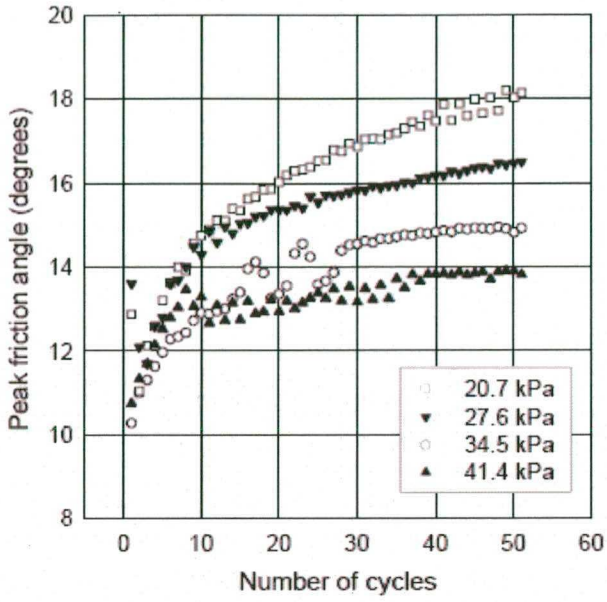

Figure 2.26: Variation of peak friction angle with number of cycles for interface tests of a geonet (transverse) with a smooth geomembrane (De and Zimmie 1998).

Orientation (Fig. 2.25)	Static friction angle		Dynamic friction angle		
	Tilt table tests	Direct shear tests	Direct shear tests	Shake table tests	
			20.7 to 40.4 kPa	2.1 kPa	21 to 84 kPa
Transverse	10.1°	11.3°	Increases from 11° to 18° (for low σ) or 14° (for high σ)	12°	7°
Longitudinal	9.8°	11.3°	Increases from 10° to 18° (for low σ) or 16.5° (for high σ)	12°	11°
Aligned	8.1°	8.1°	Increases from 9° to 18° (for both low and high σ)	--	--

Table 2.4: Shear behavior for geonet/geomembrane interface (De and Zimmie 1998).

Kim et al. (2005) also performed shake table tests on a geonet (transverse and aligned orientations) and a smooth geomembrane interface. They observed that large displacement friction angle increased with increasing displacement, noting that the geonet strands dug into and cut the surface of the geomembrane. This agrees with the observations made by De and Zimmie (1998). The effect of shear displacement rate was also investigated, with tests being performed for displacement rates ranging from 1 to 1000 mm/min under both dry and submerged conditions. They concluded that neither displacement rate nor interface dampness have an affect on the large displacement dynamic friction angle for either geonet orientation.

2.4.3 Geonet / Geotextile Interface

Due to the regular of use of both geonets and geotextiles in landfill liners, their dynamic interface behavior is also important. De and Zimmie (1998) performed cyclic direct shear tests and shake table tests using a geotechnical centrifuge for a geonet and nonwoven geotextile interface under a normal stress range of 2.1 to 84 kPa. Again, the three geonet orientations were tested (Figure 2.25). The results of the cyclic direct shear tests for the transverse geonet orientation are shown in Figure 2.27. The peak dynamic friction angle is relatively constant with increasing number of cycles, however exhibits a strong dependence on normal stress. The largest friction angle (approximately 24°) was obtained for the test with the lowest normal stress (20.7 kPa), and the lowest friction angle (approximately 17°) was obtained for the test with the highest normal stress (41.4 kPa). This decrease in friction angle with increasing normal stress was attributed to the highly deformable nature of the nonwoven geotextile when subjected to high normal

stress (De and Zimmie 1998). Results of cyclic tests on the longitudinal and aligned geonet orientations showed that the friction angle was relatively constant with increasing number of cycles, however these interfaces were not dependent on normal stress. In fact, the dynamic friction values obtained for these orientations were close to those obtained from monotonic experiments reported by other researchers (De and Zimmie). Shake table tests using a centrifuge also showed that the transverse geonet orientation was strongly dependent on normal stress. A slight dependence was also observed for the longitudinal orientation, however no tests were performed in the aligned direction. Friction angle data for the geonet/geotextile interface is provided in Table 2.5.

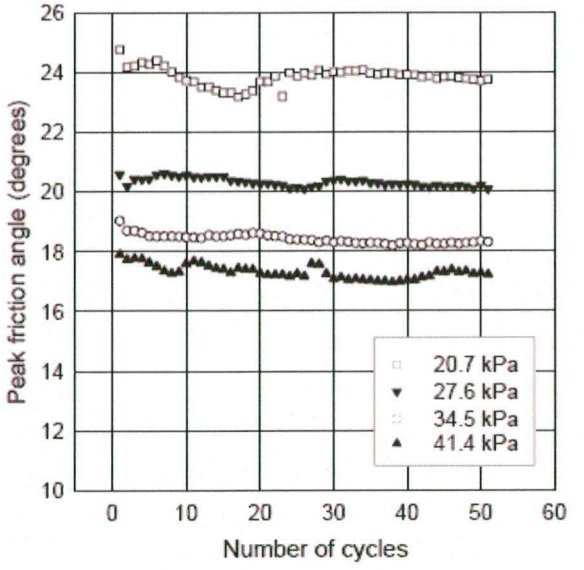

Figure 2.27: Variation of peak friction angle with number of cycles for interface tests of a geonet (transverse) with a geotextile (De and Zimmie 1998).

Orientation (Fig. 2.25)	Static friction angle		Dynamic friction angle		
	Tilt table tests	Direct shear tests	Direct shear tests	Shake table tests	
			20.7 to 40.4 kPa	2.1 kPa	21 to 84 kPa
Transverse	24.5°	From 22° (at low σ) to 14.5° (at high σ)	From 24° (at low σ) to 17° (at high σ)	24°	8°
Longitudinal	13.9°	From 22° (at low σ) to 14.5° (at high σ)	15°	19°	11°
Aligned	13.1°	10.5°	11 to 10°	--	--

Table 2.5: Shear behavior for geonet/geotextile interface (De and Zimmie 1998).

2.5 Dynamic Shear Characteristics of Geosynthetic Clay Liners

The internal and interface static shear behavior of geosynthetic clay liners has been discussed in detail in Section 2.3. However, the dynamic shear behavior for these materials has been investigated to a far lesser extent and therefore is not as well understood. This section describes the three studies that are currently available on the dynamic shearing characteristics of GCLs. The first involves the interface between a needle-punched GCL and a smooth geomembrane, the second involves the interface between an unreinforced GCL and a smooth geomembrane, and the last describes internal cyclic shearing of an unreinforced GCL. Each study has certain contributions and limitations, which will be discussed.

2.5.1 Lai et al. (1998)

Lai et al. (1998) reported the only available study of cyclic loading influence on the internal shear strength of a GCL. Direct simple shear tests (stress-controlled) were performed on an unreinforced, geomembrane-supported GCL for both static and cyclic loading. Specimens measuring 80 mm in diameter were tested under dry and hydrated conditions, with the normal stress ranging from 23 to 320 kPa for the dry and 23 to 113 kPa for the hydrated condition. The gripping system consisted of several 16-guage brass nails embedded into the geomembrane to force shear failure to occur within the bentonite. Cyclic tests were conducted at select cyclic stress ratios (cyclic shear stress divided by the undrained static shear strength). With this stress-controlled setup, no post-peak response could be measured, therefore all reported data refer to peak shear strengths.

First the shear characteristics of the GCL in a dry condition will be considered. Static tests performed at a rate of 0.5 N/sec and a normal stress range of 23 to 320 kPa resulted in failure occurring at the interface between the bentonite and the base porous stone, however the authors contend that the measured strengths are not significantly less than the internal GCL strength. The failure envelope constructed for the dry condition produced a static friction angle of 31°, with nonlinearity being evident with increasing normal stress. The displacement required to reach peak strength also increased with increasing normal stress. Cyclic direct shear tests were performed on the dry specimens at two normal stresses (67 kPa and 39 kPa) with frequency of 0.09 Hz and cyclic stress ratios ranging from 0.40 to 1.18. If a specimen did not fail during cyclic loading, then it was sheared under static conditions to evaluate the influence of dynamic loading on the shear strength. It was observed that for cyclic stress ratios less than 1, failure did not

occur during the 200-cycle test, but that the post-dynamic static shear strength increased slightly. This increase was directly proportional to the applied cyclic stress ratio and was attributed to densification of the bentonite during cyclic loading. An additional series of tests were performed to evaluate the effect of frequency on the shear strength of the dry GCL. The normal stress for these tests was 39 kPa, the cyclic stress ratio was 0.81, and the frequency of loading varied from 0.09 to 0.25 Hz. No failure occurred during cyclic loading and subsequent static tests showed that the shear strength increased due to bentonite densification, however loading frequency had no effect.

Static and cyclic tests were then conducted on hydrated GCL specimens. These tests were performed under a consolidated, undrained state. Four static tests were completed at 0.5 N/sec with normal stress ranging from 23 to 113 kPa. Again, failure occurred at the interface between the bentonite and the underlying porous stone. The failure envelope constructed for the hydrated condition provided a friction angle of 11° and the displacement required to reach peak strength was less than that for the dry condition. Five cyclic tests were performed at a normal stress of 45 kPa with frequency of 0.09 Hz and cyclic stress ratio ranging from 0.53 to 0.92. Figure 2.28 shows shear stress-shear displacement curves for two specimens, one at a cyclic stress ratio of 0.53 which did not fail during the 200-cycle test, and the other with a stress ratio of 0.67 which failed after 32 cycles. It can be seen that the shear displacement increased as the number of cycles increased, whereas no significant degradation in the shear stress-shear displacement curves was observed for the dry specimens. The test performed at a cyclic stress ratio of 0.53 was subjected to static shear following dynamic loading and no change in shear strength was measured. Figure 2.29 shows the effect of cyclic loading on

(a)

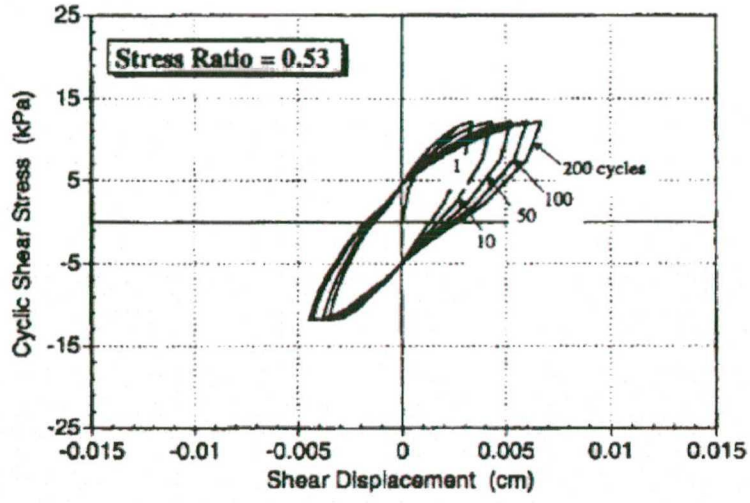

(b)

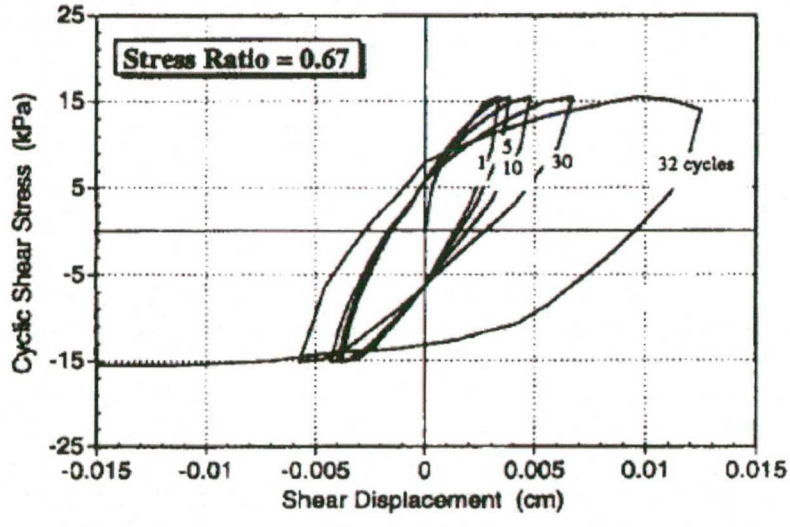

Figure 2.28: Cyclic direct shear test results of a geomembrane-supported unreinforced GCL with cyclic stress ratio of (a) 0.53 and (b) 0.67 (Lai et al. 1998).

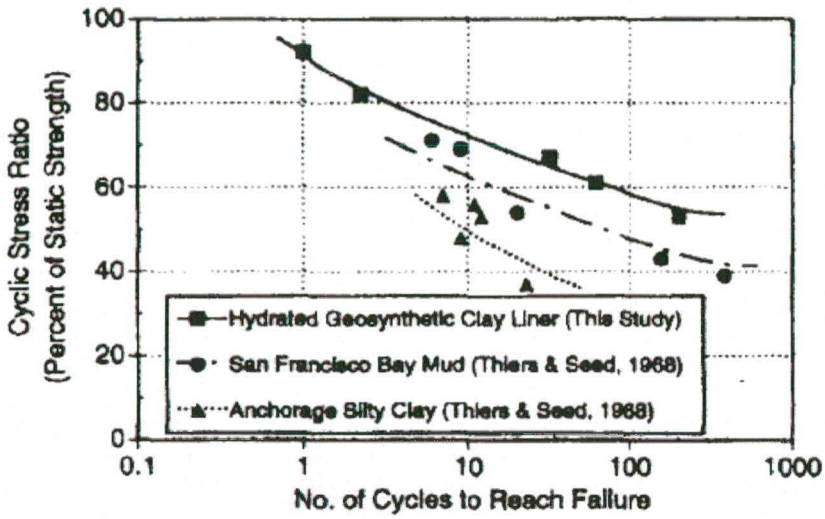

Figure 2.29: Effect of cyclic loading on shear strength of natural soils and a geomembrane-supported unreinforced GCL (Lai et al. 1998).

natural clays as well as the hydrated GCL studied by Lai et al. The figure indicates that the shear strength degrades with an increasing number of cycles, however the influence on the GCL was not as severe as on the two natural clays.

2.5.2 Lo Grasso et al. (2002)

Shake table tests were performed on a GCL/smooth geomembrane interface by Lo Grasso et al. (2002). A free-block system was used where the upper block rests on the shaking table and relative accelerations and displacements are recorded. The recording instrumentation consisted of three piezoelectric accelerometers and two LVDTs. The lower geosynthetic was attached to a table measuring 0.7 m long by 0.7 m wide and the upper geosynthetic was attached to a concrete block measuring 0.5 x 0.25 m. The normal stress for all tests reported in the paper was 3.2 kPa. The geomembrane utilized in the

study was a 2.5 mm thick, smooth HDPE product, and the GCL consisted of two woven polypropylene geotextiles supporting a layer of bentonite, however the reinforcement and hydration characteristics are not described.

Two shake table tests were performed for the GCL/geomembrane interface. In the first case, a sinusoidal displacement input increased continuously up to an amplitude of 4 mm and then decreased continuously to zero while the frequency of excitation was fixed at 5 Hz. Figure 2.30 shows the time histories of the table and block accelerations as well as the relative displacement along the interface for this test. The acceleration at which initial displacement occurs is approximately 0.30g, which corresponds to a dynamic friction angle of 17°, and the permanent displacement is 2.9 mm. Once relative displacement occurred, the block acceleration was less than that of the table and there was no phase change between the two. For the second test, the frequency was increased to 8 Hz and the amplitude increased to a maximum value of 2 mm during the first 7.5 sec, held constant for 15 sec, and then decreased to zero over the final 7.5 sec. Figure 2.31 shows the table and block accelerations and the relative displacement for this test. The critical acceleration was approximately 0.37g, corresponding to a dynamic friction angle of 21°, and the permanent displacement was 20.0 mm. For this test, once relative displacement occurred, the block acceleration reached values greater than the table and a phase change was observed between the two. This is likely the cause of the increased permanent displacement. From these two tests, the authors conclude that the dynamic friction angle is affected by the input frequency and amplitude. The test with low frequency and high amplitude resulted in lower friction angle values than the test with high frequency and low amplitude.

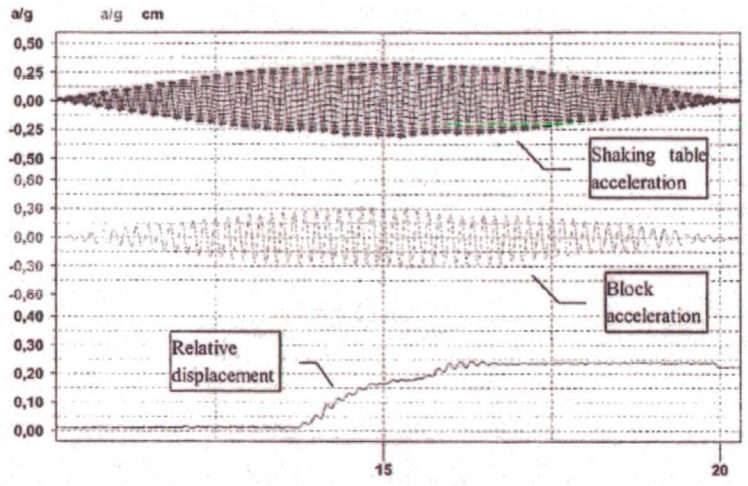

Figure 2.30: Shake table results of a smooth geomembrane/GCL interface with frequency of 5 Hz and maximum displacement of 4 mm (Lo Grasso et al. 2002).

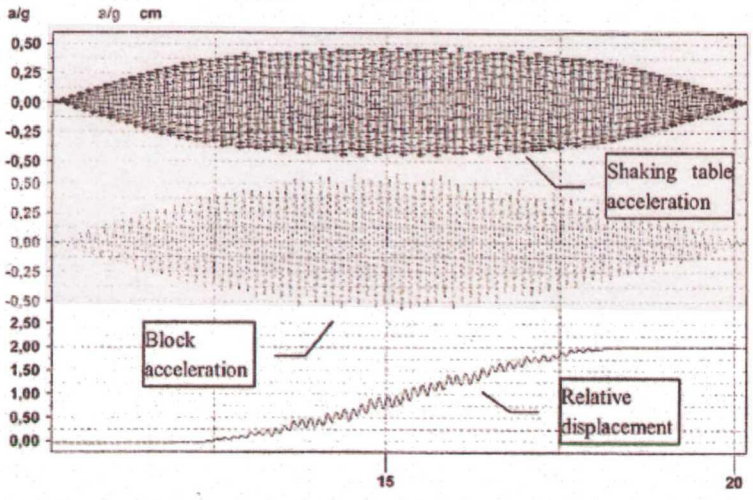

Figure 2.31: Shake table results of a smooth geomembrane/GCL interface at a frequency of 8 Hz and a maximum displacement of 2 mm (Lo Grasso et al. 2002).

A third shake table test was also performed on this interface using an actual dynamic excitation. The applied seismic time history was the East-West component of the December 13, 1990 Catania Earthquake, which had an acceleration at bedrock of 0.1g and a maximum recorded acceleration of 0.25g. The interface test showed that considerable slippage occurred during the test, reaching a maximum value of 7.7 mm, however no permanent relative displacement resulted. This presents an interesting consideration in that even if post-earthquake investigations determine that no permanent displacements occurred, substantial slippage may have taken place during the event.

2.5.3 Kim et al. (2005)

The research reported by Kim et al (2005) provided dynamic friction data from shake table tests on the interface between a needle-punched GCL and a high density polyethylene (HDPE) smooth geomembrane. A fixed-block system was utilized, where the upper block rests on the shaking table and is rigidly fixed to an exterior reaction frame so that no block movement occurs. As triangular wave excitation was applied to the table, relative displacements were measured using multiple linear variable displacement transducers (LVDTs) and all shear forces transmitted through the interface were measured using load cells. The lower geosynthetic measured 760 mm long by 400 mm wide and was attached to the table using double-sided tape. The upper geosynthetic was attached to the block using the same double-sided tape and measured 304.8 mm by 304.8 mm, which is slightly larger than the minimum 300 mm requirement by ASTM D 5321. The testing device could only test under low levels of normal stress (7.04 – 63.31 kPa), which is consistent with the overburden stress anticipated for landfill cover

systems. Tests on the GCL/geomembrane interface were performed at a normal stress of 10.94 kPa, with one test being performed at 22.5 kPa. A small water bath was also constructed so that the tests could be conducted under submerged conditions. The main objective of the study was to investigate the relationship between displacement rate and dynamic friction resistance of geosynthetic interfaces. Multiple geosynthetic interfaces were investigated in the study, however that between a GCL and a geomembrane is of interest herein.

The geosynthetic clay liner used in this study was needle-punched with two nonwoven geotextiles used to support the bentonite layer. Tests were performed using the GCL 1) in its as-received water content and 2) in a moist condition by allowing the GCL to rest submerged for one hour prior to testing. The authors observed that the shearing resistance decreased in the first few cycles due to polishing of the interface. Since multiple displacement rate tests were performed using the same specimens, 50.8 meters of cumulative displacement (i.e., 100 cycles at 127 mm amplitude) was applied to the interface prior to collecting test data. Therefore, all published results from this study refer to interface resistance on which substantial displacement has already occurred (i.e., large displacement conditions).

The test results for the needle-punched GCL/smooth geomembrane interface indicate that peak strength developed at very small displacements (typically less than 1 mm) after which shear resistance decreased continuously up to the maximum displacement of the device (250 mm). The authors plotted the mean shear strength against displacement rate for displacement amplitudes of 24 and 254 mm, under both the dry and submerged conditions, shown in Figure 2.32. The test with the larger amplitude

produced less shear resistance as compared to the smaller amplitude test. The dry condition also showed increased shear strength with increasing displacement rate while the submerged condition was relatively insensitive to displacement rate. The authors provided a failure envelope for test data at a single displacement rate, however only two normal stresses were used to create the plot. With only two points available to draw the envelope, there is no means to verify the accuracy of the data, identify any erroneous results, or establish any linearity of the resulting failure envelopes.

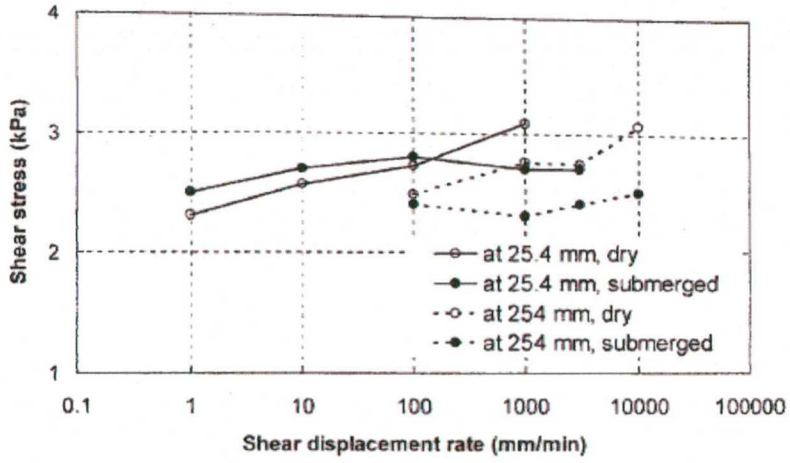

Figure 2.32: Influence of displacement rate on large displacement mean shear strength of a smooth geomembrane/needle-punched GCL interface (Kim et al. 2005).

2.6 Dynamic Shear Characteristics of Natural Clays

Analysis of dynamic shear tests on GCLs must also consider the effect of dynamic loading on the clay itself. Considerable research has been conducted on

dynamic shear behavior of natural soils and a comprehensive review is beyond the scope of this paper, however a few significant items will be discussed. The first topic is the effect of cyclic loading on shear strength. Thiers and Seed (1969) performed stress- and strain-controlled cyclic triaxial tests on three silty clays. The data revealed that the specimens weakened as the number of cycles increased and that this effect was more evident as the cyclic stress ratio increased. Vucetic and Dobry (1991) provided a landmark paper on the cyclic response of natural soils, determining that plasticity index (PI) is the main factor in controlling shear modulus reduction and damping ratio. In general, the shear modulus decreased and the damping ratio increased with increasing cyclic shear strain, where the effects were less evident for soils with higher PI. Also, as plasticity increased, further modulus degradation with additional cycles became less severe.

The second topic is the effect of cyclic loading on volume change. Chu and Vucetic (1992) and Hsu and Vucetic (2004) studied cyclic settlement of clays during simple shear. Both studies showed that settlement occurred during cyclic shear testing when the volumetric threshold shear strain of the soil was exceeded, and that the cumulative vertical strain increased as the cyclic shear strain increased. The maximum volumetric threshold shear strain reported for clay was 0.2% (Chu and Vucetic 1992). Also, vertical strain peaked as shear strain amplitude was approached, although overall settlement occurred (Hsu and Vucetic 2004).

CHAPTER 3

MACHINE DESCRIPTION

3.1 Introduction

Many factors effect the internal and interface shear strength of geosynthetic clay liners, which have been discussed in detail in Chapter 2. There are also many factors that influence the laboratory measurement of GCL shear strength. These include specimen size, hydration and consolidation procedures, specimen gripping or clamping mechanism, applied normal stress, and shear displacement rate. Fox et al. (1997) described a novel direct shear device for measurement of internal and interface GCL shear behavior. This machine incorporated several improved design features, including large specimen size (406 × 1067 mm), large displacement capability (203 mm), large range of displacement rate, an improved specimen gripping system, negligible machine friction, and measurement of specimen volume change during hydration, consolidation, and shearing. GCL pore pressure measurements were also attempted and met with limited success. This machine produced some of the highest quality static shear data yet obtained for GCLs and GCL interfaces (Fox et al. 1998, Triplett and Fox 2001). This section describes the design of a new shear machine that incorporates several improvements over the Fox et al. (1997) device and, in particular, can impose dynamic shear loading to a test

specimen. The majority of the information presented in this chapter is taken directly from Fox et al. (2006).

3.2 Machine Overview and Specifications

The dynamic direct shear machine is a freestanding apparatus that measures 3.8 m long, 1.0 m wide, and 1.2 m tall. The basic design is similar to the Fox et al. (1997) static shear device with the exception that the shearing system is capable of applying bidirectional (i.e., back-and-forth) dynamic loading to a test specimen. A photograph of the machine is shown in Figure 3.1, plan and profile scale drawings are shown in Figure 3.2, a detailed profile view of the test chamber is shown in Figure 3.3, and specifications are provided in Table 3.1. The test chamber measures 308 × 1067 mm in plan and can accommodate specimens up to 250 mm in thickness. The main components of the machine, described below, are: (1) the shearing system, (2) the normal stress and vertical displacement measurement system, (3) the specimen hydration system, and (4) the process control and data acquisition system.

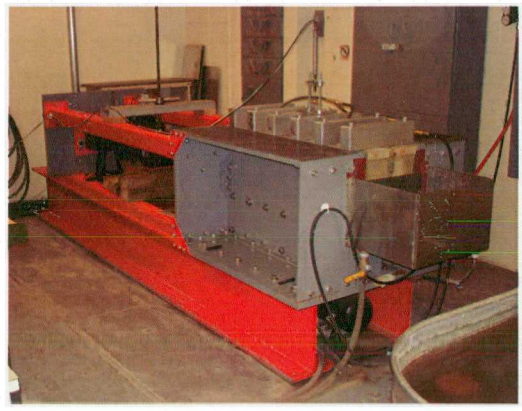

Figure 3.1: Dynamic direct shear machine.

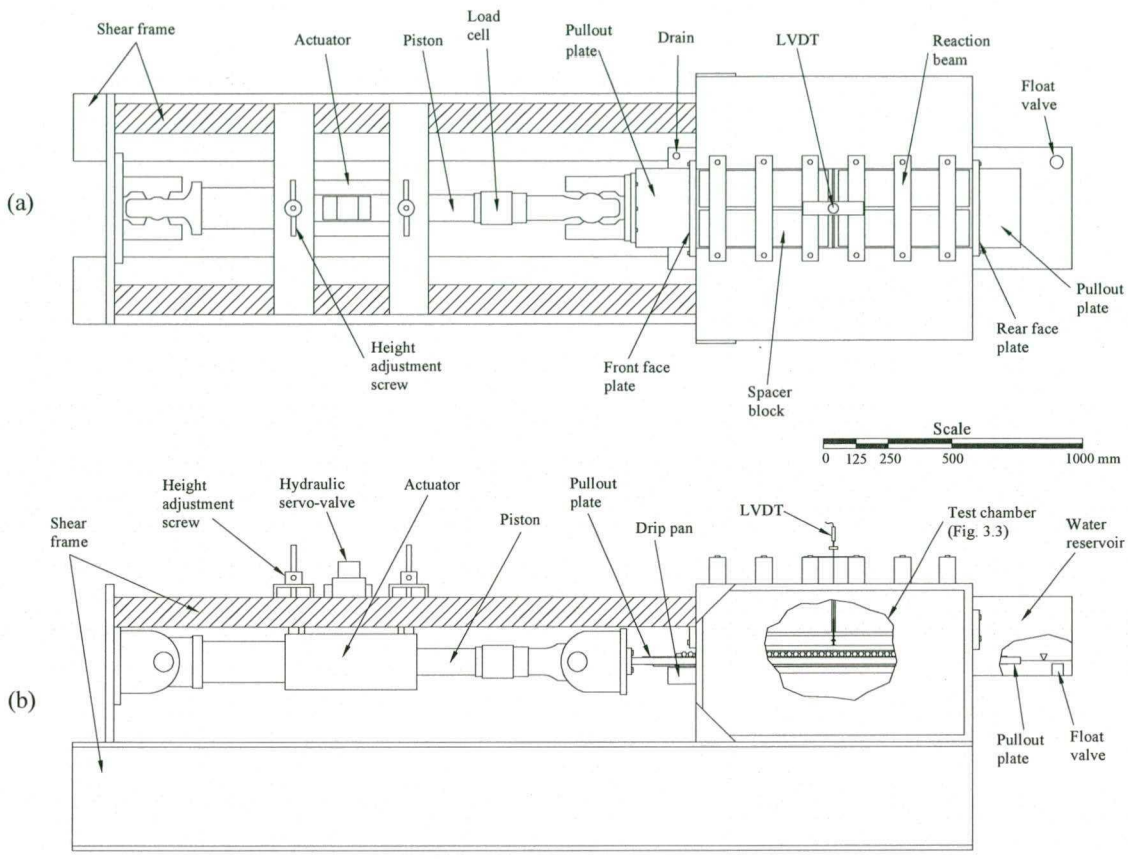

Figure 3.2: Dynamic direct shear machine: (a) plan view, and (b) profile view.

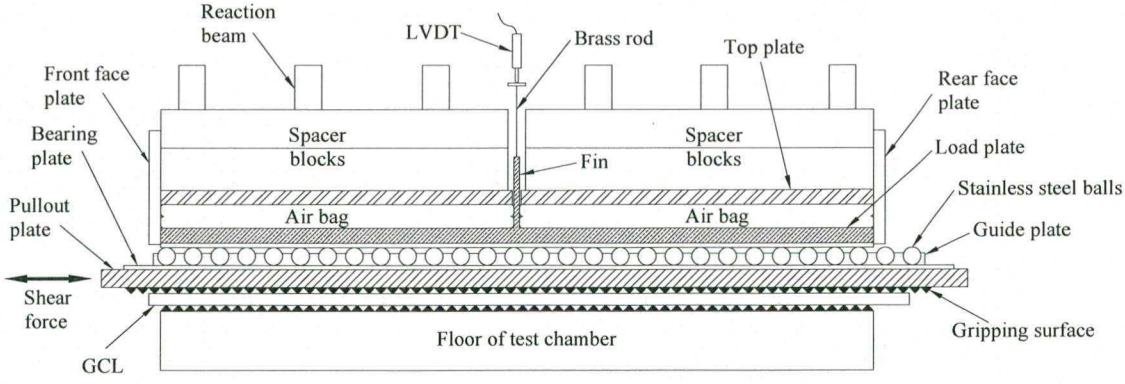

Figure 3.3: Detailed profile view of test chamber.

Feature	Specification
Specimen size	305 mm × 1067 mm
Maximum specimen thickness	250 mm
Maximum normal stress	2000 kPa
Maximum shear stress	750 kPa
Maximum horizontal displacement	254 mm
Vertical displacement measurement	Midpoint of specimen
Specimen gripping system	Modified metal connector plates
Minimum displacement rate	0.01 mm/min
Maximum sustained sinusoidal frequency (± 25 mm)	4 Hz
Maximum burst displacement rate (100 mm)	1 m/s

Table 3.1: Specifications for dynamic direct shear machine.

3.2.1 Shearing System

The mechanical shearing system used in the Fox et al. (1997) device is too slow for general dynamic loading. The new machine uses a hydraulic shearing system to achieve the necessary accelerations. A GCL test specimen is placed in the test chamber and sheared by a hydraulic actuator positioned horizontally in front of the specimen. The maximum displacement of the actuator piston is 254 mm, which is sufficiently large to allow for the measurement of residual or near-residual shear strengths in most cases. The actuator (model 244.31) was manufactured by MTS Systems Corporation of Eden Prairie, Minnesota, and has a capacity of 245 kN, which corresponds to a maximum applied shear stress of 750 kPa. An axial load cell designed for dynamic loading is incorporated into the piston to measure applied shear forces on the test specimen. The actuator also contains a linear variable displacement transformer (LVDT) for measurement of piston displacement.

The actuator is driven by a 340 liter/min hydraulic pump and a hydraulic manifold that includes 19 liters of accumulation to better allow the actuator to achieve peak response. Piston motion is computer-controlled using a three-stage servo-hydraulic valve such that essentially any type of displacement-controlled or stress-controlled time-history, including monotonic loading, is possible. For static shear tests, the system is capable of displacement rates as low as 0.01 mm/min. This is ten times slower than the maximum displacement rate recommended by Fox et al. (2004) for internal shear of hydrated GCLs. Figure 3.4 shows the theoretical performance of the shearing system for sinusoidal piston motion and three values of constant axial force. These curves indicate that performance is insensitive to axial force, displacement amplitude drops off markedly

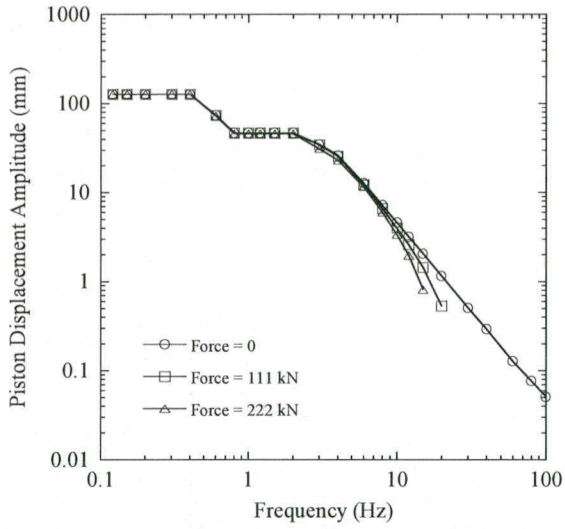

Figure 3.4: Performance curves for shearing system.

as frequency increases, and an amplitude of 25 mm can be sustained at a frequency of approximately 4 Hz. Actual tests of the system revealed similar capabilities and also indicated that a triangular wave at ±25 mm (zero force) can be sustained at a higher piston frequency of 5 Hz. For burst dynamic loading (i.e., single thrust), the accumulators allow the actuator to achieve 100 mm displacement in 0.1 sec, at zero force.

Shear forces are transferred to the test specimen through an aluminum pullout plate measuring 305 × 1500 × 22 mm. The pullout plate is coated for corrosion resistance and is bolted to the actuator at the front of the test chamber. This plate is lighter and thicker than the Fox et al. (1997) counterpart so that it has lower inertial effects and more resistance to buckling under compressive loads. The pullout plate is 433 mm longer than the test chamber, 152 mm of which is required for attachment to the actuator. The remaining 281 mm allows the pullout plate to move into the rear of the test chamber to maintain a constant shearing surface area during testing. An aggressive gripping surface is attached to the floor of the test chamber and the underside of the pullout plate, with the test specimen placed in between. To maintain alignment of the piston with the pullout plate, the actuator is bolted to the rear of the machine frame through slotted holes which, in conjunction with two height-adjustment screws, allow for 250 mm of vertical travel of the actuator assembly to accommodate specimens of varying thickness. The gripping surface consists of modified metal connector plates (i.e., truss plates) that are used for wood truss construction (Fox et al. 1997). Each truss plate measures 305 × 305 mm and contains 864 teeth protruding from one side. The teeth for the Fox et al. (1997) device were cut to have a triangular profile and a maximum height of 2 mm. For the current machine, the truss plate teeth were cut to be 1-2 mm tall and

have a flat (i.e., rectangular) profile to facilitate gripping in both directions during dynamic loading. The truss plates are made of galvanized steel and will deteriorate over time, although the original plates used by Fox et al. (1997) were still effective after two years of near-continuous use. This gripping surface is sufficiently rough that end-clamping of the geosynthetics is not needed, which allows a specimen to fail along the weakest surface and avoids possible progressive failure effects during shear (Fox et al. 1997, Fox and Stark 2004).

3.2.2 Normal Stress and Vertical Displacement Measurement System

The dynamic direct shear machine was designed to accommodate a maximum normal stress of 2000 kPa, which will allow it to produce performance shear data for landfills approaching 150 m in height. Normal stress is applied using two rubber air bags that rest on a rigid aluminum load plate. These custom-made bags are bellowed so they can expand without tensioning the rubber, which would possibly reduce the applied normal stress. Each bag reacts against a top plate, which in turn reacts against three aluminum reaction beams that transversely span the top of the test chamber. Depending on the thickness of the test specimen, wood spacer blocks of various sizes are used to fill the void space between the top plates and the reaction beams. The air bags are enclosed laterally by front and rear face plates, the walls of the test chamber, and a transverse fin that spans the middle of the load plate. Given the opportunity, the bags will burst into any small crack between the various plates, especially at high pressure. The edges and corners of the air bags are carefully protected during machine assembly with custom-made plastic forms and reinforced cloth to prevent such bursting. Vertical displacement

of the load plate due to specimen volume change is continuously monitored during hydration, consolidation, and shearing using an LVDT. This LVDT is mounted above the reaction beams and senses the motion of the load plate through a thin vertical brass rod that rests on the midpoint of the top surface of the fin.

A layer of 517 free-rolling stainless steel balls (dia. = 19.1 mm) is placed between the load plate and the pullout plate to reduce machine friction. The balls cannot roll directly on the load plate or pullout plate because the aluminum is too soft. To avoid this problem, two smooth bearing plates are placed above and below the rolling ball layer. These plates are 3.2 mm thick and are made of tempered 301 stainless steel with a Rockwell hardness of C36-C37, which was selected in order to match the hardness of the stainless steel balls. The balls are placed 25.4 mm on center over the top surface of the pullout plate. A 12.7 mm-thick plastic guide plate, having 517 holes, is used to hold the balls in position during machine assembly. As the pullout plate moves forward, rows of balls exit from underneath the front edge of the load plate and are replaced by identical rows at the rear such that the distribution of normal force on the pullout plate remains unchanged. The same rolling ball system was used for the Fox et al. (1997) device. All bearing surfaces and the 517 rolling balls are cleaned after each test to maintain consistently low frictional resistance for the machine.

Proper control of air pressure for the dynamic direct shear machine is more challenging than for a static shear machine because of potentially rapid specimen volume changes that can occur during dynamic loading. Air pressure is generated using an air amplifier that increases the building air pressure by a factor of four to a maximum of 2500 kPa. The amplifier fills a pair of 18-liter air tanks that are mounted under the shear

box. The first air tank is filled directly by the air amplifier to a pressure larger than that required for a given shear test. Air from the first tank then passes through a regulator to fill the second air tank at the desired (lower) pressure for testing. The second tank is connected directly to the air bags through a large diameter flexible hose with minimal resistance, thus the air bags have direct access to a reserve of additional air under the same pressure. The air pressure in the bags and second tank is measured using a high-accuracy digital test gage. Repeated observations have indicated that this system typically maintains the applied normal stress during dynamic loading to within 1% error. The weight of components below the air bags adds an additional 2.9 kPa to the normal stress on the test specimen.

3.2.3 Specimen Hydration System

The dynamic shear machine provides both sides of a GCL specimen with full access to water throughout hydration, consolidation, and shearing. A water reservoir at the rear of the test chamber supplies water to a series of longitudinal and transverse channels that were milled into the underside of the pullout plate and the floor of the test chamber. The truss plates are screwed to each of these surfaces with a stainless steel screen placed in between to reduce clogging of the channels and further facilitate drainage. Each 305 × 305 mm truss plate contains 432 holes (i.e., one for each pair of teeth) which, taken together, provide a GCL specimen with access to water through 3024 drainage holes. The water level in the reservoir is maintained at the top of the pullout plate using a float value. Water flow is collected at the front of the test chamber in a drip

pan and channeled to a floor drain. Water content measurements have indicated that GCL specimens are uniformly hydrated using this system (see section 4.4.7).

3.2.4 Process Control and Data Acquisition System

The dynamic direct shear machine has a fully automated process control and data acquisition system developed by MTS. The system consists of a FlexTest SE digital servocontroller that has channels for the hydraulic pump, manifold, servo-hydraulic valve, load cell, piston displacement LVDT, vertical displacement LVDT, and PC interface. The PC interface provides complete control over the testing system, including pump and manifold functions, piston motion, and data sampling rates. Data acquisition has 16 bit resolution and a maximum sampling rate of 6 kHz.

3.2.5 Machine Calibration

The load cell within the dynamic shear machine piston was calibrated to verify its accuracy in force measurement. This was accomplished by first calibrating an auxiliary load cell using dead weights. A spring was then compressed between the auxiliary load cell and the actuator by moving the piston to various displacements. In this manner, force measurements from the two load cells could be compared to one another, as shown in Figure 3.5. This plot indicates that the actuator load cell is accurate to within 99%, even in the low range. This accuracy was found to repeatable by conducting multiple calibration tests.

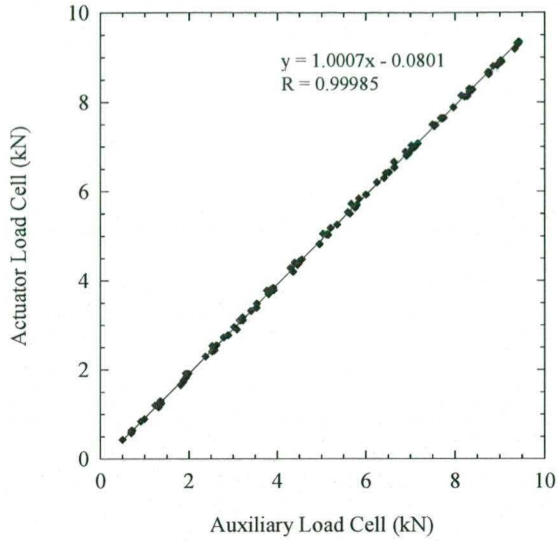

Figure 3.5: Dynamic shear machine load cell calibration data.

The frictional resistance of the rolling ball system was also assessed in order to account for its contribution to measured force during testing. To conduct this calibration, the test chamber floor (which has water channels milled into and gripping teeth attached to it) was replaced with a smooth plate of equal dimension. A layer of 440 rolling steel balls, held in place by a guide plate, along with a set of bearing plates was placed on the smooth test chamber floor. A pullout plate, smooth on both sides but otherwise identical to that used for shear testing, was placed on this lower layer of steel balls. The remainder of the machine components were then constructed in the normal fashion. The actuator was connected to the smooth pullout plate and force measurements were recorded while the piston displaced 25 mm. Frictional resistance remained nearly constant throughout the shear displacement, and the total average stress value is plotted against applied normal stress in Figure 3.6. Three separate trials were conducted using this procedure. Trial 1 consisted of sequential increases in normal stress without disassembling the

machine, thus the balls traveled in the same grooves in the bearing plates at all normal stresses. For Trial 2, the normal stress was reduced to the lowest value without disassembling the machine and an identical repeat of Trial 1 was completed. The measured resistances are lower, as expected, since the balls were again traveling within the same grooves. In Trial 3, the machine was completely disassembled, the balls were moved position on the bearing plates, and the machine was then reassembled prior to application of each normal stress. Thus this trial represents the balls bearing on virgin material that has experienced no prior deformation. As expected, Trial 3 exhibited the highest frictional resistance.

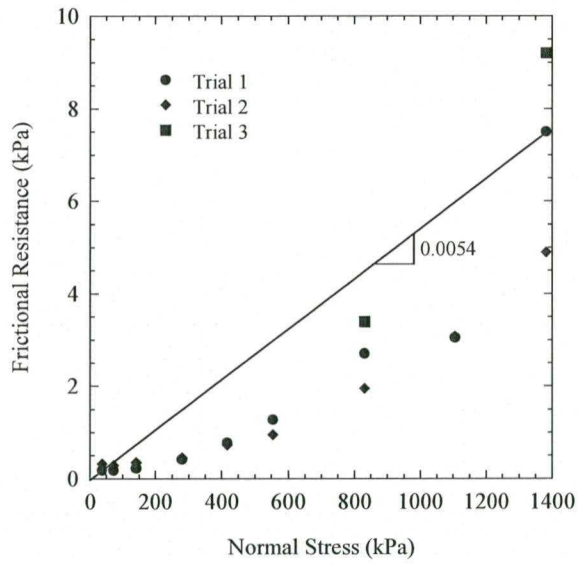

Figure 3.6: Dynamic shear machine friction calibration (two sets of rolling balls).

The measured machine resistance to shearing indicates a nonlinear increase with increasing normal stress. Since this frictional resistance is dependent on deformation of the bearing plates, which in turn depends on the exact location of the steel balls during

machine assembly, using a nonlinear function to describe this resistance would not reflect these inherent variabilities. Therefore it was decided to characterize the friction using a linear function. Since it is likely that permanent grooves will form in which the balls will travel, the resistance value of 7.5 kPa at a normal stress of 1382 kPa was used to determine the linear function. This provides a conservative estimate of the frictional resistance to be 0.54% of the applied normal stress. However, only one set of balls is used during shearing of a test specimen, therefore the shear force required to overcome rolling friction for this system is half of that shown in Figure 3.6, or 0.27% of the applied normal force with a corresponding friction angle of 0.15°. This value agrees with the 0.26% measured by Scheithe (1996), who used a similar rolling ball system.

CHAPTER 4

TESTING PROCEDURES AND RESULTS

4.1 Introduction

Although waste disposal facilities and other facilities with geosynthetic liner systems are commonly constructed in seismic regions, limited data exists for the dynamic shear behavior of some common types of geosynthetics, such as geosynthetic clay liners. Only one investigation has studied the dynamic internal shear strength (Lai et al. 1998) and two investigations have studied the dynamic interface shear strength (Lo Grasso et al. 2002, Kim et al. 2005) of GCLs. These investigations have provided some insight on the dynamic shear behavior of GCLs and GCL interfaces but have not included vital information, such as internal strengths of reinforced products, textured geomembrane/GCL interface strengths, and shear behavior at high normal stress levels. In addition, information is needed on dynamic friction angles, shear stiffness reduction and damping ratios, and the effect of various parameters (e.g., amplitude, frequency, and waveform) on response. A laboratory testing program was developed to address some of these issues for the dynamic internal shear behavior of a hydrated needle-punched GCL. Monotonic and cyclic displacement-controlled shear tests were performed to investigate the effects of displacement rate, displacement amplitude, number of cycles, excitation

frequency, and motion waveform on material response at a single normal stress level. Comparison of the test data gives insight with regard to mechanisms of dynamic shear strength as well as critical parameters and analysis methods to guide a broader testing program that includes multiple normal stress levels. Testing equipment and procedures are described, followed by test results and analyses, including post-cyclic static shear strengths and the first stiffness reduction and damping ratios reported for a GCL product. A substantial portion of the information provided herein has been presented in Nye and Fox (2006).

4.2 Laboratory Testing Program

4.2.1 GCL Material

The experimental program was conducted using Bentomat ST, a woven/nonwoven (W/NW) needle-punched (NP) GCL with no thermal bonding manufactured by CETCO (Arlington Heights, Illinois). This GCL product is composed of granular bentonite held between a woven slit-film polypropylene geotextile (105 g/m^2) and a nonwoven needle-punched polypropylene geotextile (200 g/m^2). The bentonite has a nominal minimum mass/area of 3.7 kg/m^2 at zero water content. To provide reinforcement, polypropylene fibers from the nonwoven geotextile are needle-punched through the bentonite and the woven geotextile. The average peel strength of the material used for the monotonic and cyclic tests (different rolls), as obtained from 10 peel tests each (ASTM D 6496), was 1580 N/m and 1050 N/m, respectively.

4.2.2 Procedures

GCL specimens were cut parallel to the factory roll direction of the product and hydrated using the two-stage procedure described by Fox et al. (1998) and Fox and Stark (2004). The woven geotextile for each specimen was cut to a length of 1327 mm (i.e., 260 mm longer than the test chamber) and the nonwoven geotextile was cut to a length of 1067 mm. For the first stage of hydration, each specimen was placed in a shallow pan and the appropriate amount of tap water was added to bring the specimen to the estimated final water content for the test. These final water content values vary with normal stress and were obtained from previous direct shear tests using the same GCL product. The specimens were covered to minimize evaporation and allowed to cure for two days under a 1 kPa vertical stress. For the second stage of hydration, the bottom of the test chamber was flooded with water to remove air from the drainage holes and hydration channels. The GCL specimens were placed on the lower shearing surface with the woven geotextile facing upward against the pullout plate. The normal stress system was assembled, a shearing normal stress $\sigma_{n,s}$ of 141 kPa was applied, and the specimens were hydrated for an additional one to two days with free access to water through the hydration system of the machine.

Figure 4.1 presents example volume change measurements for a GCL specimen during second-stage hydration in the shear machine under the applied normal stress of 141 kPa. Negative values of vertical displacement indicate volume decrease. Some of the initial volume change is due to seating of the machine components and embedding of the gripping teeth into the geotextiles. The specimen essentially reached constant volume within 6 h. Considering that full GCL hydration using conventional procedures will often

require 10 to 20 days (Gilbert et al. 1997), Figure 4.1 corroborates the findings of Fox et al. (1998) and Triplett and Fox (2001) that the two-stage procedure is highly effective in reducing GCL hydration time in the shear machine.

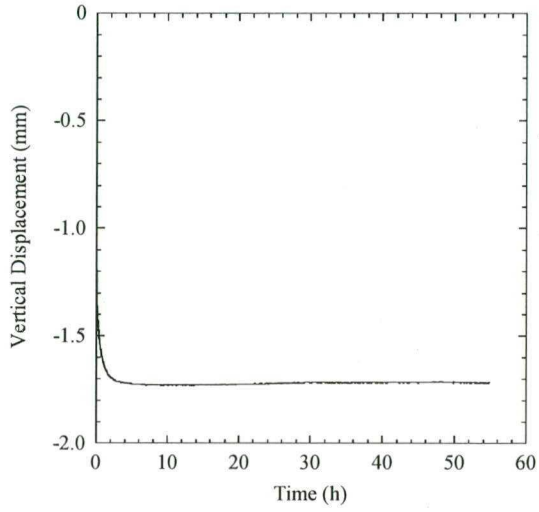

Figure 4.1: Vertical displacement during 2nd stage hydration.

Once hydrated, the GCL specimens were subjected to monotonic or cyclic internal shear at $\sigma_{n,s}$ = 141 kPa. Eighteen displacement-controlled monotonic (i.e., single direction) shear tests were conducted to evaluate the effect of shear displacement rate R on peak and residual dynamic shear strengths. Displacements rates ranged from 0.1 to 30,000 mm/min, the high end of which is approximately three orders of magnitude greater than those achieved in previous investigations (Fox et al. 1998, Eid et al. 1999). The lowest rate (R = 0.1 mm/min) is the recommended maximum value for conventional static shear testing of the internal shear strength of hydrated GCLs (Fox et al. 2004).

Fifteen displacement-controlled cyclic shear tests were conducted on the remaining hydrated GCL specimens to investigate the effects of displacement amplitude Δ_a, number of cycles N, excitation frequency f, and motion waveform on material response. The baseline test consisted of 50 cycles of sinusoidal displacement with Δ_a = 15 mm and f = 1.0 Hz. Deviations from these conditions were then made to investigate each parameter individually. Tests were conducted for Δ_a = 2, 5, 10, 15, 20, and 25 mm and f = 0.1, 0.5, 1, 2, and 3 Hz. Additional tests were performed for N = 10 and 100 as well as for square and triangular input wave motions. Following each cyclic test, the pullout plate was disconnected from the actuator and the specimen was permitted to rest under the same normal stress (141 kPa) and zero shear stress for 24 h. The specimen had free access to water during this time and could consolidate or swell as needed. Volume change measurements were continuously recorded. After the 24 h rest period, each specimen was sheared at R = 0.1 mm/min (constant) to obtain the post-cyclic, peak and residual, static shear strengths. An additional static shear test was performed on a fresh specimen of this GCL material (peel strength = 1050 N/m) for comparison with the cyclic and post-cyclic shear data.

After each test was completed, the GCL specimen was immediately removed from the test chamber and five water content measurements were taken. The mode of failure was recorded along with any indications of localized distress, such as tearing, necking, or wrinkling of the geotextiles or areas where the reinforcement had not failed.

4.3 Monotonic Shear Results

Representative shear stress τ versus shear displacement Δ relationships for the monotonic tests are shown in Figure 4.2. The curves are generally similar in shape, with

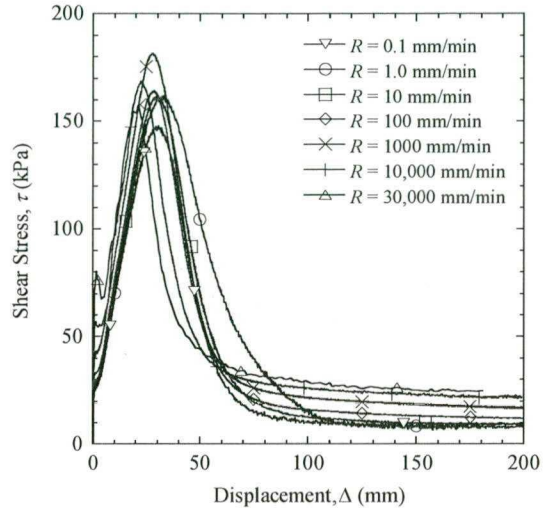

Figure 4.2: Shear stress-displacement relationships for seven monotonic shear tests.

well-defined peak shear strengths and large post-peak strength reduction due to failure of the reinforcement. Values of peak shear strength τ_p and residual shear strength τ_r are shown in Figure 4.3 as a function of displacement rate. An average static τ_p of 156 kPa was measured for R = 0.1 mm/min. With increasing displacement rate, τ_p increased to 186 kPa at R = 1000 mm/min and then decreased to 151 kPa at R = 30,000 mm/min. Thus, peak strength at the highest rate was slightly less than the static value and 20% less than the highest value measured at R = 1000 mm/min. Displacements at peak strength, also shown in Figure 4.3, were approximately 30 mm at the slow rates and progressively decreased to 21 mm at the highest rate. Residual shear strengths were relatively constant

at 11 kPa for $R \leq 10$ mm/min and then increased to 24 kPa at $R = 30{,}000$ mm/min. The secant static residual friction angle for the slow rates is 4.5°, which is in excellent agreement with values obtained in previous investigations (Müller-Vonmoos and Løken 1989, Fox et al. 1998). The secant dynamic residual friction angle at the highest rate is 9.7°, which corresponds to an increase of approximately 1° for each log cycle of R.

Plots of corresponding volume change behavior during shear are shown in Figure 4.4, where negative values indicate GCL contraction. Displacement rate had a clear effect on shear-induced volume change. Similar to Fox (2006), the data indicate that volumetric contraction decreased with increasing displacement rate, which may have resulted from less time available for compaction/restructuring of unsaturated bentonite under higher mean stress conditions during shear. Bentonite consolidation may have also played a role for the slower tests. GCL specimens experienced similar and small volume changes at the faster rates. Figure 4.4 suggests that increasing displacement rate caused increasingly positive pore pressures and that pore pressures for the faster tests were similar in magnitude.

Taken together, Figures 4.2-4.4 reveal interesting trends. Most previous studies have indicated that peak shear strength generally increases with increasing displacement rate. One notable exception is the Zornberg et al. (2005) study, which showed that peak strength of an NP GCL decreased with increasing displacement rate at high normal stress (520 kPa) – possibly due to generation of positive pore pressures. The effect of displacement rate in Figure 4.3 is more complex and cannot be readily explained on the basis of presumed pore pressures alone. As peak strengths increased from $R = 0.1$ to 1000 mm/min, volume change data suggests progressively increasing pore pressures. As

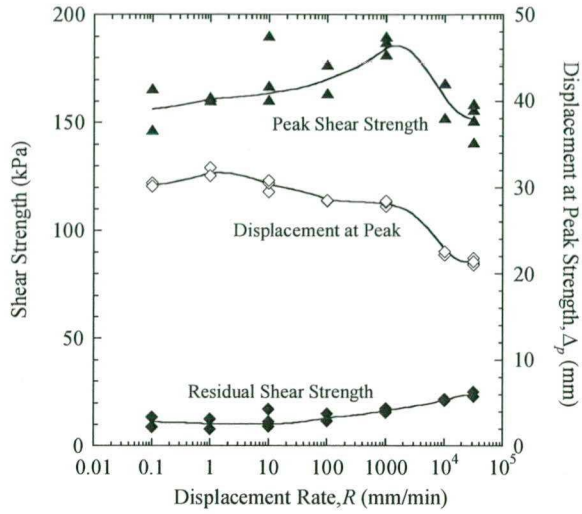

Figure 4.3: Effect of displacement rate on τ_p, Δ_p, and τ_r for monotonic shear.

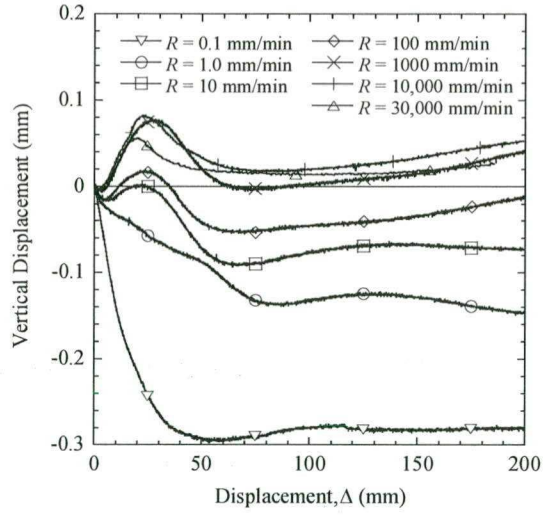

Figure 4.4: Volume change behavior for seven monotonic shear tests.

peak strengths decreased for R = 1000 to 30,000 mm/min, volume change behavior suggests similar pore pressures. Thus, a different mechanism may be primarily responsible for the observed displacement rate effect; possibly an increasing and then decreasing resistance of reinforcing fibers as R increases. While rapid shearing has been credited with increasing reinforcement strength (Stark and Eid 1996), shearing for R > 1000 mm/min may cause a decrease in peak strength as the reinforcing fibers are subjected to impact loads rather than being gradually tensioned. The general increase of residual shear strength with displacement rate is consistent with Fox et al. (1998) and is also not readily explained by presumed pore pressure effects. Rate-dependent shear resistance of the bentonite itself is likely responsible for this trend.

4.4 Cyclic Shear Results

4.4.1 Material Response

An example of the fundamental response of a hydrated W/NW NP GCL to cyclic shearing is presented in Figures 4.5-4.9. This specimen was subjected to 50 cycles of sinusoidal displacement with Δ_a = 10 mm and f = 1.0 Hz. Shear displacement for the first 6 s of the ±15 mm cyclic shear test is shown in Figure 4.5. Negative values correspond to piston extension. Shear displacement followed a sinusoidal wave with the required constant amplitude and frequency. Measured shear stresses for the full duration of this test are shown in Figure 4.6. The maximum shear stress τ_m was 98 kPa for the first cycle and decreased nonlinearly for subsequent cycles to a near-steady value of 46 kPa for the 50th cycle. The shear stress versus displacement diagram, shown in Figure 4.7, indicates the same progressive softening behavior during cyclic loading. The

hysteretic response is broadly similar to that for natural soils (e.g., Kramer 1996), although some differences are observed. First, the tangent modulus increases as the displacement amplitude is approached for each cycle and the needle-punched reinforcement is engaged. Second, the plot indicates essentially constant shear strength during the middle of each cycle. Since the reinforcement is not tensioned, these values correspond to the dynamic shear strength of hydrated bentonite and are essentially constant due to the thin failure zone and the large displacements involved. Figures 4.6 and 4.7 show that this dynamic strength decreases slightly with increasing N, which may reflect progress toward a residual shear condition or the generation of pore pressures along the shearing surface. The dynamic shear strength of the bentonite was 25.4 kPa during the 50^{th} cycle, which corresponds to a secant dynamic friction angle of 10.2°. The post-cyclic static shear test on this specimen yielded a residual friction angle of 5.0°. Considering that the average displacement rate for the cyclic test (40 mm/s) was 24,000 times faster than that for the static test (0.1 mm/min), the bentonite friction angle at 50 cycles increased, on average, by 1.2° for each log cycle of R.

Volume change behavior for the hydrated GCL during cyclic shear is shown versus time and displacement in Figures 4.8 and 4.9, respectively. This data indicates a progressively decreasing rate of contraction and is surprisingly similar to the behavior of drained sand during cyclic shear (Youd 1972). In general, the majority of volumetric contraction is achieved on the return stroke of each half-cycle. Early cycles also display

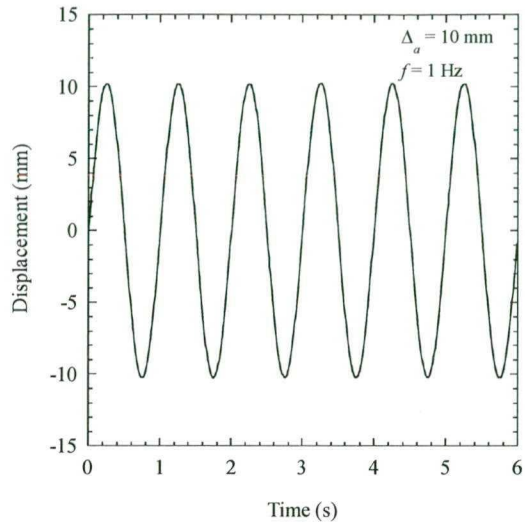

Figure 4.5: Displacement vs. time for first 6 s of ± 10 mm cyclic test.

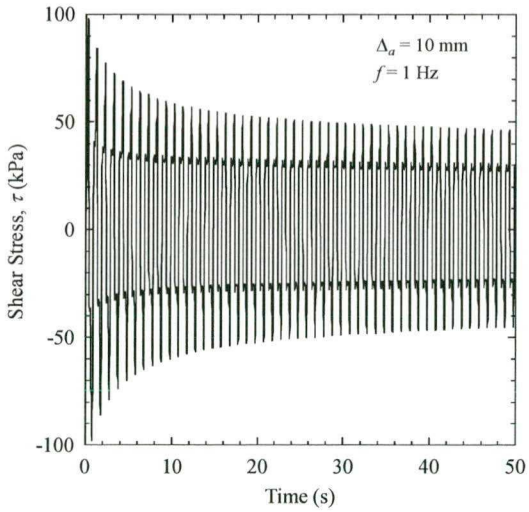

Figure 4.6: Shear stress for ±10 mm cyclic shear test.

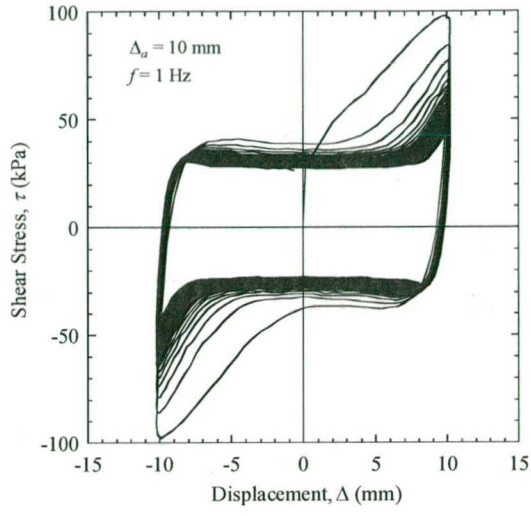

Figure 4.7: Shear stress vs. displacement for ±10 mm cyclic shear test.

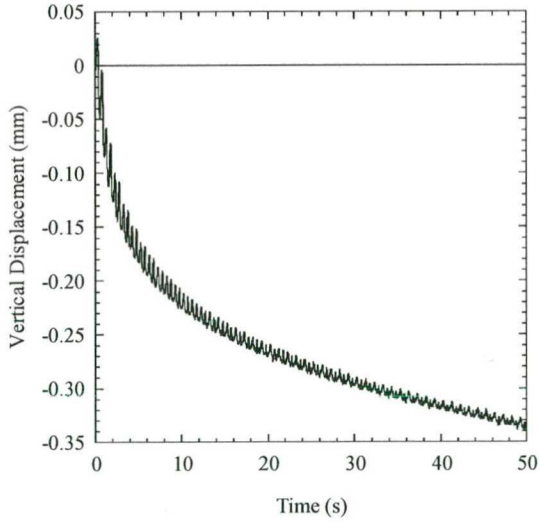

Figure 4.8: Volume change vs. time for ±10 mm cyclic shear test.

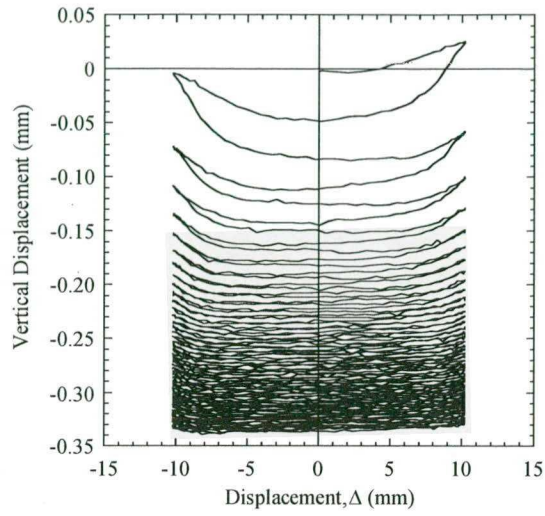

Figure 4.9: Volume change vs. displacement for ±10 mm cyclic shear test.

a pronounced expansive response as the displacement amplitude is approached and the reinforcement is engaged. Interestingly, tensioning of the reinforcement near the displacement limit might be expected to produce specimen contraction but Figure 4.9 clearly shows this was not the case. This volume change behavior appears similar to that shown by Hsu and Vucetic (2004) for a nearly saturated undisturbed low plasticity clay and may likewise be due primarily to compaction/restructuring of unsaturated bentonite into a denser configuration at constant water content. The contractive behavior may have also resulted from gradual embedment of the gripping teeth into the geotextiles, vertical extrusion of bentonite into voids of the geotextiles, and lateral migration of bentonite out of the edges of the specimen during cyclic shear. The displacement rate for this test was too fast for bentonite consolidation to play a significant role.

4.4.2 Effect of Displacement Amplitude

To study the effect of displacement amplitude on cyclic shear behavior, five additional tests were conducted with Δ_a = 2, 5, 15, 20 and 25 mm (f = 1 Hz, N = 50). The upper half of each shear stress envelope (i.e., τ_m for each cycle) is plotted in Figure 4.10. Maximum shear stress for the first cycle increased with increasing displacement amplitude, with bounding values of 39.8 and 142 kPa measured for the ±2 and ±20 mm tests, respectively. The ±25 mm test produced a slightly lower value (134 kPa), which is attributed to material variability. Similar to Figure 4.6, τ_m decreased nonlinearly for subsequent cycles in each case. The tests with lower Δ_a (2 to 15 mm) showed gradual decreases in peak stress with cycling, whereas more abrupt decreases occurred for high Δ_a (20 and 25 mm) due to failure of the reinforcement during the first few cycles. Interestingly, the ±10 mm test had the highest values of maximum shear stress after the first cycle. Corresponding volume change measurements, shown in Figure 4.11, indicate that each specimen contracted at a decreasing rate with continued cycling. The magnitude of volume reduction increased with increasing Δ_a up to 15 mm and then this trend reversed, with the ±20 and ±25 mm tests experiencing less overall contraction. This reversal is uncharacteristic of the vertical strain behavior of natural and compacted clays under cyclic loading (Chu and Vucetic 1992, Hsu and Vucetic 2004) and likely results from the effect of reinforcement failure.

The shear stress vs. displacement relationship for the first cycle of each test is compared in Figure 4.12. The curves are nearly identical for the first quarter cycle, with slight deviations attributed to material variability and displacement rate effects. The

remaining part of each curve is reasonably symmetric for tests with $\Delta_a \leq 15$ mm; however, the ±20 and ±25 mm tests experienced a marked decrease in shear strength and stiffness during the second half-cycle due to reinforcement failure. Shear stresses for subsequent cycles of the ±20 and ±25 mm tests (not shown in Figure 4.12) remained nearly constant for all shear displacements and were essentially controlled by the bentonite once the reinforcement was ruptured during the initial cycle (see related figures

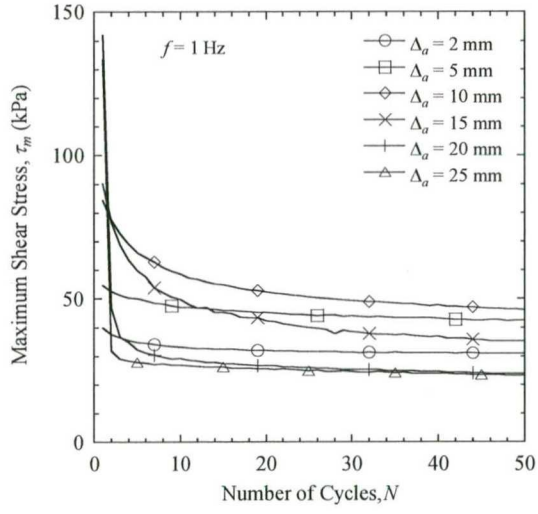

Figure 4.10: Shear stress envelopes for six cyclic shear tests with varying displacement amplitude.

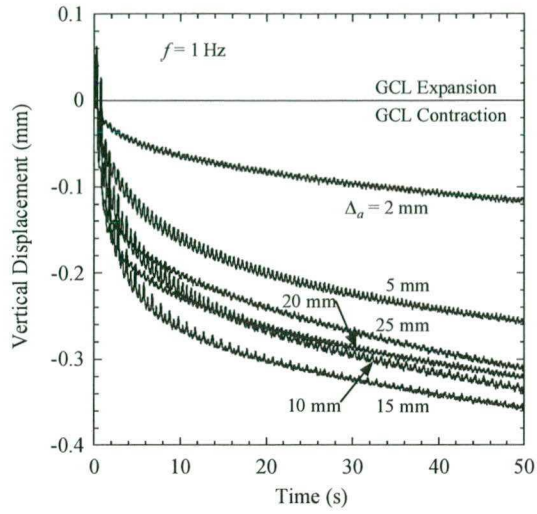

Figure 4.11: Volume change behavior for six cyclic shear tests with varying displacement amplitude.

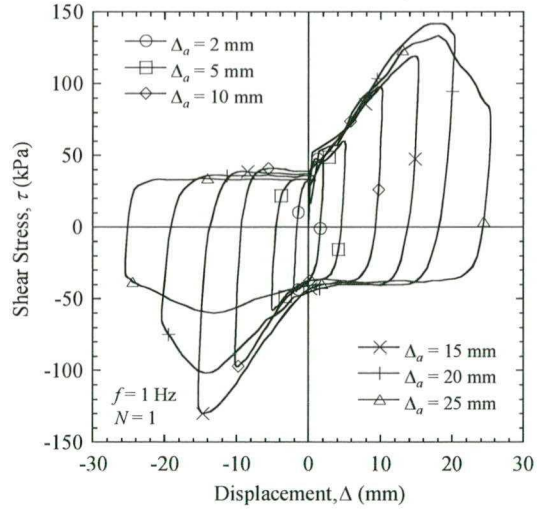

Figure 4.12: Shear stress-displacement curves for first cycle of six cyclic shear tests with varying displacement amplitude.

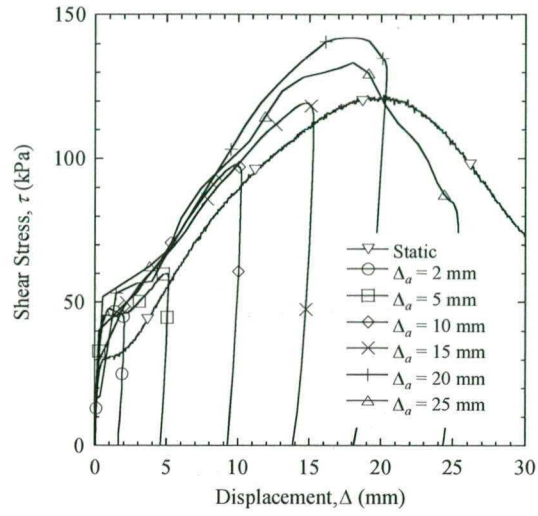

Figure 4.13: Comparison of initial cyclic shear and static shear data.

in Appendix A). The final dynamic friction angle ($N = 50$) for the ±25 mm test was 9.4°, which is in good agreement with the value of 10.2° obtained for the ±10 mm test. A detail view of the first quarter-cycle curves is shown in Figure 4.13, along with the initial portion of the static shear test conducted on a fresh GCL specimen with no prior cyclic loading. This figure shows that static shear data may provide a reasonable approximation for the initial dynamic response until displacement reversal occurs. Cyclic shear stresses exceed corresponding static values at each displacement and appear to be due to displacement rate effects.

During the 24 h rest period after each cyclic test, the GCL specimens either did not change volume or experienced slight swelling with a maximum vertical displacement of 0.01 mm. A static shear test was then conducted on each specimen for $R = 0.1$ mm/min. The τ vs. Δ relationships are shown in Figure 4.14 along with the corresponding relationship from the static shear test ($\Delta_a = 0$). Peak and residual shear

strengths are plotted in Figure 4.15. These figures clearly show that increasing cyclic displacement amplitude yielded progressively lower post-cyclic static peak strength, which is due to greater levels of damage to the needle-punched reinforcement. The reinforcement was almost completely destroyed during the ±25 mm test, leaving the specimen with essentially residual shear strength. Post-cyclic residual shear strengths were unaffected by previous cyclic loading and yield a secant residual friction angle of 4.9°.

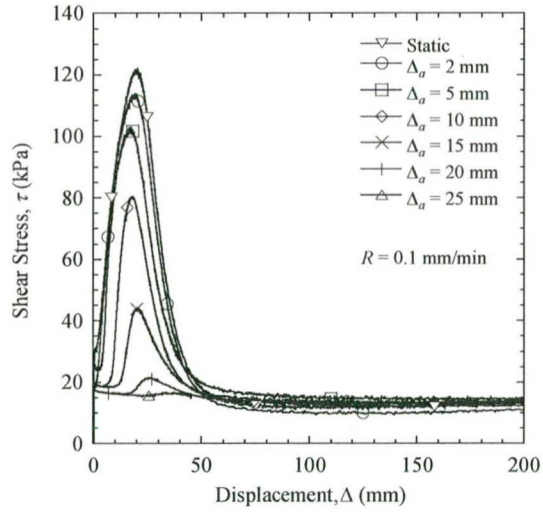

Figure 4.14: Effect of cyclic displacement amplitude on post-cyclic static shear strength.

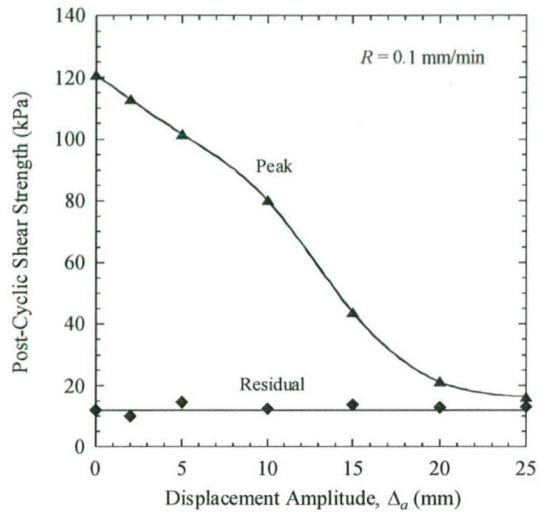

Figure 4.15: Post-cyclic peak and residual static shear strengths.

4.4.3 Equivalent Linear Parameters

An effective means to characterize general shear stiffness and energy dissipation in natural soils under dynamic loading is through the secant shear modulus and damping ratio, as typically used in equivalent linear ground motion analyses (Idriss and Seed 1968). This method was modified for a sand/concrete interface by Desai et al. (1985) and applied to a smooth geomembrane/geotextile interface by Yegian et al. (1998). Similarly, we define a secant shear stiffness K (shear stress per unit displacement) as,

$$K = \frac{K_1 + K_2}{2} = \frac{\tau_{m,1} + \tau_{m,2}}{2\Delta_a} \tag{4-1}$$

where K_1 and $\tau_{m,1}$ are average shear stiffness and maximum shear stress for the first half-cycle, respectively, and K_2 and $\tau_{m,2}$ are corresponding values for the second half-cycle (Figure 4.16). The secant shear stiffness for the entire cycle is taken as the average of

two half-cycle values due to asymmetry in the hysteresis loop, which is observed primarily for large Δ_a and low N. Likewise, damping ratio β is defined as,

$$\beta = \frac{\beta_1 + \beta_2}{2} = \frac{1}{2}\left(\frac{A}{4\pi A_1} + \frac{A}{4\pi A_2}\right) = \frac{A}{4\pi\Delta_a}\left(\frac{1}{\tau_{m,1}} + \frac{1}{\tau_{m,2}}\right) \tag{4-2}$$

where β_1 and β_2 are damping ratios for the first and second half-cycles, respectively, A is the total area enclosed by the loop, and A_1 and A_2 are the areas defined in Figure 4.16.

Figure 4.17 is a plot of maximum shear stress vs. displacement amplitude – the so-called "backbone curve" – for the cyclic shear tests at various N values. Although these points are not taken directly from the stress-displacement curves (Figure 4.16), this method provides a reasonable characterization of material behavior for conditions prior to

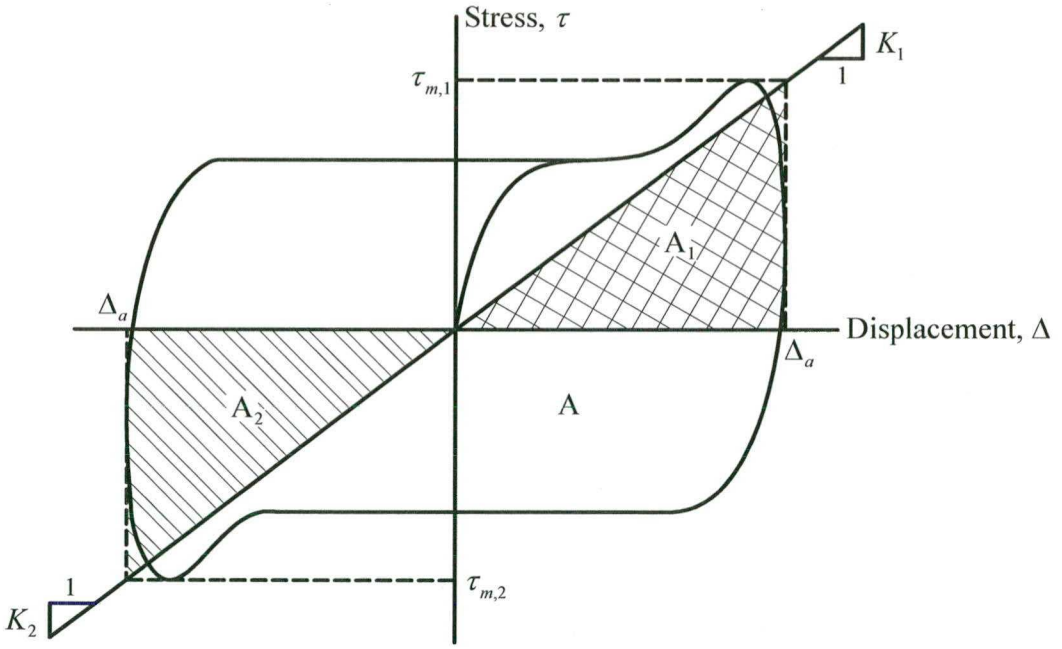

Figure 4.16: Calculation of secant shear stiffness and damping ratio from hysteresis loop.

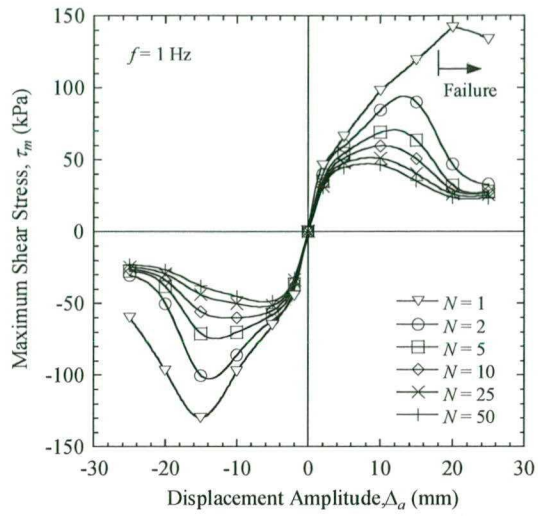

Figure 4.17: Backbone curves for six cyclic shear tests.

failure and has been applied to natural clays (Vucetic 1988) as well as geosynthetic interfaces (Yegian et al. 1998). Figure 4.13 indicates that failure occurred during the first cycle of the ±20 and ±25 mm tests at Δ = 18 mm. Points for these tests have been included for comparison in Figure 4.16 although applicability of the linear equivalent method may be suspect at large displacement levels.

The backbone curves are largely symmetric about the origin but display some asymmetries at higher displacement amplitudes due to reinforcement failure. Corresponding values of shear stiffness K are plotted versus Δ_a in Figure 4.18. These curves indicate strong stiffness reduction with increasing displacement amplitude and stiffness degradation with continued cycling. Both effects are augmented by reinforcement failure for Δ_a > 18 mm, where τ_m drops markedly from the first to second cycles. Figure 4.18 also contains a plot of stiffness reduction obtained directly from the static shear test (Figure 4.13). In this case, static shear data yielded a stiffness reduction

curve that is a reasonable first approximation to that obtained from cyclic testing. The maximum GCL shear stiffness K_{max} is approximately 150 kPa/mm for both static and cyclic tests. K_{max} occurs at very small displacements ($\Delta \approx 0.1$ mm) and reflects the stiffness of the bentonite without the influence of reinforcement. This value was not used to prepare normalized stiffness reduction curves (i.e., K/K_{max}) because its relevance is questionable for typical conditions involving much larger displacements where GCL reinforcement controls behavior.

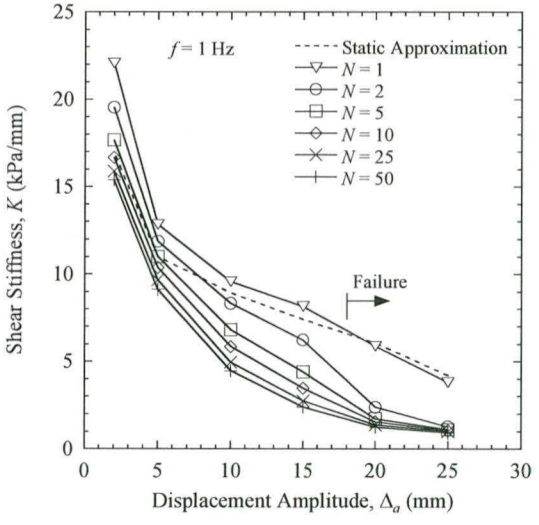

Figure 4.18: Shear stiffness reduction curves.

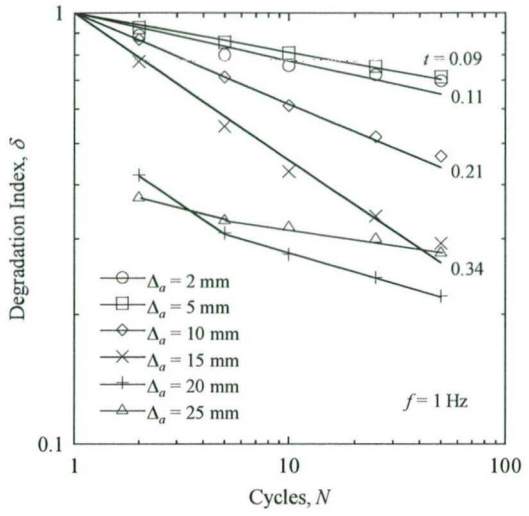

Figure 4.19: Degradation index for six cyclic shear tests.

Stiffness degradation is often characterized using the degradation index δ defined as,

$$\delta = \frac{K_N}{K_1} \tag{4-3}$$

where K_1 and K_N are values of secant shear stiffness for the 1^{st} and N^{th} cycles, respectively. Figure 4.19 shows a plot of log δ vs. log N for each displacement amplitude. These curves are approximately linear and through the origin for $\Delta_a < 18$ mm, and thus define a constant value of the degradation parameter t, where $\delta = N^{-t}$ (Idriss et al. 1978). Similar to natural clays (Vucetic and Dobry 1988), t increases with increasing displacement amplitude. For GCL specimens that failed during the first cycle ($\Delta_a > 18$ mm), the plots do not pass through the origin and $\delta \neq N^{-t}$.

Values of damping ratio β, shown in Figure 4.20, were little influenced by N for $\Delta_a \leq 10$ mm but then increased with increasing N for larger Δ_a. Similar to Figure

4.18, material failure during the first cycle resulted in a strong increase of damping ratio from the first to second cycles. GCL damping ratios in Figure 4.20 are significantly higher than those typically reported for natural clays at much lower shear strain levels (Vucetic and Dobry 1991) and are generally consistent in magnitude with the value of 0.43 calculated by Yegian et al. (1998) for a smooth geomembrane/geotextile interface.

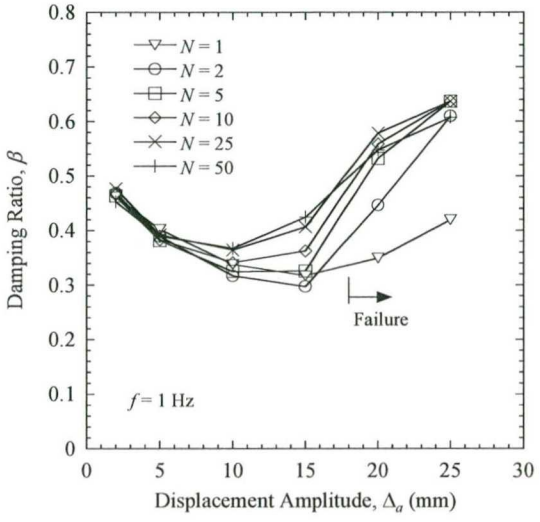

Figure 4.20: Damping ratio for six cyclic shear tests.

4.4.4 Effect of Number of Cycles

Two additional cyclic shear tests were performed to evaluate the effect of 10 and 100 cycles of loading on subsequent static shear strength (Δ_a = 15 mm, f = 1 Hz). Peak and residual post-cyclic static strengths, along with values from the N = 50 test and the static test (N = 0), are shown in Figure 4.21. Peak strengths are relatively constant for the cyclic tests, indicating the majority of reinforcement damage occurred within the first

10 cycles of loading. Similar to Figure 4.15, static residual shear strength was unaffected by prior cyclic shearing.

4.4.5 Effect of Frequency

The effect of input motion frequency on cyclic and post-cyclic GCL shear behavior was investigated by performing four additional sinusoidal tests for f = 0.1, 0.5, 2, and 3 Hz (Δ_a = 15 mm, N = 50). Shear stress envelopes, plotted in Figure 4.22, show no clear trend and indicate that excitation frequency had an insignificant effect on dynamic shear behavior. The maximum difference in τ_m between any two tests is 17% and the majority of data is within 10%. Figure 4.23 presents post-cyclic static shear strengths. Although the data exhibit some scatter, likely due to material variability, the post-cyclic response also appears to be unaffected by frequency.

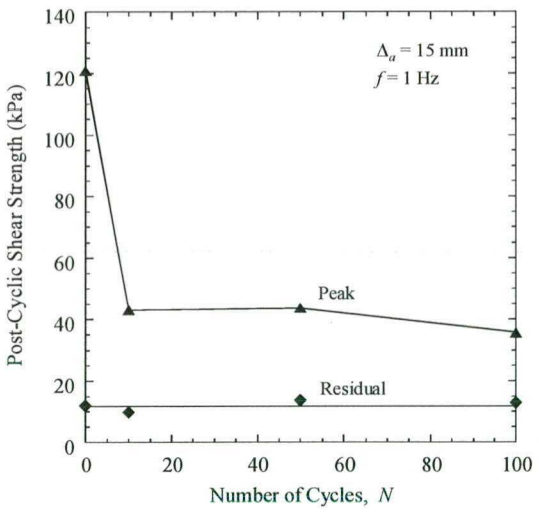

Figure 4.21: Effect of number of cycles on post-cyclic static shear strength.

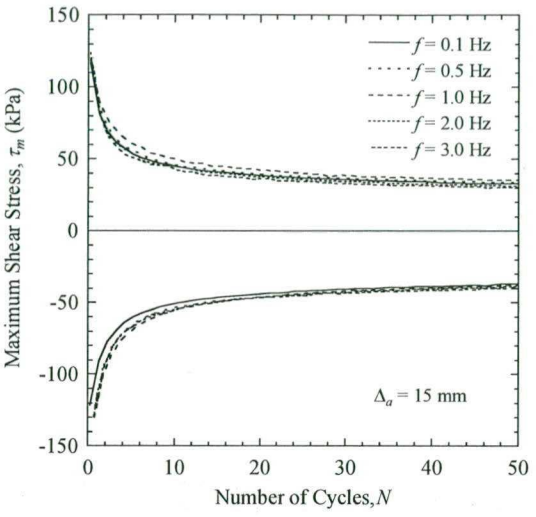

Figure 4.22: Effect of loading frequency on shear stress envelope.

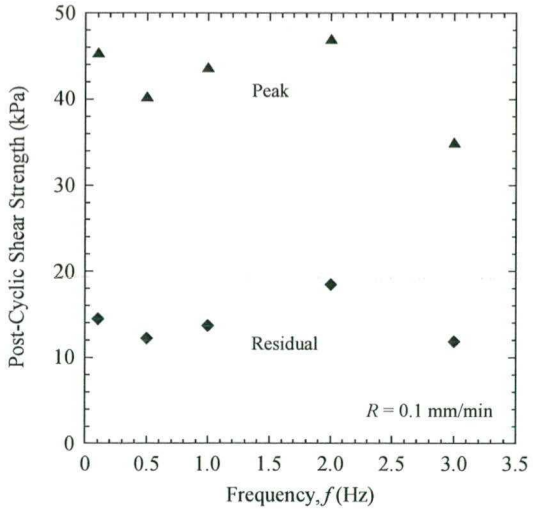

Figure 4.23: Effect of loading frequency on post-cyclic static shear strength.

4.4.6 Effect of Waveform

Shear stress envelopes for three cyclic tests performed using sinusoidal, square, and triangular waves (Δ_a = 15 mm, f = 1 Hz, N = 50) are compared in Figure 4.24. Similar to Figure 4.22, waveform had essentially no effect on the measured dynamic response. This observation is also supported by the post-cyclic static shear tests, shown in Figure 4.25, where shear stress is normalized by dividing by residual shear strength. Tests were performed for two sine wave, one square wave, and one triangular wave specimen. The post-cyclic data resulted in essentially equal values for peak and residual strength, with no sensitivity to waveform.

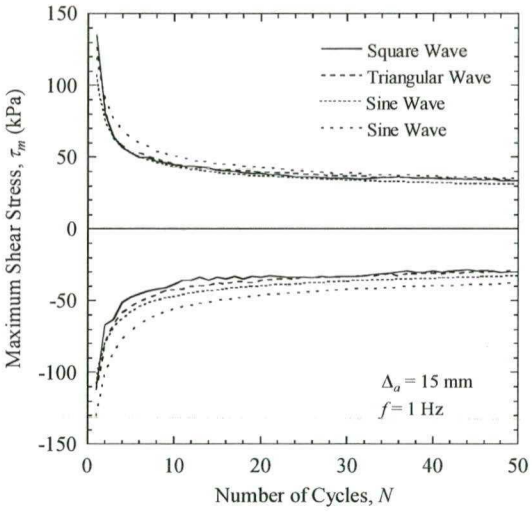

Figure 4.24: Effect of waveform on shear stress envelope.

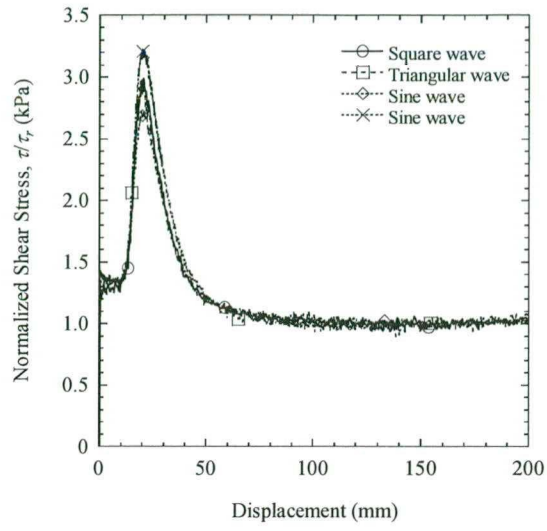

Figure 4.25: Effect of waveform on post-cyclic static shear strength.

4.4.7 Failure Mode and Final Water Content

Inspection of the failed GCL specimens indicated that, in all cases, internal shear failure occurred at or just inside the woven geotextile/bentonite interface. The failures were completely uniform and showed no indications of localized distress, such as wrinkling, necking, or tearing of the geotextiles. In general, more bentonite was extruded laterally from the edges of the cyclic specimens than from static or monotonic specimens, which suggests that some of the observed volume change during cyclic loading may have been due to this mechanism. Figure 4.26 shows a representative photograph of a failed specimen following cyclic and static shearing, where the woven geotextile is pulled back to expose the failure surface. Final water contents for the monotonic and cyclic specimens are provided in Tables 4.1 and 4.2, respectively. No clear trend is apparent for the monotonic specimens, with values ranging from 125 to 172%; however, water contents for the fifteen cyclic specimens were very consistent, with an overall average of

130% and a coefficient of variation (standard deviation/mean) of 3.7%. This data also indicates that GCL specimens are uniformly hydrated using the machine hydration system, where the average value of the coefficient of variation for the distribution of water content within a single GCL specimen is 9.4% for the monotonic tests and 6.0% for the cyclic tests.

Figure 4.26: Failure surface for a hydrated W/NW NP GCL specimen after cyclic and static shearing.

Displacement Rate (mm/min)	Water content (%)					Mean (%)	Standard Deviation (%)	Coefficient of Variation (%)
	Sample 1	Sample 2	Sample 3	Sample 4	Sample 5			
0.1	146.4	137.8	114.1	133.0	176.7	141.6	22.91	16.18
	132.5	125.0	125.5	118.6	122.8	124.9	5.05	4.04
1	206.9	141.5	169.4	148.5	196.0	172.4	28.64	16.61
	162.6	158.6	167.9	147.1	151.5	157.5	8.37	5.31
10	157.0	142.0	159.2	173.8	193.9	165.2	19.63	11.88
	157.0	142.0	159.2	173.8	193.9	165.2	19.63	11.88
	140.8	159.9	154.6	146.0	155.2	151.3	7.70	5.09
100	138.4	149.9	172.4	144.9	144.4	150.0	13.15	8.77
	162.0	154.0	161.9	139.6	136.2	150.7	12.21	8.10
1000	133.0	148.5	154.2	158.9	185.7	156.0	19.25	12.34
	132.7	132.7	161.4	150.0	155.0	146.4	13.08	8.94
	145.9	166.6	162.8	145.0	156.4	155.4	9.74	6.27
10000	123.2	141.6	147.1	135.1	167.0	142.8	16.17	11.32
	128.0	139.2	154.6	150.7	173.9	149.3	17.25	11.55
30000	138.9	129.2	165.3	128.0	153.9	143.1	16.18	11.31
	124.8	130.2	148.7	138.4	153.7	139.2	12.12	8.71
	145.6	163.9	149.1	156.0	168.4	156.6	9.62	6.15
	159.6	145.1	150.6	156.5	142.6	150.9	7.25	4.80
Average for all specimens:						151.0%	14.33%	9.40%
Standard deviation of mean						7.57%		
Coefficient of variation of mean						5.01%		

Table 4.1: Final water contents for monotonic shear specimens.

Test	Water content (%)					Mean (%)	Standard Deviation (%)	Coefficient of Variation (%)
	Sample 1	Sample 2	Sample 3	Sample 4	Sample 5			
1	120.4	138.7	157.1	119.7	135.7	134.3	15.39	11.46
2	118.0	128.6	133.8	142.3	136.9	131.9	9.23	7.00
3	144.6	137.5	121.5	127.5	116.6	129.5	11.46	8.85
4	131.5	118.8	127.5	140.5	134.8	130.6	8.16	6.25
5	130.8	142.2	145.7	137.7	135.5	138.4	5.81	4.20
6	141.4	137.4	115.7	126.4	148.6	133.9	12.96	9.68
7	118.1	127.3	132.7	131.2	114.8	124.8	7.98	6.40
8	138.4	131.9	133.9	127.1	128.5	131.9	4.48	3.40
9	106.4	118.7	132.7	120.9	130.5	121.8	10.51	8.63
10	193.3	120.5	136.1	76.7	122.8	129.9	41.93	32.28
11	123.3	128.3	130.0	135.8	130.9	129.7	4.52	3.49
12	120.3	123.7	129.6	120.2	128.7	124.5	4.50	3.62
13	126.1	129.8	137.0	129.9	130.6	130.7	3.94	3.02
14	126.9	124.2	129.4	121.3	118.5	124.1	4.34	3.50
15	139.8	146.9	134.6	132.8	131.1	137.1	6.41	4.67
Average for all specimens (except Test 10):						130.2%	7.84%	6.01%
Standard deviation of mean						4.79%		
Coefficient of variation of mean						3.68%		

Table 4.2: Final water contents for cyclic shear specimens.

CHAPTER 5

CONCLUSIONS

5.1 Summary

The main objective of this research was to characterize the shear behavior of a hydrated needle-punched (NP) geosynthetic clay liner (GCL) with no thermal bonding when subjected to dynamic loading. To accomplish this task, a dynamic direct shear machine was developed based on the Fox et al. (1997) device that is capable of applying bi-directional (i.e., back-and-forth) loading to a test specimen. Monotonic and cyclic displacement-controlled shear tests were performed to investigate the effects of displacement rate, displacement amplitude, number of cycles, excitation frequency, and motion waveform on material response at a single normal stress level. These tests provided insight with regard to mechanism of dynamic shear strength as well as critical parameters and analysis methods that can be used for future studies.

5.2 Conclusions

The following conclusions are reached based on the design of the new dynamic direct shear machine for GCLs and GCL interfaces:

1. The dynamic direct shear machine tests GCL specimens measuring 305 × 1067 mm. The maximum shear displacement is 254 mm, which is sufficient to measure the residual internal shear strength of hydrated needle-punched GCLs. The machine has a maximum normal stress of 2000 kPa, a maximum shear stress of 750 kPa, and the capability for general stress-controlled or displacement-controlled dynamic loading. The maximum frequency for sinusoidal shearing with a displacement amplitude of 25 mm is 4 Hz. The maximum displacement rate for burst loading (i.e., single thrust) at zero piston force is 1 m/s. Specimen volume change can be measured during hydration, consolidation, and shearing. The machine utilizes an aggressive gripping system that enforces uniform shear failure of a GCL specimen.
2. The machine hydration system is capable of uniformly hydrating GCL specimens, where the average value of the coefficient of variation (standard deviation/mean) for the distribution of water content within a single GCL specimen is 6%.
3. Results presented in this paper corroborate the effectiveness of the two-stage accelerated hydration procedure of Fox et al. (1998). In general, GCL specimens essentially reached constant volume during hydration within 6 h after placement in the shear machine.

The following conclusions are drawn based on an experimental investigation of the monotonic and cyclic shear behavior of a hydrated woven/nonwoven NP GCL at a normal stress of 141 kPa:

1. A series of displacement-controlled monotonic (i.e., single direction) shear tests indicated that peak shear strength first increased and then decreased with

increasing displacement rate R. Peak strength at R = 30,000 mm/min was slightly less than the static peak strength (R = 0.1 mm/min) and 20% less than the highest value measured at R = 1000 mm/min. Residual shear strengths more than doubled from the slowest to the fastest displacement rates. These trends could not be explained solely on the basis of presumed pore pressures and suggest an increasing and then decreasing resistance of reinforcing fibers as R increases.

2. A series of displacement-controlled cyclic shear tests indicated that dynamic response was primarily controlled by displacement amplitude Δ_a. Excitation frequency and waveform had little effect on cyclic shear behavior or post-cyclic static shear strengths. Number of cycles ($N \geq 10$) also had little effect on post-cyclic static shear strengths.
3. For a given cyclic displacement amplitude, hydrated GCL specimens showed nonlinear strength reduction and volumetric contraction with continued cycling. Tests with lower Δ_a (2 to 15 mm) showed gradual decreases in maximum shear stress, whereas more abrupt decreases occurred at higher Δ_a (20 and 25 mm) due to failure of the reinforcement during the first few cycles. Shear stress versus displacement diagrams displayed hysteresis similar to those for natural soils with some differences observed due to presence of reinforcement. GCL specimens experienced essentially no volume change during the 24 h rest period.
4. Cyclic tests with increasing displacement amplitude yielded progressively lower post-cyclic static peak strengths due to greater levels of reinforcement damage. Post-cyclic static residual strengths were unaffected by prior cyclic loading.

5. Secant shear stiffness showed strong reduction with increasing Δ_a and degradation with continued cycling. Both effects were augmented by reinforcement failure for Δ_a > 18 mm, where shear strength dropped markedly from the first to second cycles. Static shear data yielded a stiffness reduction curve that is a reasonable first approximation to that obtained from cyclic testing. For non-failure conditions (Δ_a < 18 mm), degradation index δ could be characterized using the conventional degradation parameter t, where $\delta = N^{-t}$.
6. Damping ratio was essentially independent of N for low displacement amplitudes and increased with increasing N for larger displacement amplitudes. GCL damping ratios were significantly higher than those typically reported for natural clays at lower shear strain levels.
7. Both monotonic and cyclic tests indicated that the secant dynamic residual friction angle increased, on average, approximately 1° for each log cycle of displacement rate.

5.3 Recommendations for Future Study

1. The results of this paper may be used to guide a broader testing program which examines the influence of normal stress on the dynamic shear behavior of a hydrated NP GCL. The capabilities of the dynamic direct shear machine allow for a wide range of normal stresses (maximum of 2000 kPa) to be investigated.
2. Dynamic shear behavior of GCL interfaces, particularly GCL/geomembrane, is important for sustainable design of landfill and other hydraulic liner systems.

Limited studies exist for such interfaces, and reliable data would greatly contribute to the understanding of these materials.

3. Monotonic shear tests performed at other normal stress levels would provide dynamic friction angles that may be used for geosynthetic liner design.
4. At least one monotonic shear test should be performed at a rate slower than those presented in Figure 4.3 (such as 0.01 mm/min) to further define material trends.
5. Subsequent laboratory testing programs should include stress-controlled testing, which would allow for application of specific cyclic stress ratios (shear stress amplitude divided by static shear strength) to determine strength degradation due to cyclic loading.

LIST OF REFERENCES

Anderson, R.L. (1995). "Earthquake Related Damage and Landfill Performance," *Earthquake Design and Performance of Solid Waste Landfills*, Geotechnical Special Publication No. 54, ASCE, pp. 1-16.

ASTM D 5321 (2002). Test Method for Determining the Coefficient of Soil and Geosynthetic or Geosynthetic and Geosynthetic Friction by the Direct Shear Method, American Society for Testing and Materials, Philadelphia, Pennsylvania.

ASTM D 6243 (1998). Test Method for Internal and Interface Shear Resistance of Geosynthetic Clay Liner by the Direct Shear Method, American Society for Testing and Materials, Philadelphia, Pennsylvania.

ASTM D 6496 (2004). Test Method for Determining Average Bonding Peel Strength Between Top and Bottom Layers of Needle-Punched Geosynthetic Clay Liners, American Society for testing and Materials, Philadelphia, Pennsylvania.

Augello, A.J., Matasovic, N., Bray, J.D., Kavazanjian, E. and Seed, R.B. (1995). "Evaluation of Solid Waste Landfill Performance During the Northridge Earthquake," *Earthquake Design and Performance of Solid Waste Landfills*, Geotechnical Special Publication No. 54, ASCE, pp. 17-50.

Berard, J.F. (1997). "Evaluation of Needle-Punched Geosynthetic Clay Liners Internal Friction," *Proceedings of Geosynthetics '97*, Vol. 1, pp. 351-362.

Briancon, L., Girard, H. and Poulain, D. (2002). "Slope Stability of Lining Systems – Experimental Modeling of Friction at Geosynthetic Interfaces," *Geotextiles and Geomembranes*, Vol. 20, No. 3, pp. 147-172.

Chiu, P. and Fox, P.J. (2004). "Internal and Interface Shear Strengths of Unreinforced and Needle-Punched Geosynthetic Clay Liners," *Geosynthetics International*, Vol. 11, No. 3, pp. 176-199.

Chu, H. and Vucetic, M. (1992). "Settlement of compacted clay in a cyclic direct simple shear device," *Geotechnical Testing Journal*, Vol. 15, No. 4, pp. 371-379.

De, A. and Zimmie, T.F. (1998). "Estimation of Dynamic Interfacial Properties of Geosynthetics," *Geosynthetics International*, Vol. 5, No. 1-2, pp. 17-39.

Desai, C. S., Drumm, E. C. and Zaman, M. M. (1985). "Cyclic Testing and Modeling of Interfaces," *Journal of Geotechnical Engineering*, Vol. 111, No. 6, pp. 793-815.

Eid, H.T. and Stark, T.D. (1997). "Shear Behavior of an Unreinforced Geosynthetic Clay Liner," *Geosynthetics International*, Vol. 4, No. 6, pp. 645-659.

Eid, H.T., Stark, T.D. and Doefler, C.K. (1999). "Effect of Shear Displacement Rate on Internal Shear Strength of a Reinforced Geosynthetic Clay Liner," *Geosynthetics International*, Vol. 6, No. 3, pp. 219-239.

Fox, P. J. (2006). Discussion of "Analysis of a Large Database of GCL Internal Shear Strength Results," by Zornberg, J. G., McCartney, J. S., and Swan, R. H., Jr., *Journal of Geotechnical and Geoenvironmental Engineering*, in press.

Fox, P.J., Nye, C.J., Morrison, T.C., Hunter, J.G. and Olsta, J.T. (2006). "Large Dynamic Direct Shear Machine for Geosynthetic Clay Liners," *Geotechnical Testing Journal*, Vol. 29, No. 5, in press.

Fox, P.J., Rowland, M.G. and Scheithe, J.R. (1998). "Internal Shear Strength of Three Geosynthetic Clay Liners," *Journal of Geotechnical and Geoenvironmental Engineering*, Vol. 124, No. 10, pp. 933-944.

Fox, P.J., Rowland, M.G., Scheithe, J.R., Davis, K.L., Supple, M.R. & Crow, C.C. (1997). "Design and Evaluation of a Large Direct Shear Machine for Geosynthetic Clay Liners," *Geotechnical Testing Journal*, Vol. 20, No. 3, pp. 279-288.

Fox, P.J. and Stark, T.D. (2004). "State-of-the-art report: GCL Shear Strength and its Measurement," *Geosynthetics International*, Vol. 11, No. 3, pp. 141-175.

Fox, P. J., Stark, T. D., and Swan, Jr. R. H. (2004). "Laboratory Measurement of GCL Shear Strength," *Advances in Geosynthetic Clay Liner Technology: 2nd Symposium*, STP 1456, R. E. Mackey and K. von Maubeuge, eds., ASTM International, West Conshohocken, Pennsylvania, USA, 92-109.

Gilbert, R.B., Liu, C.N., Wright, S.G. and Trautwein, S.J. (1995). "A Double Shear Test Method for Measuring Interface Strength," *Proceedings*, Geosynthetics 95, pp. 1017-1029.

Gilbert, R.B., Fernandez, F. and Horsfield, D.W. (1996). "Shear Strength of Reinforced Goesynthetic Clay Liner," *Journal of Geotechnical and Geoenvironmental Engineering*, Vol. 122, No. 4, pp. 259-266.

Gilbert, R.B., Scranton, H.B. and Daniel, D.E. (1997). "Shear Strength Testing for Geosynthetic Clay Liners," *Testing and Acceptance Criteria for Geosynthetic Clay Liners, STP 1308*, ASTM International, West Conshohocken, PA, pp. 121-135.

Hillman, R.P. and Stark, T.D. (2001). "Shear Strength Characteristics of PVC Geomembrane-Geosynthetic Interfaces," *Geosynthetics International*, Vol. 8, No. 2, pp. 135-162.

Hsu, C. and Vucetic, M. (2004). "Volumetric threshold shear strain for cyclic settlement," *Journal of Geotechnical and Geoenvironmental Engineering*, Vol. 130, No. 1, pp. 58-70.

Idriss, I. M. and Seed, H. B. (1968). "Seismic Response of Horizontal Soil Layers," *Journal of the Soil Mechanics and Foundations Division*, Vol. 94, SM4, pp. 1003-1031.

Idriss, I. M., Dobry, R., and Singh, R. D. (1978). "Nonlinear Behavior of Soft Clays During Cyclic Loading," *Journal of the Geotechnical Engineering Division*, Vol. 104, GT12, pp. 1427-1447.

Kim, J., Riemer, M. and Bray, J.D. (2005). "Dynamic Properties of Geosynthetic Interfaces," *Geotechnical Testing Journal*, Vol. 28, No. 3, pp. 1-9.

Koerner, R.M., Daniel, D.M. and Bonaparte, R. (1996). "Current Status of the Cincinnati GCL Test Plots," *Proceedings of the 10th GRI Conference on Field Performance of Geosynthetics and Geosynthetic Related Systems*, Drexel University, Philadelphia, Pennsylvania, pp. 147-175.

Koerner, R.M. (2005). *Designing with Geosynthetics*, 5th ed., Prentice Hall, Inc., Upper Saddle River, NJ, 816 pp.

Kramer, S.L. (1996). *Geotechnical Earthquake Engineering*, Prentice Hall, Inc., Upper Saddle River, New Jersey, 653 pp.

Lai, J., Daniel, D.E. & Wright, S.G. (1998). "Effects of Cyclic Loading on Internal Shear Strength of Unreinforced Geosynthetic Clay Liner," *Journal of Geotechnical and Geoenvironmental Engineering*, Vol. 124, No. 1, pp. 45-52.

Lalarakotoson, S., Villard, P. and Gourc, J.P. (1999). "Shear Strength Characterization of Geosynthetic Interfaces on Inclined Planes," *Geotechnical Testing Journal*, Vol. 22, No. 4, pp. 284-291.

Ling, H.I., Burke, C., Mohri, Y. and Matsushima, K. (2002). "Shear Strength Parameters of Soil-Geosynthetic Interfaces Under Low Confining Pressure Using a Tilting Table," *Geosynthetics International*, Vol. 9, No. 4, pp. 373-380.

Lo Grasso, S.A., Massimino, M.R. and Maugeri, D.I.C.A (2002). "Dynamic Analysis of Geosynthetic Interfaces by Shaking Table Tests," *Proceedings, 7th International Conference on Geosynthetics*, Nice, Vol. 4, pp. 1335-1338.

Martin, J.P., Koerner, R.M. and Whitty, J.E. (1984). "Experimental Friction Evaluation of Slippage Between Geomembranes, Geostextiles and Soils," *Proceedings*, International Conference on Geomembranes, pp. 191-196.

Mitchell, J.K. (1993). *Fundamentals of Soil Behavior*, John Wiley and Sons, Inc., New York, New York, 456 pp.

Mesri, G. and Olson, R.E. (1970). "Shear Strength of Montmorillonite," *Geotechnique*, Vol. 20, No. 3, pp. 261-270.

Müller-Vonmoos, M. and Løken, T. (1989). "The Shearing Behavior of Clays," *Applied Clay Science*, Vol. 4, No. 2, pp. 125-141.

Narejo, D.B. (2003). "A Simple Tilting Table Device to Measure Index Friction Angle of Geosynthetics," *Geotextiles and Geomembranes*, Vol. 21, No. 1, pp. 49-57.

Nye, C.J. and Fox, P.F. (2006). "Dynamic Shear Behavior of a Needle-Punched Geosynthetic Clay Liner," *Journal of Geotechnical and Geoenvironmental Engineering*, in review.

Qian, X., Koerner, R. and Gray, D. (2002). *Geotechnical Aspects of Landfill Design and Construction*, Prentice Hall, Inc., Upper Saddle River, NJ, 768 pp.

Scheithe, J.R. (1996). "Research on the internal shear strength of a needle-punched geosynthetic clay liner," Master of Science thesis, Department of Civil Engineering, Purdue University, West Lafayette, Indiana.

Stark, T.D. and Poeppel, A.R. (1994). "Landfill Liner Interface Strengths from Torsional-Ring-Shear Tests," *Journal of Geotechnical Engineering*, Vol. 120, No. 3, pp. 597-615.

Stark, T.D. and Eid, H.T. (1996). "Shear Behavior of Reinforced Geosynthetic Clay Liners," *Geosynthetics International*, Vol. 3, No. 6, pp. 771-786.

Stark, T.D., Arellano, D., Evans, W.D., Wilson, V.L. & Gonda, J.P. (1998). "Unreinforced Geosynthetic Clay Liner Case History," *Geosynthetics International*, Vol. 122, No. 3, pp. 197-203.

Thiers, G.R. and Seed, H.B. (1969). "Strength and Stress-Strain Characteristics of Clays Subjected to Seismic Loading Conditions," *Vibration Effects of Earthquakes on Soils and Foundations*, ASTM STP 450, American Society for Testing Materials, pp. 3-56.

Triplett, E.J. and Fox, P.J. (2001). "Shear Strength of HDPE Geomembrane/Geosynthetic Clay Liner Interfaces," *Journal of Geotechnical and Geoenvironmental Engineering*, Vol. 127, No. 6, pp. 543-552.

Viswanadham, V.S. and Jessberger, H.L. (2005). "Centrifuge Modeling of Geosynthetic Reinforced Clay Liners of Landfills," *Journal of Geotechnical and Geoenvironmental Engineering*, Vol. 131, No. 5, pp. 564-574.

Vucetic, M. (1988). "Normalized Behavior of Offshore Clay Under Uniform Cyclic Loading," *Canadian Geotechnical Journal*, Vol. 25, pp. 33-41.

Vucetic, M. and Dobry, R. (1988). "Degradation of Marine Clays Under Cyclic Loading," *Journal of Geotechnical Engineering*, Vol. 114, No. 2, pp. 133-149.

Vucetic, M. and Dobry, R. (1991). "Effect of Soil Plasticity on Cyclic Response," *Journal of Geotechnical Engineering*, Vol. 117, No. 1, pp. 89-107.

Yegian, M.K. and Lahlaf, A.M. (1992). "Dynamic Interface Shear Strength Properties of Geomembranes and Geotextiles," *Journal of Geotechnical and Geoenvironmental Engineering*, Vol. 118, No. 5, pp. 760-779.

Yegian, M.K. and Harb, J.N. (1995). "Slip Displacements of Geosynthetic Systems Under Dynamic Excitation," *Earthquake Design and Performance of Solid Waste Landfills*, Geotechnical Special Publication No. 54, ASCE, pp. 212-236.

Yegian, M.K., Harb, J.N. and Kadakal, U. (1998). "Dynamic Response Analysis Procedure for Landfills with Geosynthetic Liners," *Journal of Geotechnical and Geoenvironmental Engineering*, Vol. 124, No. 10, pp. 1027-1033.

Yegian, M.K. and Kadakal, U. (1998). "Geosynthetic Interface Behavior Under Dynamic Loading," *Geosynthetics International*, Vol. 5, No. 1, pp. 1-16.

Yegian, M.K., Yee, Z.Y. and Harb, J.N. (1995). "Seismic Response of Geosynthetic/Soil Systems," *Geoenvironmental 2000*, Geotechnical Special Publication No. 46, ASCE, Vol. 2, pp. 1113-1125.

Youd, T. L. (1972). "Compaction of Sands by Repeated Shear Straining," *Journal of the Soil Mechanics and Foundations Division*, Vol. 98, SM7, pp. 709-725.

Zornberg, J.G., McCartney, J.S. and Swan, R.H. (2005). "Analysis of a Large Database of GCL Internal Shear Strength Results," *Journal of Geotechnical and Geoenvironmental Engineering*, Vol. 131, No. 3, pp. 367-380.

APPENDIX A

SUPPLEMENTARY TEST DATA

A.1 Introduction

This appendix provides a compilation of additional test data collected throughout this study. The intent is to supplement the data discussed in Chapter 4. First, the monotonic test results will be shown and then the cyclic test results. The vertical displacement data for second-stage hydration is withheld to prevent redundancy.

A.2 Monotonic Shear Data

Monotonic shear tests were performed for displacement rates ranging from 0.1 to 30,000 mm/min. This section provides shear stress and vertical displacement behavior during each test.

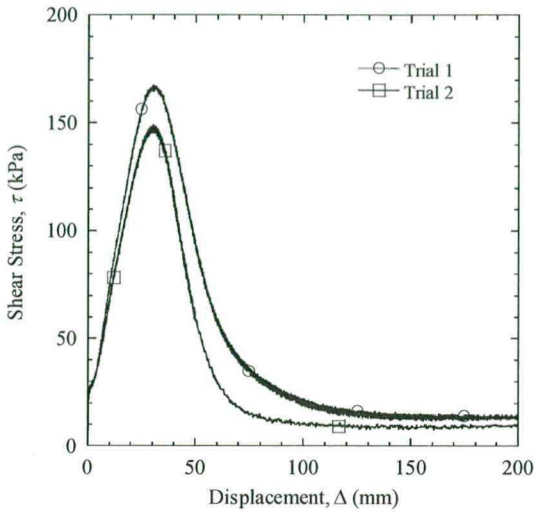

a)

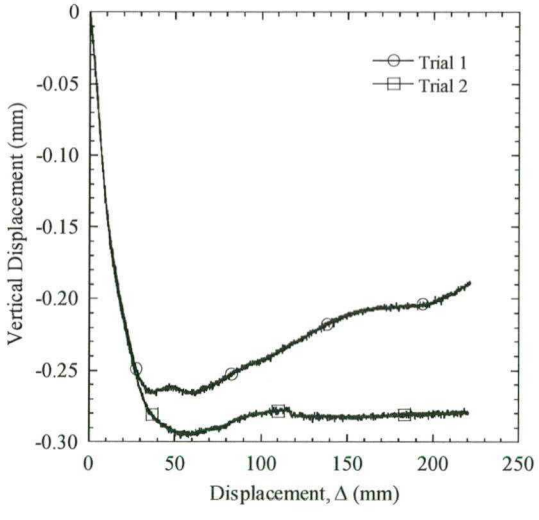

b)

Figure A.1: Monotonic shear test with displacement rate of 0.1 mm/min.

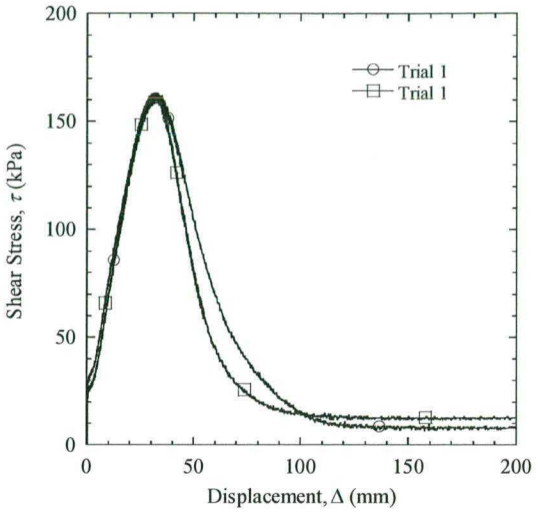

a)

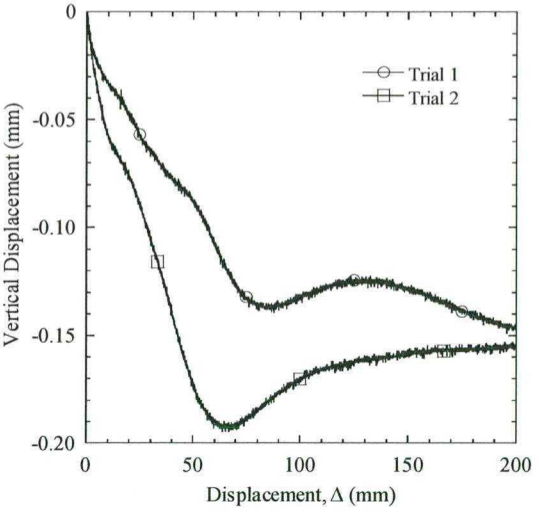

b)

Figure A.2: Monotonic shear test with displacement rate of 1 mm/min.

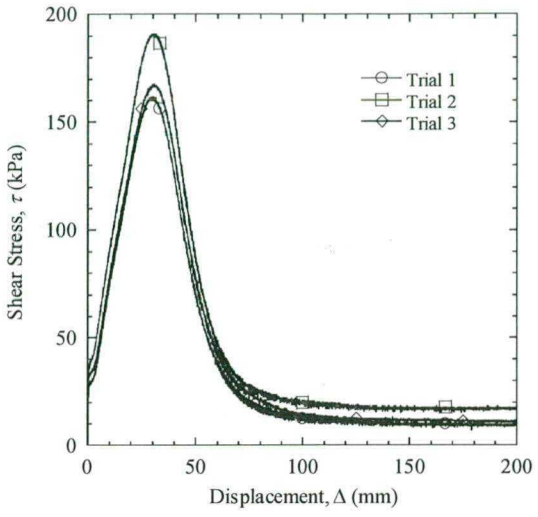

a)

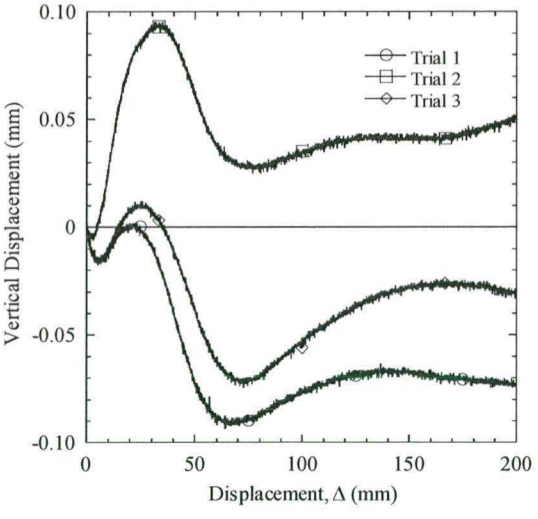

b)

Figure A.3: Monotonic shear test with displacement rate of 10 mm/min.

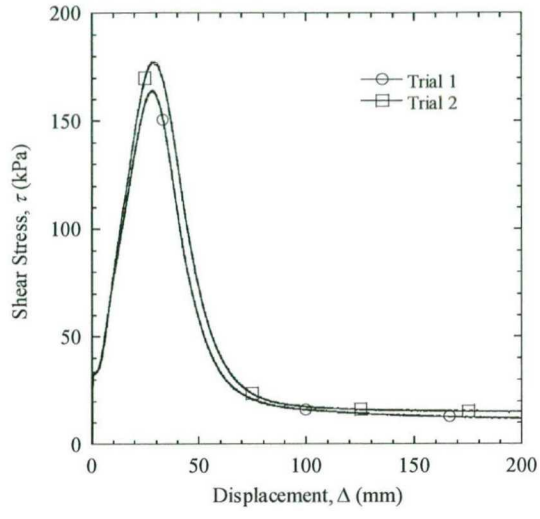

a)

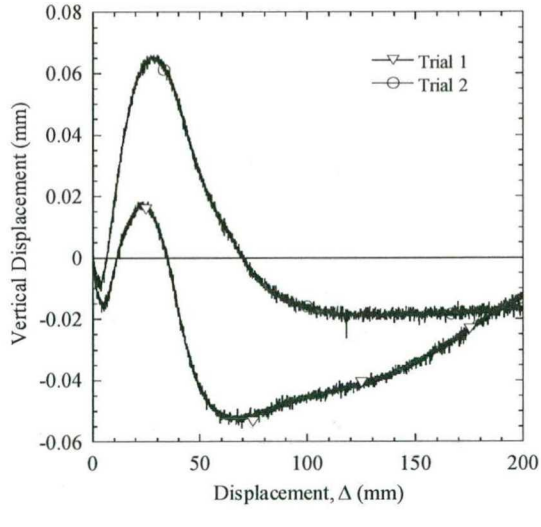

b)

Figure A.4: Monotonic shear test with displacement rate of 100 mm/min.

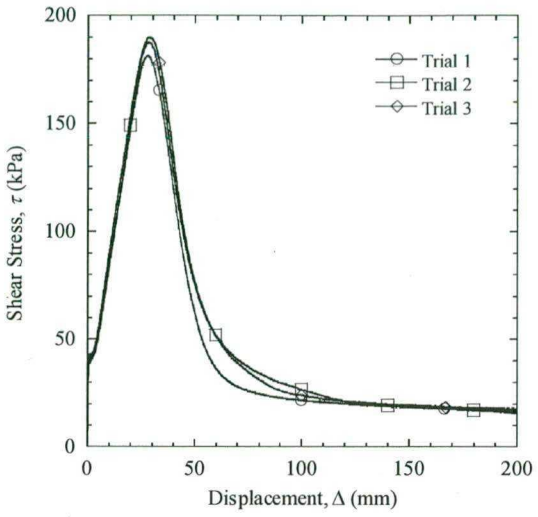

a)

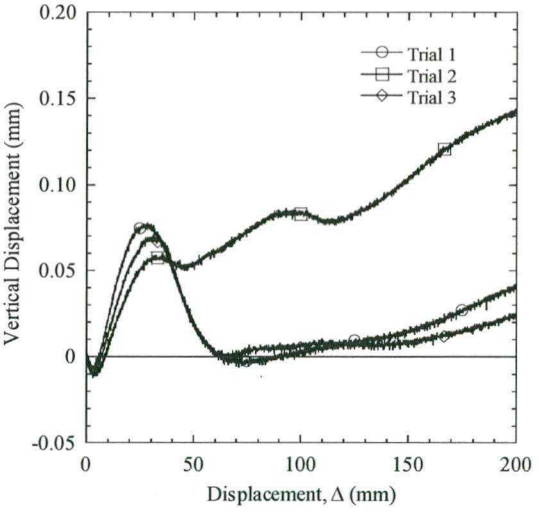

b)

Figure A.5: Monotonic shear test with displacement rate of 1000 mm/min.

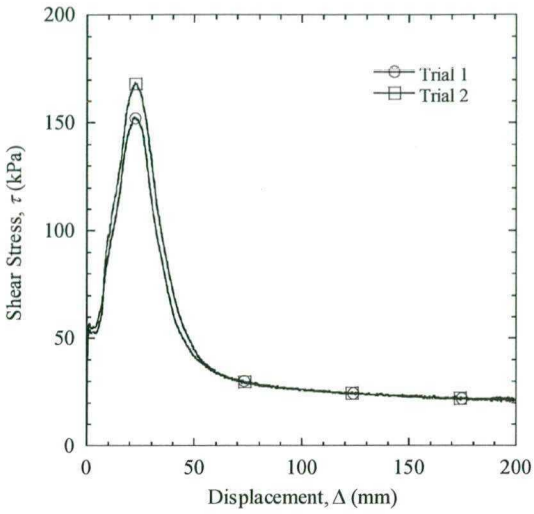

a)

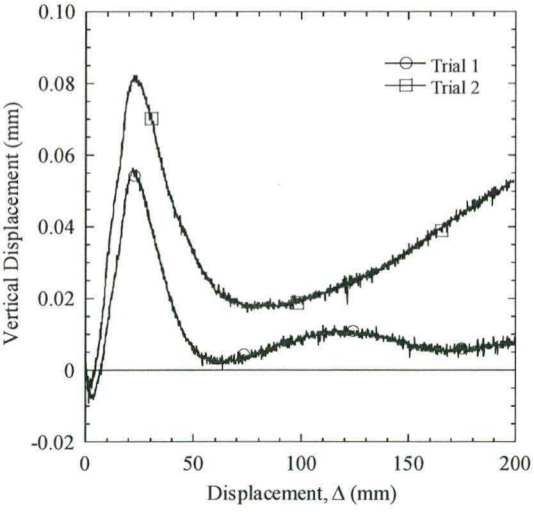

b)

Figure A.6: Monotonic shear test with displacement rate of 10,000 mm/min.

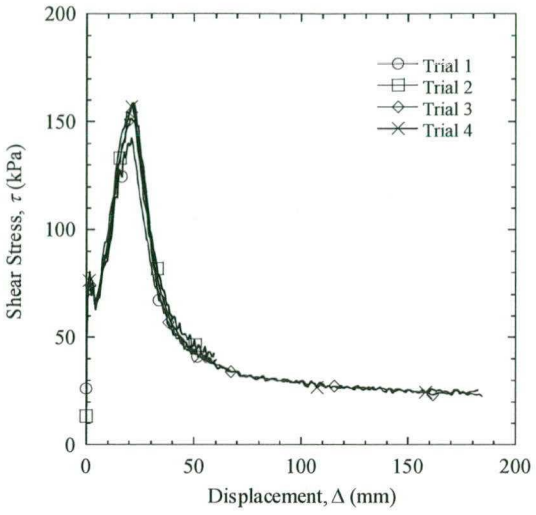

a)

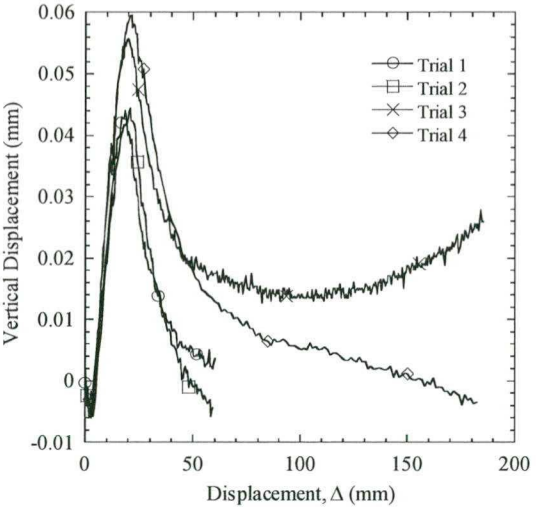

b)

Figure A.7: Monotonic shear test with displacement rate of 30,000 mm/min.

A.3 Cyclic Shear Data

This section provides additional test data for the cyclic shear tests performed to investigate the influence of displacement amplitude on shear behavior. Specifically, shear stress-displacement behavior during cyclic shear and vertical displacement during the 24 h rest period are shown. Table A.1 lists each cyclic test and the corresponding test parameters. These test numbers correlate with those from Table 4.2.

Test	File Name	Parameter Changed	Cyclic Amplitude (mm)	Cyclic Frequency (Hz)	No. of cycles	Static rate (mm/min)	Waveform
1	Test 1-27-06	amplitude	2	1.0	50	0.1	sine
2	Test 2-2-06	amplitude	5	1.0	50	0.1	sine
3	Test 11-6-05	amplitude	10	1.0	50	0.1	sine
4	Test 11-1-05	amplitude	15	1.0	50	0.1	sine
5	Test 11-10-05	amplitude	20	1.0	50	0.1	sine
6	Test 11-14-05	amplitude	25	1.0	50	0.1	sine
7	Test 11-19-05	frequency	15	0.1	50	0.1	sine
8	Test 12-4-05	frequency	15	0.5	50	0.1	sine
9	Test 2-6-06	frequency	15	2.0	50	0.1	sine
10	Test 1-17-06	frequency	15	3.0	50	0.1	sine
11	Test 11-25-05	cycles	15	1.0	10	0.1	sine
12	Test 1-8-06	cycles	15	1.0	100	0.1	sine
13	Test 3-28-06	waveform	15	1.0	50	0.1	sine
14	Test 2-15-06	waveform	15	1.0	50	0.1	square
15	Test 2-24-06	waveform	15	1.0	50	0.1	triangular

Table A.1: Cyclic shear test parameters.

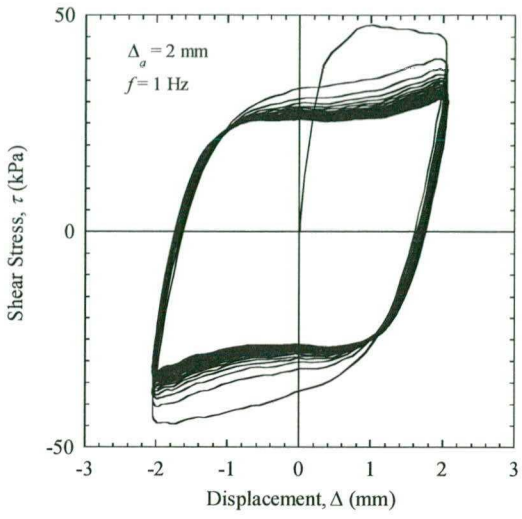

Figure A.8: Shear stress vs. displacement for Test 1.

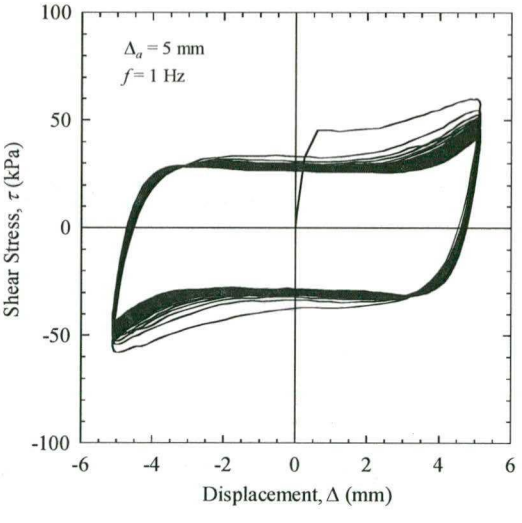

Figure A.9: Shear stress vs. displacement for Test 2.

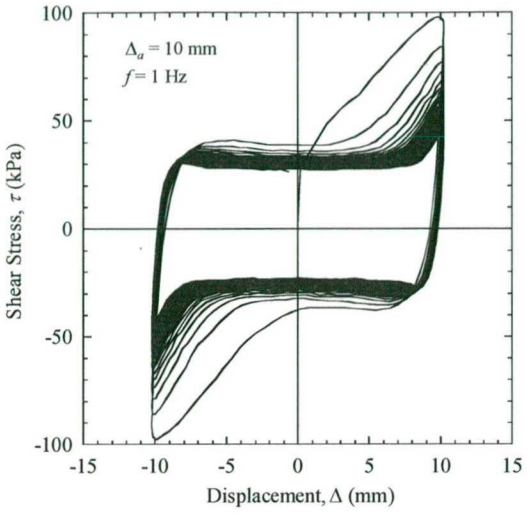

Figure A.10: Shear stress vs. displacement for Test 3.

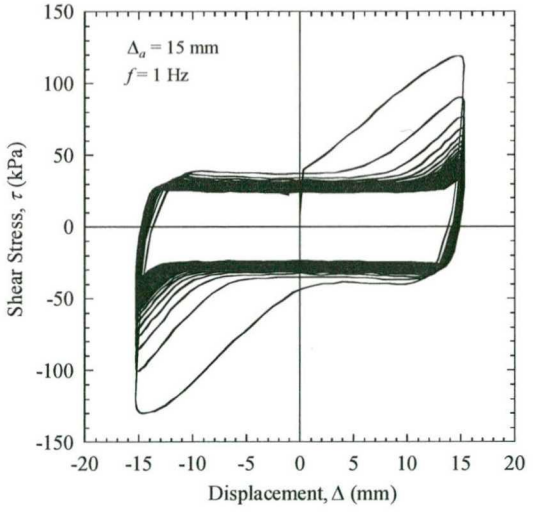

Figure A.11: Shear stress vs. displacement for Test 4.

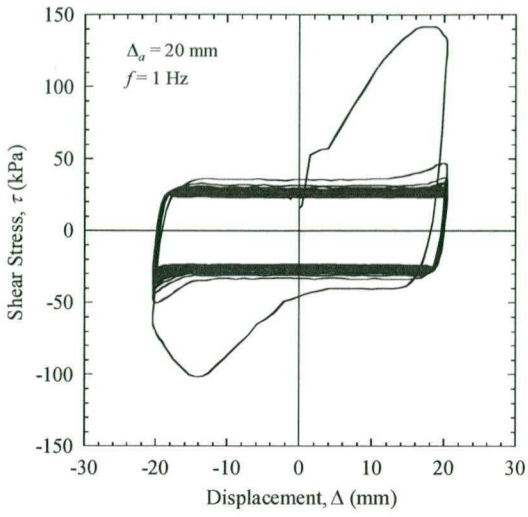

Figure A.12: Shear stress vs. displacement for Test 5.

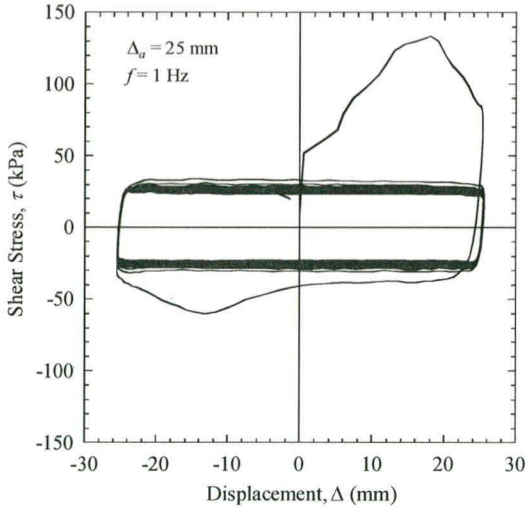

Figure A.13: Shear stress vs. displacement for Test 6.

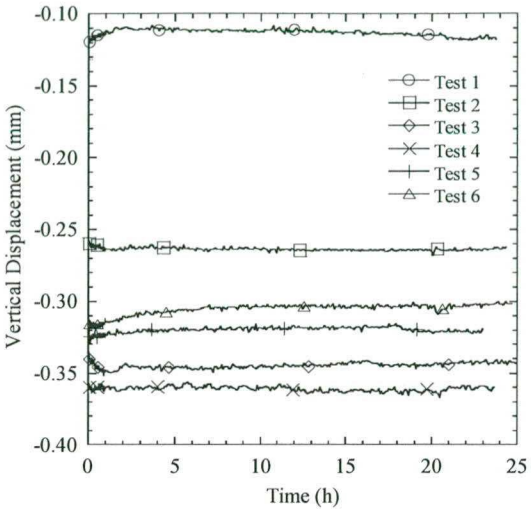

Figure A.14: Volume change during 24 h rest period for six cyclic shear tests.

APPENDIX B

DYNAMIC SHEAR MACHINE CONFIGURATION

B.1 Introduction

This appendix provides a detailed account of the specific techniques used in the laboratory for configuration of test specimens, machine components, machine software, and data analysis. It is anticipated that this information will be used for subsequent testing of GCL specimens using the dynamic direct shear machine.

B.2 Specimen Preparation

A shipment of four rolls of Bentomat ST were packed by the CETCO Fairmount facility on 2/22/05 and shipped to Ohio State University on 2/24/05. This material was used in the research testing program described herein, with the exception of the monotonic shear data in Section 4.3. The material for the monotonic shear tests came from twelve rolls of Bentomat ST that were packed by the CETCO Lovell facility and shipped to Ohio State on 2/10/06. After specimens were trimmed from these rolls, they were hydrated using the described two-stage procedure. The geotextiles for each specimen were separated for a length of approximately 25 mm at the front and over a sufficient length at the rear such that 1067 mm of reinforcement was left intact. All loose

bentonite was removed from the separated areas prior to placing it in the pan for the first stage of hydration. Assuming an initial water content of 20%, enough water was then added to bring the specimen to a water content of 160%. This value was sufficient for a normal stress of 141 kPa, however it will change for other normal stresses. Once the specimen was placed in the test chamber, the needle-punched reinforcement was checked to ensure that there was no area of GCL that was reinforced outside of the chamber.

B.3 Shear Machine Assembly

During the physical assembly of the shear machine, several specific items should be considered. First, keep the piston clear of the pullout plate (and any other obstructions) when pressuring the manifolds. Due to the machine not being precisely tuned, the piston tends to displace erratically (typically within ± 10 mm) during this process. The actuator is calibrated such that zero displacement is measured when the piston is fully retracted and 254 mm when the piston is fully extended. Dynamic shear tests have been typically conducted with the pullout plate set at an absolute displacement of 220 mm. This allows for dynamic displacements of up to ± 25 mm without the pullout plate colliding with the drip pan or float valve. For dynamic displacements greater than ± 25 mm, the pullout plate clearance must be verified.

Given the opportunity, the air bags will burst into any small crack between the various confining plates, especially at high pressure. The edges and corners of the bags are carefully protected during machine assembly with custom-made plastic forms and reinforced cloth to prevent such bursting. These plastic forms tend to deform with significant specimen volume change, which occurs at high normal stress. Also, the cloth

may tear with repeated use and may require replacement. When the middle two reaction beams are bolted to the machine frame, one is labeled "L" and the other "R." This corresponds to "left" and "right," respectively, when facing the machine with the piston on the left. These are labeled so that the LVDT assembly will fit properly onto the reaction beams. A final consideration when assembling the machine is that the drainage valve on the water reservoir should be left slightly open to ensure proper performance of the float valve.

B.4 Shear Machine Software

The software used to control the dynamic direct shear machine was developed by MTS Systems. To open the software, click on the "Station Manager" icon on the computer desktop. You will then be asked to select a configuration file, which is located in C:/ftse/Controllers/Ctlr_01468813/config/ShearFrameFTSE.cfg. Then select a Parameter Set, which depends on the valve that is currently connected to the machine. Use "3StageValveNEW" for the 3-stage valve, however the parameter settings for the single stage valve are likely incorrect since the files were accidentally erased from the computer, therefore they should be recreated. All the tests in this thesis were conducted using the 3-stage valve. This will open the Station Manager. Click "Reset" for the Interlock 1, and also select "Exclusive Control" (A and B in Figure B.1). To turn on the hydraulic pumps, first look at the control screen on the pumps to verify which pumps are currently activated. Then select the Power Low button for the Hydraulic Power Unit (HPU) (C in Figure B.1), wait for the oil temperature to stabilize (typically around 100° F) and then select the Power High button (D in Figure B.1). Next power up the

Hydraulic Service Manifolds (HSM 1) by selecting Power Low and Power High sequentially (E and F in Figure B.1). The piston tends to move erratically during this process due to deficiencies in the machine tuning. To depressurize the manifolds and turn off the pumps, complete this process in reverse.

The actuator is calibrated such that zero displacement corresponds to the piston being fully retracted and a displacement of 254 mm corresponds to the piston being fully extended. To manually move the piston, select Manual Command under Station Controls in the Station Manager (G in Figure B.1) and a popup controller opens. Select "Enable Manual Command" in this new window and you can change the piston position manually using this controller.

B.4.1 Hydration Test

A procedure has been developed to measure vertical displacement using the LVDT during 2nd stage hydration. First, select MPT from the Station Manager and then define a specimen (H and I in Figure B.1). By defining a specimen, the software creates a folder with this name in which the test data will be saved, located under C:/My Documents/specimens. Next, select Procedure Editor from the Station Manager (J in Figure B.1) and then File/Open Procedures/My Documents/Procedures/ LVDT hydration (Figure B.2). In this procedure, four different data collection processes are defined. The first three collect data at time intervals of 5, 15, and 30 s respectively for a specified time period. The fourth process collects data every 5 min indefinitely until the process is stopped. When you are ready to begin the hydration test, select the Toggle Execute/Edit

Mode button from the Station Manager and press Program Run (K and L in Figure B.1). When hydration is complete, then press Program Stop (M in Figure B.1).

B.4.2 Dynamic Test

Procedures have also been established to perform a dynamic test which is immediately followed by LVDT monitoring during a 24 h rest period. In the Procedure Editor window, select File/Open Procedures/My Documents/Procedures/dynamic-LVDT test (Figure B.3). The following processes are present:

- data initial – this takes a single data point at the onset of the test to provide an initial value of force, displacement, and LVDT,
- dynamic – this provides the cyclic command function, where you can modify displacement amplitude, frequency and test duration,
- data dynamic – this collects data points at a specified time interval, which can be modified depending on the desired sampling frequency (typically 100 data points per cycle),
- LVDT5-8 – these are the same data collection processes used for the Hydration Test to measure vertical displacement during the rest period.

The "Start" column indicates when the process will begin and the "Interrupt" column indicates when the process will complete within the procedure, which can be modified by clicking on each. Before you start the dynamic test, verify that a sufficient number of hydraulic pumps are on for the test (at least 2 and likely all 3). When you are ready to begin, select the Toggle Execute/Edit Mode button from the Station Manager and press Program Run (K and L in Figure B.1). When the dynamic portion is complete, vertical

displacement measurement will begin immediately. Disconnect the pullout plate from the actuator as quickly and gently as possible, and leave the pumps running during the 24 h rest period. When this rest period is complete, press the Program Stop button (M in Figure B.1).

B.4.3 Static Test

To open the procedure created for monotonic shear tests, in the Procedure Editor window select File/Open Procedures/My Documents/Procedures/static test (Figure B.4). The following processes are present:

- data initial – this data acquisition process collects a single point at the beginning of the test to provide an initial measure of force, displacement and LVDT,
- static – this is the command process which specifies the displacement rate and total displacement of the piston,
- data static – this data acquisition process collects data at a specified sampling rate for the duration of the test; in the case of a test at 0.1 mm/min displacement rate, it has been determined that collecting samples every 30 s works well.

The "Start" column indicates when the process will begin and the "Interrupt" column indicates when the process will complete within the procedure, which can be modified by clicking on each. Before you start the static test, verify that a sufficient number of hydraulic pumps are on for the test (1 for very slow displacement rates and all 3 for high displacement rates). When you are ready to begin, select the Toggle Execute/Edit Mode button from the Station Manager and press Program Run (K and L in Figure B.1).

This procedure was utilized when conducting the study on the effect of displacement rate. For each displacement rate, the sampling frequency was modified so that an equal number of data points was obtained for each test, with the exception of those tests at which the fastest data collection frequency (1024 Hz) was required. At the fastest displacement rate, the command function was set to 100,000 mm/min although the piston actually moved at a slower rate. Because the software considers the test to be complete once the procedure is done (as opposed to the actuator completing the desired displacement) some modification had to be made at this fastest displacement rate in order to acquire the desired data. First, the data acquisition (i.e., data static) procedure was set to collect a specific number of samples (1000 in this case) rather than sampling at a certain time interval. Also, the "Procedure is done when" line (see Figure B.4) was set to "static data.Done." This avoided the problem of the data acquisition halting prior to recording large displacement shear stresses.

B.4.4 Tuning and Compensators

In order to have proper machine response, the PID (proportional-integral-derivative) controller must be correctly tuned. To perform machine tuning, first set the mode to Tuning (N in Figure B.1) where the password is "Tuning." Next, select Station Setup (O in Figure B.1) in the Station Manager window and a new window will open. On the left hand side of the Station Setup window, select "Channels" then "ShearFrame" and then the button to the right which looks like a tuning fork (Figure B.5). Here you can adjust the P, I and D values to achieve proper response of the piston. In general, you will

not need to adjust the F gain values. Some common rules of thumb when adjusting the tuning include:

$$I \approx 0.1P,$$

$$D \approx 0.01P.$$

It is best to modify the tuning for each test sequence in order to obtain proper piston response to the command function, however the values shown in Figure B.5 work well for sinusoidal shearing with frequency of 1 Hz. Therefore it is recommended that the tuning is not adjusted for additional sinusoidal strain-controlled testing, however the tuning will definitely need to be modified if stress-controlled testing commences.

Another method for machine tuning is to use the Adaptive Compensators. These are automatic tuning programs which are installed in the software and gradually correct the tuning during a test. It is best to use the manual tuning to get the machine response close to the command and then use the compensators if necessary. To activate the compensators, double click on the command process used to run the static test (section B.4.3) within the Procedure Editor. Here a drop-down menu lists the available Adaptive Compensators. The first is the peak/valley compensator (PVC), which monitors the peak and valley of a cyclic test and adjusts the PID controller to match the command. The second is the amplitude/phase compensator (APC), which monitors the amplitude and phase of a cyclic test and again adjusts the PID controller as necessary. Either of these can be used, however the piston response will change slightly during the test due to the effects of the compensators. For this reason, it may not be advisable in general to use these compensators for our testing program.

B.5 Data Analysis

Once the raw data is collected by the MTS software, it must be reduced into a usable form for analysis. The majority of this work has been done using Excel and the final plots were created using Kaleidagraph. The raw data files were opened into Excel then copied and pasted into another spreadsheet. Next, the initial values of displacement, force and LVDT were subtracted from all data points for each portion of the test (i.e., hydration, dynamic shearing and static shearing). The measured shear force is then converted to shear stress by 1) adjusting for the load cell calibration (Figure 3.5), 2) dividing by the shearing surface area, and 3) subtracting out the machine friction (Figure 3.6). The data should also be manipulated so that shear displacements and shear stresses are positive during 1) the initial cycle of a dynamic test, and 2) the full duration of a static test. To aid in data reduction calculations, three Visual Basic codes were written in Excel, which are described in the following sections.

B.5.1 Smooth Data.xls

This spreadsheet takes a list of data points and averages the data in a specified smoothing interval. First, place the data to be smoothed in columns A and B of the spreadsheet, and then in the highlighted boxes specify the smoothing interval (odd number only) and the number of data points. The macro then averages the data and reports the averaged value at the center of each interval. In this manner, the data is smoothed, however the location is not changed. This spreadsheet is useful for smoothing the shear stress-shear displacement and vertical displacement-shear displacement curves for a static test. Figure B.6 shows the code for this macro.

B.5.2 Modulus and Damping.xls

Use this spreadsheet to aid in calculating the shear modulus, damping ratio, and evolution of peak shear stress during a cyclic test. The code for the three programs is shown in Figures B.7-9. First, place the smoothed cyclic data in columns A-D of the spreadsheet, then indicate in the highlighted cells the number of cycles and the displacement amplitude of the test. Next, specify if the displacement and stress values are both negative for the first cycle. The macro determines the maximum stress value for each half cycle and divides this by the displacement amplitude in order to determine the shear stiffness. This spreadsheet also calculates the energy dissipated during each cycle by determining the area within the shear stress vs. displacement curve. This is accomplished using the trapezoidal rule. The damping ratio is then calculated for each half cycle and the average value is reported.

B.5.3 Sort Data.xls

The final spreadsheet was created to assist in sorting the data, particularly when creating plots of the evolution of peak shear stress with number of cycles. It is especially useful to separate the stress-time data into half cycles so that each can be plotted separately. Place the shear stress and time data (obtained from the Modulus spreadsheet in Modulus and Damping.xls) in Columns A and B of the spreadsheet and the macro will separate the data by placing the first set of data in Columns D-E and the next set of data in Columns F-G, which is repeated for all data. The visual basic code for this spreadsheet is shown in Figure B.10.

B.6 Technical Contacts

There are several resources available if technical difficulties are encountered when operating the MTS FlexTest controller. First, consult the software manual, which is located in hard copy in the filing cabinet next to the lab desk or in electronic copy installed on the computer. Peter Furkey (614-507-3664), a field service engineer with MTS, has been of great assistance is answering questions regarding the machine operation. If questions arise which can not be solved through either of these sources, MTS has a HELPLine (800-328-2255) which may be contacted. In addition, Steve Carlsen (952-937-4510) is an applications engineer with MTS who has been useful in answering questions.

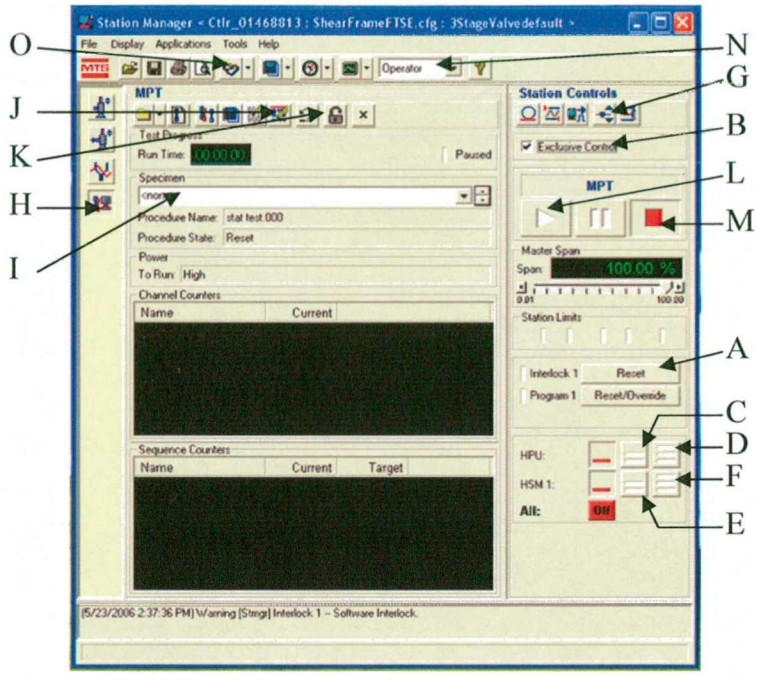

Figure B.1: Station Manager window.

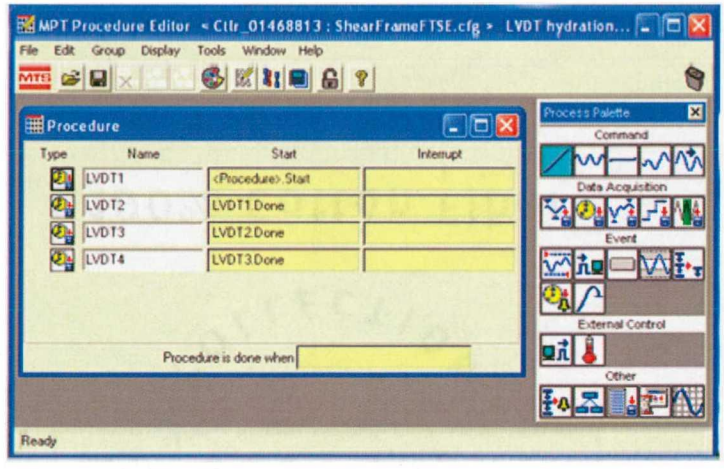

Figure B.2: Hydration test procedure.

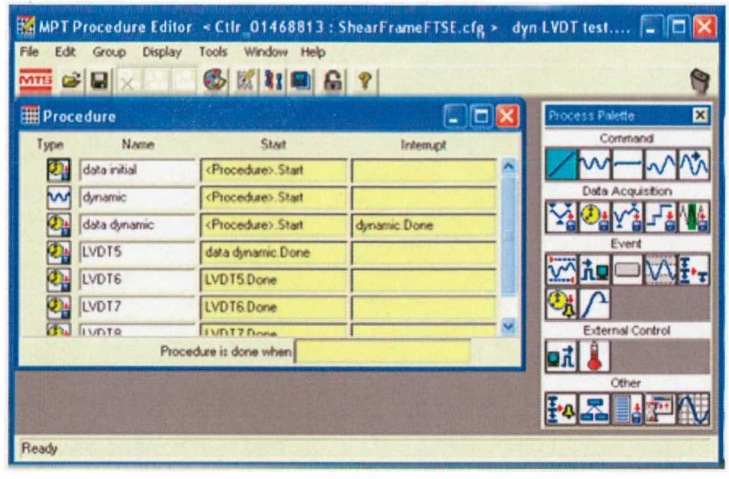

Figure B.3: Dynamic test procedure.

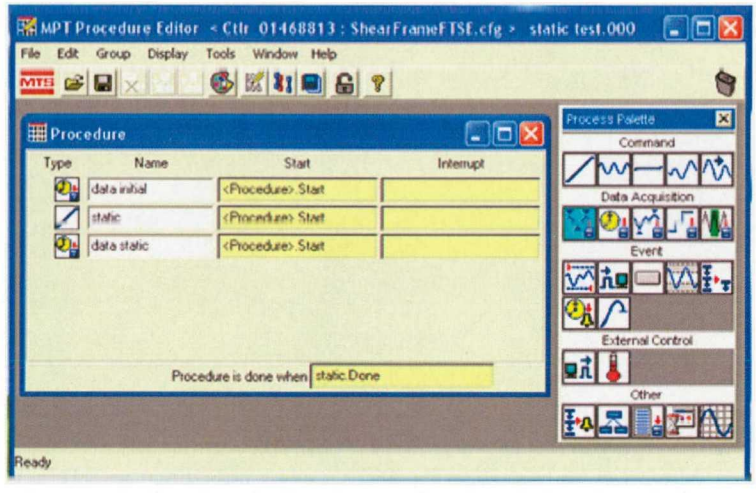

Figure B.4: Static test procedure.

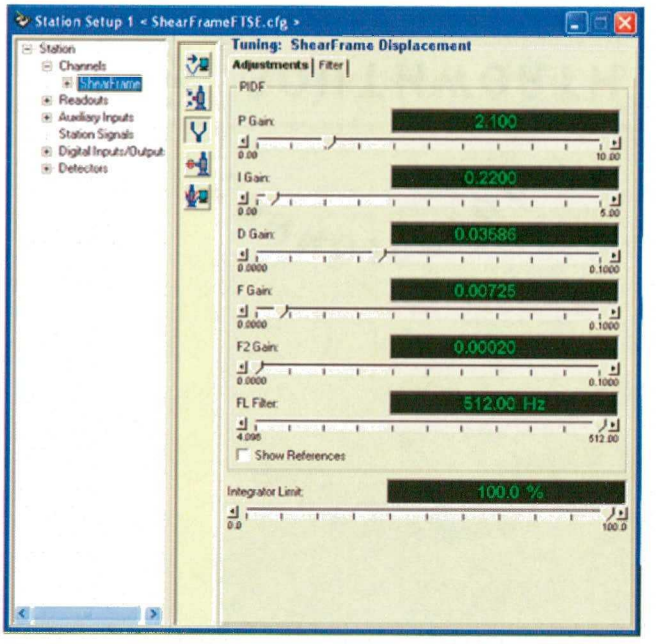

Figure B.5: Station Setup window.

```
Dim counter1 As Integer
Dim counter2 As Integer
Dim counter3 As Integer
Dim interval As Integer
Dim sum As Single
Dim avg As Single

interval = Range("n1").Value / 2 - 0.5
counter2 = 2

For counter1 = interval To Range("N2").Value / Range("n1").Value + 1

sum = 0

For counter3 = 1 To Range("n1").Value
sum = sum + Cells(counter2, 2).Value
counter2 = counter2 + 1
Next counter3

avg = sum / Range("n1").Value
num = counter2 - Range("n1") + interval

ActiveSheet.Cells(num, 4).Value = avg
ActiveSheet.Cells(num, 3).Value = ActiveSheet.Cells(num, 1)

Next counter1
```

Figure B.6: Visual Basic code for Smooth Data.xls.

```
Dim counter1 As Integer;  Dim counter2 As Integer
Dim counter3 As Integer; Dim flag As Integer
counter2 = 4
For counter1 = 5 To Range("H1").Value
   Cells(1, 9) = counter2
   flag = 0

   If Cells(1, 9) = Cells(1, 10) Then
      If Cells(counter1, 3) < Cells(counter1 + 1, 3) Then
      Cells(2, 13) = Cells(counter1, 2).Value
         If Cells(counter1, 2) < Cells(1, 15) Then
            For counter3 = 1 To 10
               Cells(2, 9) = Cells(counter1, 3).Value
               Cells(2, 11) = Cells(counter1 + counter3, 3).Value
               If Cells(2, 10) < Cells(2, 12) Then
                  If Cells(2, 10) - Cells(2, 12) < 5 Then
                  If Cells(counter1, 3) * Cells(counter1 + counter3, 3) > 0 Then
                     flag = 1
                  End If
                  End If
               End If
            Next counter3
            If flag = 0 Then
               Cells(counter2, 7) = Cells(counter1, 3).Value
               Cells(counter2, 8) = Cells(counter1, 2).Value
               Cells(counter2, 9) = Cells(counter1, 1).Value
               counter2 = counter2 + 1
            End If
         End If
      End If
   End If

   If Cells(1, 9) = Cells(1, 11) Then
      If Cells(counter1, 3) > Cells(counter1 + 1, 3) Then
      Cells(2, 13) = Cells(counter1, 2).Value
         If Cells(counter1, 2) > Cells(1, 14) Then
            For counter3 = 1 To 10
               Cells(2, 9) = Cells(counter1, 3).Value
               Cells(2, 11) = Cells(counter1 + counter3, 3).Value
               If Cells(2, 10) < Cells(2, 12) Then
                  If Cells(2, 10) - Cells(2, 12) < 5 Then
                  If Cells(counter1, 3) * Cells(counter1 + counter3, 3) > 0 Then
                     flag = 1
                  End If
                  End If
               End If
            Next counter3
            If flag = 0 Then
               Cells(counter2, 7) = Cells(counter1, 3).Value
               Cells(counter2, 8) = Cells(counter1, 2).Value
                 Cells(counter2, 9) = Cells(counter1, 1).Value
                 counter2 = counter2 + 1
              End If
           End If
        End If
     End If
Next counter1
```

Figure B.7: Visual basic code for Maximum Stress in Modulus and Damping.xls.

```
Dim counter1 As Integer
Dim counter2 As Integer
Dim odd As Integer
Dim even As Integer

counter2 = 4

For counter1 = 5 To Range("H1").Value
   Cells(1, 9) = counter2

   If Cells(1, 9) = Cells(1, 10) Then
      If Cells(counter1, 2) < Cells(counter1 + 1, 2) Then
      If Cells(counter1, 2) < Cells(counter1 + 3, 2) Then
         Cells(counter2, 7) = Cells(counter1, 3).Value
         Cells(counter2, 8) = Cells(counter1, 2).Value
         Cells(counter2, 9) = Cells(counter1, 1)
         counter2 = counter2 + 1
      End If
      End If
   End If

   If Cells(1, 9) = Cells(1, 11) Then
      If Cells(counter1, 2) > Cells(counter1 + 1, 2) Then
      If Cells(counter1, 2) > Cells(counter1 + 3, 2) Then
         Cells(counter2, 7) = Cells(counter1, 3).Value
         Cells(counter2, 8) = Cells(counter1, 2).Value
         Cells(counter2, 9) = Cells(counter1, 1)
         counter2 = counter2 + 1
      End If
      End If
   End If

Next counter1
```

Figure B.8: Visual basic code for Maximum Displacement in Modulus and Damping.xls.

```
Dim counter2 As Integer
Dim counter3 As Integer

counter2 = 2
counter3 = 4

For counter1 = 4 To Range("H1").Value

   If Cells(counter1, 2) * Cells(counter1 + 1, 2) < 0 Then
      If counter2 = 3 Then
         Cells(counter3, 10) = Cells(counter1, 7)
         counter3 = counter3 + 1
         counter2 = 1
      End If
   End If

   If Cells(counter1, 2) * Cells(counter1 + 1, 2) < 0 Then
      counter2 = counter2 + 1
   End If

Next counter1
```

Figure B.9: Visual basic code for Area in Modulus and Damping.xls.

```
Dim counter1 As Integer
Dim counter2 As Integer

counter2 = 2

For counter1 = 2 To 105

   If Cells(counter1, 1) < 0 Then
      Cells(counter2, 4) = Cells(counter1, 1)
      Cells(counter2, 5) = Cells(counter1, 2)
      Cells(counter2, 6) = Cells(counter1 + 1, 1)
      Cells(counter2, 7) = Cells(counter1 + 1, 2)
      counter2 = counter2 + 1
   End If

Next counter1
```

Figure B.10: Visual basic code for Sort Data.xls.